High Temperature Removal of H$_2$S from Coal Gasification Process Streams Using an Electrochemical Membrane System

Final Technical Report

1 September 1999 to 1 June 2003

Dr. Jack Winnick
Dr. Meilin Liu

June 2003

DISCLAIMER

This report was prepared as an account of work sponsored by an agency of the United States Government. Neither the United States Government nor any agency thereof, nor any of their employees, makes any warranty, express of implied, or assumes any legal liability or responsibility for the accuracy, completeness, or usefulness of any information, apparatus, product, or process disclosed, or represents that its use would not infringe privately owned rights. Reference herein to any specific commercial product, process, or service by trade name, trademark, manufacturer, or otherwise does not necessarily constitute or imply its endorsement, recommendation, or favoring by the United States Government or any agency thereof. The views and opinions of authors expressed herein do not necessarily state or reflect those of the United States Government or any agency thereof.

ABSTRACT

A bench scale set-up was constructed to test the cell performance at 600-700˚ C and 1 atm. The typical fuel stream inlet proportions were 34% CO, 22% CO_2, 35% H_2, 8% H_2O, and 450-2000 ppm H_2S. The fundamental transport restrictions for sulfur species in an electrochemical cell were examined. Temperature and membrane thickness were varied to examine how these parameters affect the maximum flux of H_2S removal. It was found that higher temperature allows more sulfide species to enter the electrolyte, thus increasing the sulfide flux across the membrane and raising the maximum flux of H_2S removal. The results identify sulfide diffusion across the membrane as the rate-limiting step in H_2S removal. The maximum H_2S removal flux of 1.1 x 10^{-6} gmol H_2S min^{-1} cm^{-2} (or 3.5 mA cm^{-2}) was obtained at 650˚ C, with a membrane that was 0.9 mm thick, 36% porous, and had an estimated tortuosity of 3.6.

Another focus of this thesis was to examine the stability of cathode materials in full cell trials. A major hurdle that remains in process scale-up is cathode selection, as the lifetime of the cell will depend heavily on the lifetime of the cathode material, which is exposed to very sour gas. Materials that showed success in the past (i.e. cobalt sulfides and $Y_{0.9}Ca_{0.1}FeO_3$) were examined but were seen to have limitations in operating environment and temperature. Therefore, other novel metal oxide compounds were studied to find possible candidates for full cell trials. Gd_2TiMoO_7 and $La_{0.7}Sr_{0.3}VO_3$ were the compounds that retained their structure best even when exposed to high H_2S, CO_2, and H_2O concentrations.

TABLE OF CONTENTS

LIST OF TABLES

LIST OF FIGURES

NOMENCLATURE

Symbols:

a_i = activity of species i
A = area of electrode, cm^2
c_i = liquid mole fraction of species i, mol mol^{-1}
C_i = concentration of species i, mol cm^{-3}
D = diffusivity coefficient, cm^2 s^{-1}
e = quantity of electron charge, C
$E°$ = standard state potential, V
E = actual cross-cell potential, V
F = Faraday's constant, C
i = current density, A cm^{-2}
K_{eq} = equilibrium constant
k_m = mass transfer coefficient, cm s^{-1}
M_W = molecular weight, g mol^{-1}
n = number of equivalents/mole, mol^{-1}
$n^{\cdot}$ (with dot) = molar flow rate, mol s^{-1}
p_i = partial pressure of species i, atm
r_i = radius of ionic species i, cm
t_i = transference or transport number
T = temperature, K
u_i = mobility of ionic species i, cm^2 V^{-1} s^{-1}
$V^{\cdot}$ (with dot) = volumetric flow rate, cm^3 s^{-1}
x = thickness of membrane, cm
y_i = gaseous mole fraction of species i, mol mol^{-1}
z_i = molar charge of transferred species i, mol^{-1}
ε = void volume of membrane
ρ = molar density, mol cm^{-3}
τ = tortuosity
υ = viscosity, kg m^{-1} s^{-1}
μ = electrochemical potential, J mol^{-1}
$\Delta\Phi$ = potential drop across membrane, V

subscripts:
elec = electrolyte
fg = fuel gas
diff = diffusion

SUMMARY

Sulfur is a natural contaminant in nearly all fossil fuel supplies. When a fuel stream is gasified or reformed, the sulfur manifests itself in the form of hydrogen sulfide, H_2S. Extraordinary effort is put forth to remove H_2S to at least ppm levels before the fuel can be used for power generation. To compete with current methods, an electrochemical membrane system (EMS) is now being studied to remove H_2S in one step at high temperature. This process offers continuous H_2S removal at an estimated operating cost of \$0.32 / kg H_2S removed (see Appendix G) and a capital cost that is roughly half that of a Claus plant with tail-gas clean-up. Other advantages are the considerable savings in energy and space compared to current methods.

A bench scale set-up was constructed to test the cell performance at 600-700° C and 1 atm. The typical fuel stream inlet proportions were 34% CO, 22% CO_2, 35% H_2, 8% H_2O, and 450-2000 ppm H_2S. The fundamental transport restrictions for sulfur species in an electrochemical cell were examined. Temperature and membrane thickness were varied to examine how these parameters affect the maximum flux of H_2S removal. It was found that higher temperature allows more sulfide species to enter the electrolyte, thus increasing the sulfide flux across the membrane and raising the maximum flux of H_2S removal. Also, membrane thickness was found to be a critical parameter in cell design. A thinner membrane decreases the distance that sulfide ions must travel to be oxidized at the anode. These results identify sulfide diffusion across the membrane as the rate-limiting step in H_2S removal. The maximum H_2S removal flux of 1.1×10^{-6} gmol H_2S min^{-1} cm^{-2} (or 3.5 mA cm^{-2}) was obtained at 650° C, with a membrane that was 0.9 mm thick, 36% porous, and had an estimated tortuosity of 3.6.

Using this maximum H_2S removal flux, 160 m^2 of cell area would be needed to remove H_2S at 1 g s^{-1} (3.6 kg day^{-1}). If the inlet stream has a contamination level of 1000 ppm H_2S, then the flow rate of gas that could be treated is 4700 SCFM at 650° C and 1 atm. With each cell being 1 m^2, 160 cells would be used. Each cell would be, at most, 2 cm thick, as molten carbonate cells are, making the total volume of the system 3.2 m^3. A conservative estimate is that at least 90% of the H_2S would be removed in this system. Additional cells or metal adsorbents could remove the remaining contaminants.

Economic analysis has shown a promising niche for this technology in industry as it provides continuous H_2S removal and scalability. However, the membranes used in this study did not have optimized design (porosity, tortuosity, and thickness). Having an optimized membrane should permit higher H_2S removal fluxes and better overall cell performance. In addition, it should be noted that the bulk diffusion of H_2S to the cathode/electrolyte surface might be limiting if membrane properties were optimized and the temperature were high enough. This limiting current would be about 28 mA cm^{-2}.

Another focus of this thesis was to examine the stability of cathode materials in full cell trials. A major hurdle that remains in process scale-up is cathode selection, as the lifetime of the cell will depend heavily on the lifetime of the cathode material, which is exposed to very sour gas. Materials that showed success in the past (i.e cobalt sulfides and $Y_{0.9}Ca_{0.1}FeO_3$) were examined but were seen to have limitations in operating environment and temperature. Therefore, other novel metal oxide compounds were studied to find possible candidates for full cell trials.

Gd_2TiMoO_7 and $La_{0.7}Sr_{0.3}VO_3$ were the compounds that retained their structure best even when exposed to high H_2S, CO_2, and H_2O concentrations. They also showed no

sign of melting at operating temperatures. But Gd_2TiMoO_7 was seen to have better

stability with electrolyte present, whereas $La_{0.7}Sr_{0.3}VO_3$ was seen to have better stability

in the pure sour gas stream without electrolyte present. A layered electrode that could

help preserve a stable environment for each of these compounds should be explored in

future research.

CHAPTER 1. INTRODUCTION

1.1 Significance of H₂S Removal

Fossil fuels supply a majority of the world's electricity and combustible fuel. Before
these fuels are used for power generation, contaminants must be removed from the fuel.
Sulfur is perhaps the most predominant and problematic contaminant. In fuel reforming
or gasification at high temperature, hydrogen sulfide is formed. H_2S is not only toxic to
humans at levels below 1000 ppm, but it is also capable of corroding metals--irreversibly
damaging equipment such as turbines and electrodes. It can also poison catalysts such as
those used in Fischer-Tropsch and hydrotreating processes.

Once sufficiently cleansed of sulfur and other harmful impurities, these fuels can be
combusted in gas turbines to generate power at efficiencies of 30-40%.   Fuel cells have
been shown to be more promising, reaching efficiencies over 50%. Integration of these
two technologies could be the most beneficial; a fuel cell/turbine hybrid has a theoretical
efficiency approaching 80%.

Even though fuel cells are thermodynamically superior devices, turbines are still
favored when using fossil fuels because of the scale-up advantages and the resistance to
higher levels of contaminants such as H_2S. Turbines can withstand up to 100 ppm H_2S
versus less than 1 ppm for high temperature fuel cells (MCFC and SOFC).

Current methods of removing H_2S usually involve low temperature absorption or
high temperature adsorption followed by post-regeneration of the sorbent. To compete
with these methods, research towards optimizing a high temperature, continuous,
electrochemical membrane system (EMS) has been underway for some time. First
patented in 1980,[1] full cell runs utilizing graphite cell housing and electrodes showed the

first results of process feasibility.[2] The sulfide reaction mechanism was then explored in half cell runs,[3] and further trials showed favorable kinetics for bench scale runs.[4] NiO was shown to be a viable cathode material for polishing applications (i.e. H_2S levels below 60 ppm)[5,6,7], and optimum cell performance was modeled at low, intermediate, and high contamination levels.[8] Various membrane, electrode, and cell housing materials were tested in bench scale runs, but the choice of cathode material remains the major obstacle in scale-up.

1.2 Hot-gas Clean-up in Coal Gasification Processes

McDermott, Inc. has been working with BWX Technologies to develop a small fuel cell system that can supply the electrical demands. In their design, a low temperature PEM fuel cell generates electricity, and RVS-1 adsorbent is used to remove H_2S.[9] Hot-gas adsorption processes offer an energy-efficient route for dry fuel streams, but the regeneration of the metal-oxide sorbent is an expensive and involved process.[10] There is also a limit to the number of cycles that the sorbent pellets can withstand. In addition, by using a PEM fuel cell, the reformed hot-gas stream must be cooled to remove CO and to reach the operating temperature of the PEM fuel cell. The PEM fuel cell platinum anode is susceptible to H_2S chemsorption, thus requiring removal to below at least 5 ppb.[11]

EMS would negate the need for both catalyst regeneration and stream reheating/cooling as long as high temperature fuel cells or combustion turbines were employed. These high temperature fuel cells (MCFC and SOFC) are also tolerant to CO and have shown resistance to slightly higher H_2S levels (100 ppm).[12] But it is generally accepted that H_2S levels will have to be reduced below 1 ppm for fuel cell application.

The idea is appealing because the resulting fuel gas stream is both cleansed of the highly corrosive H_2S as well as further enriched by H_2. Elemental sulfur is the only sulfur by-product, which is benign (CO_2 may also be produced at the anode). Being a continuous process, waste materials do not have to be handled and regenerated as in a sorbent method. This saves manpower and operating costs while avoiding exposure of personnel to potentially harmful materials. An efficiently designed cell stack may also ensure that the physical space required is minimal.

Coal power plants currently provide 51% of the US electricity demands,[13] and this figure is expected to increase based on the limit of natural gas and oil reserves. On a global scale, coal supplies 23% of all energy, and with the vast coal reserves in the US, China and Russia, this number will also likely increase. But even if the percentages do not change much or even decrease, the increasing world energy demands and the stable price of coal dictate that coal usage will grow for years to come.

Coal gasification processes operate from 550-2000º C at 1-35 bar. Typical stream composition for oxygen-blown processes is shown in Table 1. At present, low temperature absorption processes and Claus plants are used to remove sulfur and salvage it as a salable by-product. These removal procedures can often be as extensive as the rest of the process.[14] High temperature adsorption processes offer an energy efficient route for dry fuel streams, but the regeneration of the metal-oxide sorbent may be hazardous and is non-continuous. In addition, the high flow rates of fuel processing (on the order of 7000 lb/day) would cause vast amounts of adsorbent to be used and then treated.[15] Maintaining operation at temperatures at or above 600º C can theoretically cut the energy needs of an IGCC (Integrated Gasification Combined Cycle) process by approximately

Component	Molar Concentration %
CO	30-45
CO_2	5-25
H_2O	0-12
H_2	20-35
H_2S	< 2

Table 1. Typical Composition of Coal Gas Leaving Gasifier.
Heavy Metal Impurities and other contaminants
such as ammonia are not listed.

20%. Additionally, the IGCC process offers reduction of CO_2 emissions by 35%.[16]

Comparison between the current IGCC design and that using electrochemical cells is

shown in Figures 1 and 2. With many other contaminants in the coal stream (i.e. heavy

metals, ammonia, halide gases, and ash), the focus needs to be on processes that conserve

cost and physical plant space while striving for zero emissions.

High temperature EMS potentially offers such a solution, because it conserves plant

space and operating cost. EMS negates the need for both catalyst regeneration and fuel

stream reheating. Preliminary capital cost analysis indicates that EMS would also be

roughly half the price of a Claus/Sulfinol plant with tailgas clean-up.[5]
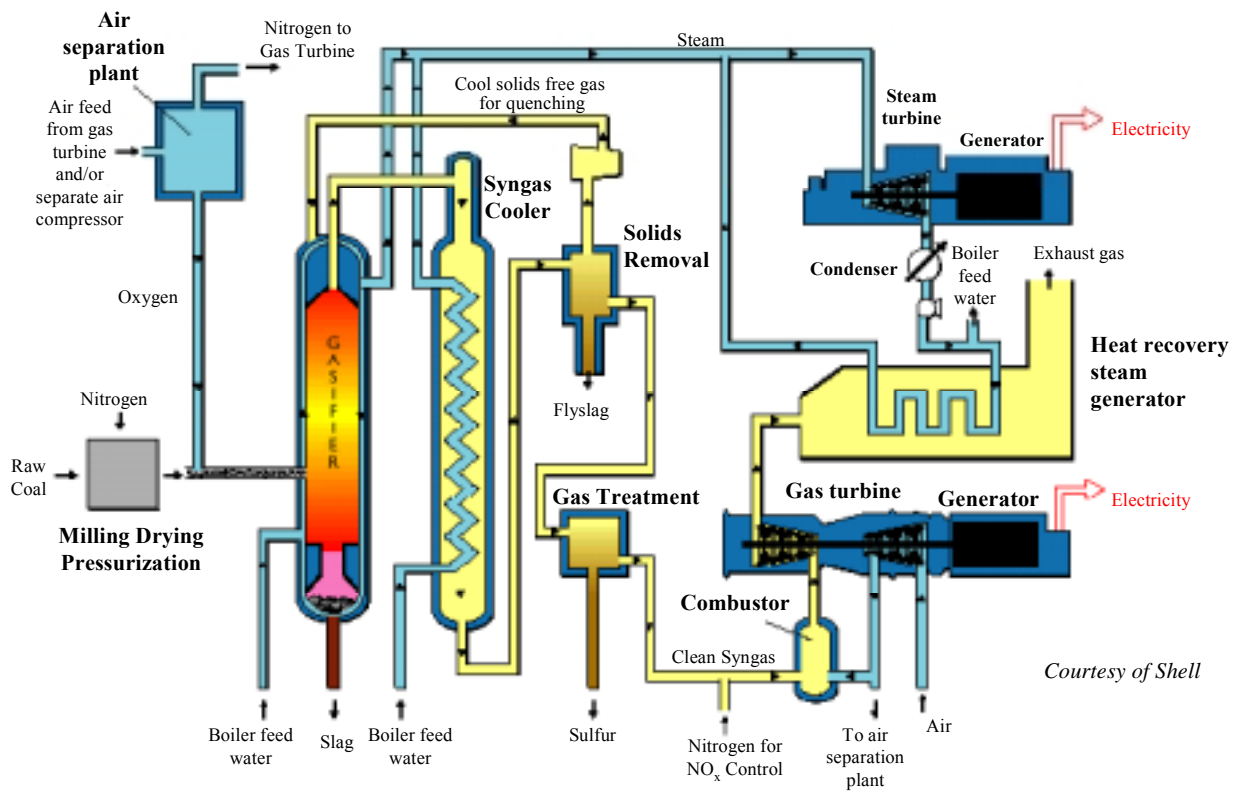
Figure 1. Integrated Gasification Combined Cycle (IGCC)
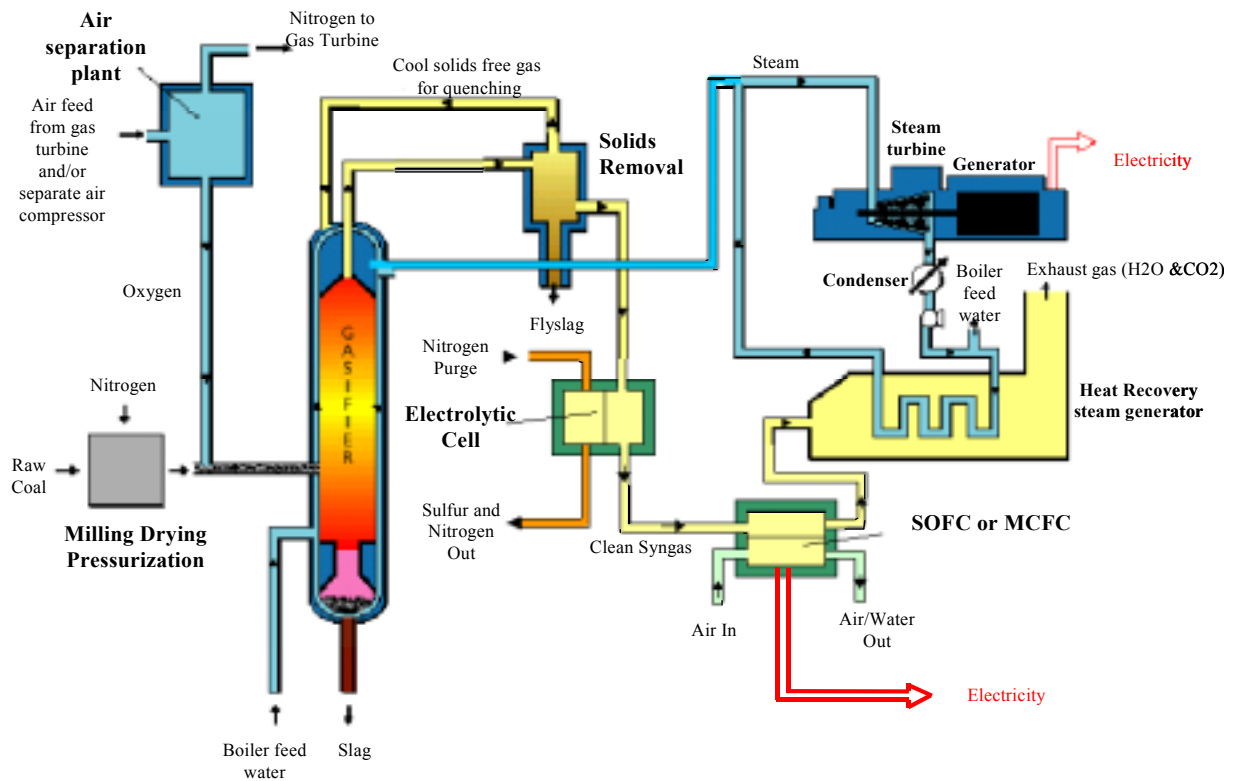
Figure 2. IGCC with Electrochemical Cells
No large heat exchanger is needed after the gasifier,
and sulfur is removed in one step.

1.3 Objectives

In order to expedite the scale up of EMS, the following research objectives were the focus of this study:

1. Inspect the rate-determining step in H_2S removal and determine the maximum H_2S removal rate for a given cell design and operating conditions

2. Test and develop novel cathode materials

3. Make preliminary economic calculations based on full cell performance runs

CHAPTER 2. BACKGROUND

2.1 Theory

2.1.1 Electrochemical Membrane Separation

Selective membrane separation is a well-established unit operation. The basic principle relies on a chemical potential gradient as the driving force for separation of certain molecular species. A pressure or concentration gradient usually provides the necessary driving force for mass transfer across the membrane:

$$\Delta\mu_I = \mu_I - \mu_I' = RT\ln(a_i/a_i') \tag{1}$$

where prime represents the extract side. Typically these processes are not very species selective; therefore, they do not produce high purity products.

If the component to be removed is the strongest Lewis acid (electron acceptor) in a gas mixture, as is the case with the proposed H_2S process, the component can be ionized into an electrolyte. Thus an electrochemical potential gradient can provide the driving force for the charged species across the membrane:

$$\Delta\bar{\mu} = \bar{\mu}_i - \bar{\mu}_i{}' = RT\ln\left(\frac{a_i}{a_i'}\right) + z_iF\Delta\phi \tag{2}$$

which is established by applying an electric potential, $\Delta\phi$. The symbol, F, is Faraday's constant, and z_i is the charge of given species, i. The electrochemical membrane method requires only an external electric potential and no pressure or concentration gradient. Moreover, it can actually overcome an opposing concentration gradient. Compared to pressure-driven membrane separations, electrochemical membrane separation (EMS) can

produce selectivity considerably higher because the applied electric field affects only charged species.

This concept has been successfully applied to a hot gas electrochemical membrane process for the removal of H_2S from process gas streams. Such a process is presented in Figure 3. Its construction resembles that of a molten carbonate fuel cell (MCFC). The process gas passes over the cathode, where the strongest Lewis acid, H_2S, is reduced:

$$H_2S + 2e^- \rightarrow H_2 + S^{2-} \tag{3}$$

A membrane, which contains sulfide ions in a molten state, acts to transport sulfide ions across the cell to the anode, where they are oxidized to elemental sulfur, S_2. An inert sweep gas is used to remove the sulfur vapor, which is condensed downstream:

$$S^{2-} \rightarrow \tfrac{1}{2}S_2 + 2e^- \tag{4}$$
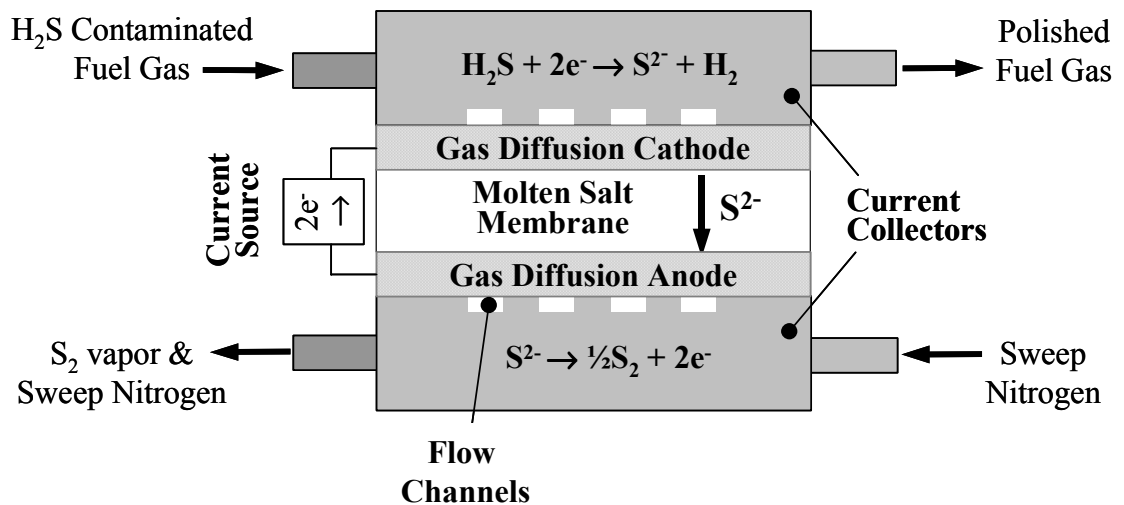
Figure 3. Electrochemical Membrane Removal of H$_2$S

2.1.2 Steps in Removal

At steady state, the overall rate of any process is determined by the slowest step: electrode kinetics; transport away from the electrode; or transport to the electrode. In the proposed electrochemical cell, which involves the use of gas-diffusion electrodes and an electrolyte-saturated membrane, the conversion of H_2S proceeds through a series of distinct steps, which can be modeled by electrochemical equations:

1. gas-phase diffusion of H_2S from the bulk stream to the electrode surface

2. gas-phase diffusion of H_2S in the electrode pores

3. liquid-phase diffusion of H_2S through a thin film of electrolyte coating the electrode pores

4. reduction of H_2S at the cathode-electrolyte interface, resulting in sulfide (S^{2-}) ions

5. migration/diffusion of sulfide ions across the electrolyte-saturated membrane

6. sulfide ion oxidation at the anode-electrolyte interface, resulting in elemental sulfur (S_2)

7. liquid-phase diffusion of sulfur through a thin film of electrolyte coating the electrode pores

8. gas-phase diffusion of sulfur through the electrode pores

9. gas-phase diffusion of sulfur from the electrode surface to the sweep stream

Analysis has shown that the rate-limiting step of H_2S removal will be dictated by the diffusion fluxes in steps 1 and 4. Whichever one is smaller will determine the maximum rate of sulfur removal.

2.1.3 Sulfide Diffusion Limitation across the Membrane

The limiting current density carried by sulfide ions is directly proportional to the maximum H_2S removal flux and can be estimated from the sulfide diffusion rate across the membrane.

$$Molar\_Flux = \frac{i_{diff}}{nF} = D_{S^{2-}-Elec} \frac{\varepsilon \rho_{Elec}}{\tau} \frac{C_{S^{2-}}^{cath}}{x} \tag{5}$$

where n is the number of electrons transferred per mole reacted (2 mol^{-1} in this reaction), ε the porosity of the membrane, τ membrane tortuosity, ρ_{Elec} electrolyte molar density in mol cm^{-3}, x membrane thickness in cm, c_{S2-}^{cath} the molar fraction of sulfide species at the cathode, and $D_{S2-/Elec}$ the diffusivity of sulfide ions in the electrolyte (10^{-5} cm^2 s^{-1})[17]. Equation (5) results from consideration of the diffusive flux of sulfide ions through the membrane. Contribution to this flux by migration is assumed to be negligible due to the presence of supporting electrolyte, alkali carbonate. The low sulfide concentration will result in a small transport number for sulfide compared to carbonate, thus rendering the sulfide migration term negligible compared to its diffusion term. Other key assumptions are that c_{S2-}^{cath} is at the thermodynamic equilibrium percentage for that temperature and that the concentration of sulfide at the anode is zero. The quantity, c_{S2-}^{cath}, is calculated from the equilibrium ratio of Reaction (6), with H_2S concentration being the log-mean bulk concentration of H_2S in the cathode gas.

$$(Li_{0.62}K_{0.38})_2CO_3 + H_2S \rightarrow (Li_{0.62}K_{0.38})_2S + CO_2 + H_2O \tag{6}$$
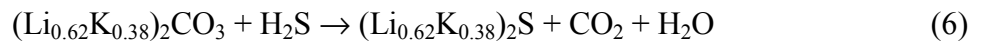
Also, the concentration profiles of carbonate and sulfide across the membrane are assumed to be linear. All parameters in Equation (5) except τ are independently evaluated. For a derivation of Equation (5), please see Appendix D.

2.1.4 Gas Mass Transfer Limitations

Mass transfer of H_2S from the process gas to the electrode-electrolyte interface could also be a rate-limiting factor. The mass transfer coefficient, k_m, can be estimated using Sherwood number correlations based upon rectangular channels in laminar flow regimes.[8,18] For this system, $k_m \sim$ 10-12 cm s^{-1}. The log-mean average offers the most accurate estimate of the average H_2S concentration present. The inlet and outlet mole fractions of H_2S are y_{inlet} and y_{outlet}, and ρ_{fg} is the fuel gas molar density.

$$Flux = \frac{i_L}{nF} = k_m \rho_{fg} \frac{(y_{inlet} - y_{outlet})}{\ln(y_{inlet} / y_{outlet})} \tag{7}$$

The mass transfer coefficient, k_m, can also be estimated directly from experimental data if the flux is actually limited by mass diffusion from the bulk fuel stream to the cathode surface. The term, i_L, is the mass transfer limited current density.

2.1.5 Stoichiometric Limitations

Finally, the stoichiometric limiting current is determined by Faraday's law. For example, if H_2S is the only electroactive species, then the current given below is the minimum needed to remove all inlet H_2S.

$$i_{theo} \cdot A = nF\dot{n}_{H_2S} \approx nF \frac{P\dot{V}}{RT} y_{inlet,H_2S} \tag{8}$$

For instance, if the fuel flow rate is 100 cm^3 min^{-1} and the inlet H$_2$S concentration is 1000 ppm, then the maximum i$_{theo}$ that can be passed by sulfur ions is 1.69 mA cm^{-2} over an electrode area of 7.9 cm^2.

If other reactions occur, then higher currents will have to be applied and the H$_2$S removal current efficiency will decrease. One concern is cracking in the membrane, which could allow H$_2$ to diffuse to the other side. If hydrogen is present at the anode, then the parasitic reaction below will take place.

$$H_2 + CO_3{}^{2-} \rightarrow H_2O + CO_2 + 2e^- \tag{9}$$
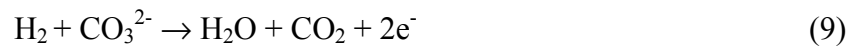
Pressure gradients may also drive Reaction (9) by pushing H$_2$ through the membrane. Electrolyte solidification or excessive evaporation may also result in gas crossover.

2.1.6 Application of Theory

A key assumption in Equations (5), (7), and (8) is that sulfide is the ONLY electroactive species. But because some current is usually lost to CO$_2$ transport, the required applied current is much higher than the currents calculated in these equations. [*] In analysis of the system, the molar fluxes in Equations (5), (7), and (8) are taken to be the H$_2$S removal rate seen in experimentation at the cathode side.

By stepping up the current until the H$_2$S removal rate reaches a maximum, the maximum H$_2$S removal rate at a certain temperature, inlet H$_2$S concentration, and flow rate can be found. From this maximum H$_2$S removal rate, a membrane tortuosity and mass transfer coefficient can be back-calculated from Equations (5) and (7), respectively. Reproducibility of these values under various operating conditions can help one gain insight as to which process is rate limiting. Also, Equations (5), (7), and (8) are derived

[*] Note that this loss of current efficiency results in hydrogen enrichment of the fuel stream, due to the reverse of Reaction (9).

24

under steady-state conditions. The current must be held after each alteration for several hours to achieve steady state and acquire valid, reproducible data points.

2.1.7 Theoretical Potentials

H_2S is readily reduced in hot gas mixtures, even at ppm levels. However, if other reactions occur, higher currents must be applied, and the H_2S removal current efficiency will decrease. When carbon dioxide and water are present in the fuel gas, they may react at the cathode by Reaction (10).

$$CO_2 + H_2O + 2e^- \rightarrow H_2 + CO_3^{2-} \tag{10}$$

The respective ionic flux of each ion through the electrolyte membrane depends on both the relative diffusivity of carbonate and sulfide ions as well as their concentrations.

Preventing oxidation of carbonate at the anode is necessary for truncating its transport through the membrane, the desired anodic reaction being:

$$S^{2-} \rightarrow \frac{1}{2}S_2 + 2e^- \tag{4}$$

This occurs at a standard potential some 700 mV lower than the oxidation of carbonate:

$$CO_3^{2-} \rightarrow CO_2 + \frac{1}{2}O_2 + 2e^- \tag{11}$$

Summing the half-cell reactions (3) and (4) results in this overall, preferred reaction at 650° C:

$$H_2S \rightarrow H_2 + \frac{1}{2}S_2 \qquad E^\circ = -0.239 \text{ V} \tag{12}$$

When the competing half-cell reactions (10) and (11) are summed:

$$H_2O \rightarrow H_2 + \frac{1}{2}O_2 \qquad E^\circ = -1.030 \text{ V} \tag{13}$$

The relative extent of each of these reactions is determined by chemical equilibrium; each will occur at the potential predicted by the Nernst relation:

$$E_{eq} = E^{\circ} - \frac{RT}{nF} \ln \left\{ \frac{a_{S^{2-}_{cathode}} \, P_{H2\,cathode} \, P_{S2\,anode}^{\frac{1}{2}}}{a_{S^{2-}_{anode}} \, P_{H2S_{cathode}}} \right\} \tag{14}$$

$$E_{eq} = E^{\circ} - \frac{RT}{nF} \ln \left\{ \frac{a_{CO_3^{2-}_{cathode}} \, P_{H_2\,cathode} \, P_{CO2_{anode}} \, P_{O2\,anode}^{\frac{1}{2}}}{a_{CO_3^{2-}_{anode}} \, P_{CO2_{cathode}} \, P_{H2O\,cathode}} \right\} \tag{15}$$

The Nernst equation is only strictly true for the special case of equilibrium, as it provides no information on the overall reaction rate. But true equilibrium, as discussed in kinetic theory, is not achieved in an electrochemical cell under load; a better phrase to describe the system is steady state, and the Nernstian relation is applicable here.

In addition to the Nernstian potential, electrochemical systems require additional potential necessary to overcome a series of irreversible losses, which occur due to activation barriers with respect to electron transfer, mass transfer limitations of electroactive species, and internal resistances. The Nernstian potential, activation overpotential (η_{act}), concentration overpotential (η_{conc}), and ohmic polarization (IR_{cell}) terms are summed to give the total cross-cell potential required to induce chemical reaction:

$$E_{cell} = E_{eq} + |\eta_{act}| + |\eta_{conc}| + IR_{cell} \tag{16}$$

2.1.8 Overpotentials

The concentration polarization is the additional voltage required due to mass transport limitations. The concentration polarization at the cathode can be calculated by:

$$\eta_{conc,Cath} = \frac{RT}{nF} \ln\left(\frac{i_L - i}{i_L}\right) \tag{17}$$

where i_L represents the mass transfer current density that is limited by bulk diffusion of H_2S to the cathode surface. This current density, i_L, can be estimated by Equation (7). The concentration overpotential at the anode can be estimated by substituting i_{diff} for i_L. However, because of the competing reaction of CO_2 transport, these calculations are flawed in that they only consider sulfide transport. Once the overpotential resulting from sulfide species transport becomes high enough for carbonate to start reacting at the anode, the individual overpotentials are not easily separated from each other.

Steps 4 and 6 of the H_2S removal system are based on electron transfer. The activation overpotential is the additional voltage required to drive the electrochemical reactions occurring at the electrodes. The expression relating activation overpotential to the flux, or current density, is the Butler-Volmer equation:

$$i = i_o \left\{ \exp\left(\alpha_a \frac{nF}{RT} \eta_{act,An} \right) - \exp\left(-\alpha_c \frac{nF}{RT} \eta_{act,cath} \right) \right\} \tag{18}$$

where i is the current density, i_o is the exchange current density, α_a and α_c are transfer coefficients for the anodic and cathodic processes respectively, R is the universal gas constant, T is the temperature, and η_{act} is the activation overpotential. The term i_o is an important parameter, which is analogous to the rate coefficient in chemical reactions. In

cases of high negative overpotential, the cathodic term dominates, rendering the anodic term negligible. Also at high overpotentials, there are two competing reactions, making it difficult to separate the individual overpotential values. Double layer effects are also a problem since they can affect i_o. From the resulting simplified Butler-Volmer equation, η_{act} can be plotted versus $\ln(i)$ to solve for an apparent or pseudo rate-constant, i_o, that is specific to that system.

2.1.9 H_2 Solubility and Diffusivity in the Electrolyte

Another mechanism that could be responsible for H_2 presence at the anode besides membrane cracking/holes is its potential dissolution into the electrolyte and diffusion across the membrane. Experimental results show that the solubility of H_2 in a Li_2CO_3-K_2CO_3-Na_2CO_3 eutectic melt follows Henry's law and at 600º C and 1 atm is equal to 18×10^{-6} mol cm^{-3}.[19] The diffusivity of H_2 in carbonate melts was determined to be 5.3×10^{-4}, 6.2×10^{-4}, and 6.7×10^{-4} cm^2 s^{-1} at 600, 650 and 700º C, respectively.[20] Assuming that these parameters are applicable to the system used here, H_2 diffusion through the membrane should not be a problem. The low solubility of H_2 implies very low transfer rates via this route. The main contribution to H_2 crossover will be from H_2 bubbling through the membrane caused by either a pressure drop across the cell or simple crossover in regions where the membrane is cracked or depleted of electrolyte.

2.1.10 Carbon Deposition

With the presence of significant amounts of CO and CO_2 in these fuel streams, one concern is carbon deposition by means of the Boudouard reaction:

$$2CO \rightarrow C_{(s)} + CO_2 \qquad\qquad K_{eq(650C)} = 3.18 \qquad\qquad (19)$$

This carbon deposition can clog the porous cathode and shut off diffusion paths for H_2S transfer. By adding water vapor to the stream, this reaction can be minimized. Higher temperature also lowers K_{eq} rather significantly. It should also be noted that a recent study suggests that the Boudouard reaction is extremely unfavorable at transition metal surfaces. It is, instead, a pitting mechanism that causes metal dusting and degradation.[21]

Formation of COS species is also another concern. This can occur by

$$H_2S + CO_2 \leftrightarrow H_2O + COS \qquad K_{eq\ (650\ C)} = 0.026 \qquad (20)$$

$$H_2S + CO \leftrightarrow H_2 + COS \qquad K_{eq(650\ C)} = 0.048 \qquad (21)$$

Once again, the presence of H_2O can inhibit formation of an undesirable product. Weaver showed that COS is removed along with H_2S by the electrochemical membrane system. This removal was attributed to the rapid equilibration between H_2S and COS via Reaction (21).[22]

2.2 Previous Work

2.2.1 Sulfur Removal Calculations

Past studies have revealed that diffusion of sulfur species is the limiting process in this cell, but questions remain whether gas or liquid phase diffusion limit this process. Evaluation of Equations 5 and 7 at different temperatures can help gain insight into which process should be limiting. Using a fuel stream that has a log-mean H_2S concentration of 1000 ppm, the limiting current will be calculated at 600, 650, and 700° C for each process. From Equation (7), the gas phase limited H_2S removal current density would be 27, 28, and 28.5 mA cm^{-2} at each respective temperature. So one can see that temperature does not have a large impact on a system limited by gas phase mass transfer.

Now consider diffusion of sulfide species through the membrane using Equation (5). Assume, as a starting case, that the ratio of membrane porosity to tortuosity is 0.2 and that its thickness is 0.9 mm. The respective sulfide concentrations calculated by the equilibrium of Reaction (6) are 0.033, 0.072, and 0.14 at 600, 650, and 700º C, respectively. Now assuming that the diffusivity of sulfide species remains relatively constant at 10^{-5} cm^2 s^{-1}, the current densities of H_2S removal would be 3.0, 6.5, and 13 mA cm^{-2} at 600, 650, and 700º C, respectively. There is a dramatic increase in removal performance with temperature increase, and these values are much lower than the gas phase H_2S diffusion limitations. These calculations are valuable in predicting the maximum H_2S removal rate achievable, but experimental evidence has not yet been gathered to support the sulfide membrane-diffusion limited theory.

2.2.2 Sulfide Reaction Kinetics

Studies in "free" (molten) electrolyte showed the exchange current, i_o, to be on the order of 100 mA cm^{-2} at 830° C for H_2S reduction.[4] The transfer coefficients were both found to be equal to 0.6. Because they do not sum to 2 as they should, this means that the cathodic and anodic processes are not the opposite of each other. Factors that should be noted from White's study were that it was performed with an initial electrolyte composed of pure sulfide (no carbonate species), the electrodes were graphite, and the temperature was also higher than what looks promising for an EMS industrial setting (kinetic rates will be slightly lower at 650-700° C). However, this work still provides evidence that reaction kinetics will not limit this system.

To calculate the exchange current density, White used transient techniques that allow analysis under real conditions, in which the experiment may have mass transfer

limitations, potentiostat rise-time, double-layer capacitance, and interface resistance. Alternatively, the Butler-Volmer equation can be rearranged to measure i_o experimentally in a full cell run that has sufficiently large cathodic overpotential: $i = i_o \exp(-\alpha_c n f \eta_{act,cath})$.

When mass transfer effects are not present and no chemical reactions impede the overall process, the overpotential measured in experiment, the quantity, $E_{cell} - E_{eq} - IR$, will be equal to the activation overpotential, η_{act}. But in this system, the concentration overpotential is also a factor; therefore, η_{conc} must also be subtracted as seen in Equation (16). A plot of the activation overpotential versus applied current will yield a y-intercept from which the exchange current density can be calculated. For instance, consider a system in which a current density of $i = 12.7$ mA cm^{-2} is applied over 7.9 cm^2. From measurements of concentrations on each side of the cell, $E_{eq} = -0.75$ V at 600° C and the log-mean concentration of H_2S is 1000 ppm. From earlier calculations and Equation (17), $\eta_{conc,Cath} = -0.001$ V, and $\eta_{conc,An} = -0.06$ V. With the IR = -0.3 V, $\eta_{act} = -0.075$ V. Now, by changing i and reiterating this process for a series of data, a plot of i versus η_{act} can be used to find i_o. See Figure 4 for a sample plot that yields $i_o \sim 10$ mA cm^{-2} from noticing that the y-intercept $= \ln(i_o)$. Additionally, the slope can be used to calculate the transfer coefficient, α_c, which is equal to 0.08 here.
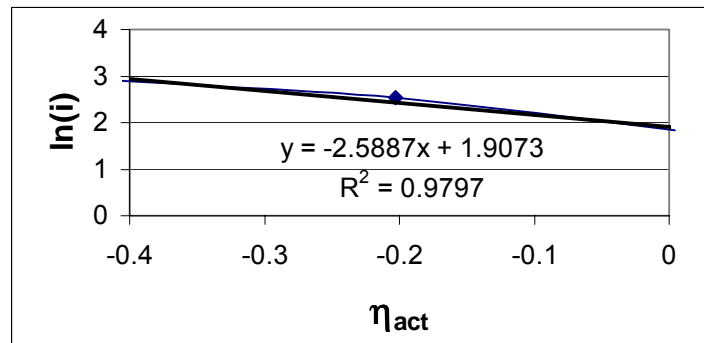
Figure 4. Sample plot of η_{act} vs. ln(i) to solve for i_o

However, the exchange current density acquired this way from real data is only a pseudo rate constant for all combined electrochemical reactions because there are multiple reactions occurring. It is difficult to establish which parts of the potential result from overpotentials and not from the competing reaction of CO_2 transport occurring. Once the competing reaction begins, E_{eq} is then a mixed potential. In this scenario, each overpotential needs to be representative of the contributions of both species being transported or activated. Last of all, there is another overpotential, η_{Rxn}, that is related to other side reactions such as Reaction (6). This other overpotential, η_{Rxn}, is probably what is responsible for the low i_o and α_c values calculated from this data set.

2.2.3 Mechanism of Sulfide Reaction

Concerning the mechanism of reaction, there is consensus that polysulfide catalyzes H_2S reduction via

$$S_2^{2-} + 2e^- \rightarrow 2S^{2-} \tag{22}$$

and is supplied by

$$H_2S + S^{2-} \rightarrow H_2 + S_2^{2-} \tag{23}$$

Cyclic voltammogram data from Banks support this claim.[3] Polysulfide is also an active participate at the anode, being oxidized by

$$S_2^{2-} \rightarrow S_2 + 2e^- \tag{24}$$

and supplied by

$$S_2 + 2S^{2-} \rightarrow 2S_2^{2-} \tag{25}$$

With CO and CO_2 included in the sour stream, exchange current densities were more than doubled,[4] and the H_2S removal rate was also drastically increased.[3] Upon the water-gas shift reaction, the sour stream in each of these studies consisted of roughly 5.8% CO_2,

27.2% CO, 17.8% H_2, 2.2% H_2O, 6500 ppm H_2S, and balance N_2 (as determined

experimentally at 1000 K). Under this gas, H_2S reduction may be catalyzed by the

following reaction scheme at the cathode:

$$CO_2 + H_2O + 2e^- \rightarrow H_2 + CO_3^{2-} \tag{10}$$

$$CO_3^{2-} + H_2S \rightarrow CO_2 + H_2O + S^{2-} \tag{26}$$
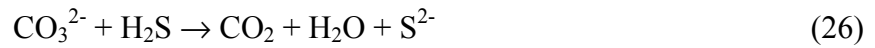
But as the concentrations of CO_2 and H_2O increase and temperature decreases,

thermodynamic equilibrium favors carbonate displacement of sulfide in the electrolyte.

2.2.4 Cathode Materials Selection

Simple sulfides, such as FeS, NiS, CuS, and MoS_2 do not have adequate electrical

conductivity and/or long-term stability because of the low melting points, solubility in the

carbonate electrolyte, or poor reduction tolerance. Nb-doped TiO_2 has good electronic

conductivity, reduction tolerance and H_2S tolerance, but it changes to a non-conductive

phase under the presence of CO_2 and H_2O at high temperature. Mg- and Sr-doped $LaCrO_3$

and $LaGaO_3$ have poor electrical conductivity in the reductive environments although their

chemical stability in H_2S and CO_2 atmosphere is good. Sr-doped $LaCoO_3$ and $SrCo_{1-x}Fe_xO_3$

readily reacts with the sulfide electrolyte and H_2S, resulting in compounds with low melting

points. $Y_{1-x}Ca_xFeO_3$ was reported to have suitable performance in the working environment;

it reacts with H_2S to form FeS, Y_2O_2S and $YFeO_3$, which are stable under the testing

conditions.[23] However, the lifetime of this material is a concern, especially at higher

temperatures.[24] Further experiments are necessary to find out the suitable cathode materials

for the practical application of this H_2S removal cell system.

2.2.5 Cobalt Sulfide Cathode

Under the operating conditions of this process, phase diagrams predict that the pentlandite,Co_9S_8, is stable.[25] Past work has shown that Co_9S_8 is a stable phase under operating conditions, but questions still remain concerning its versatility in operating environment and preparation. Work by Weaver has been promising, reaching an H_2S removal flux of 4.8×10^{-6} mol min^{-1} cm^{-2} at 650º C.[22] His gas composition consisted of 41.0% H_2, 1.6% CO_2, 1.285% H_2S, 5.7% CO, and balance N_2 after water-gas shift reaction. The membrane was composed of $LiAlO_2$ and was 0.18 cm thick. To date, these results have not been duplicated. Cell failure was attributed to gas crossover on account of density changes in the electrolyte upon sulfurization, resulting in membrane cracking.

Smith started with $LiCoO_2$, which was converted to Co_9S_8 in situ.[26] He showed H_2S removal flux as high as 1.9×10^{-6} mol min^{-1} cm^{-2} at a fuel flow of 328 mL min^{-1}. The gas composition was 3.9% H_2, 2.85% CO_2, 0.61% CO, 8.14% H_2O, 2800 ppm H_2S, and balance N_2 at 650º C. The Zircar pre-fabricated membranes used here were reportedly 69% porous and 0.062 cm thick. Failure was attributed to cathode pore flooding after excessive electrolyte had been added.

While these results look promising, another issue is the preparation and optimized structure of this material. During sulfurization, a cobalt compound grows by outward diffusion of cations through the lattice, which is defected as a result of this movement. This phenomenon is capable of doubling the size of the initial pure cobalt sample. While the rate of cation vacancy diffusion is independent of sulfur pressure, non-stoichiometry is a function of sulfur vapor pressure and is still being studied.[27] If a cobalt sulfide cathode is to be prepared in situ, its changes in volume and porosity upon sulfidation

must be taken into account. The dependence of its structure and stoichiometry on H_2S vapor pressure must also be considered.

2.2.6 Metal Oxide Cathodes

A selection of oxide materials were tested for conductivity and stability under sour conditions by Wang.[23] The following perovskite metal oxides were tested: $Y_{0.9}Ca_{0.1}FeO_3$, $La_{0.9}Sr_{0.1}Ga_{0.8}Cr_{0.2}O_3$, $LaCr_{0.9}Ti_{0.1}O_3$, and $SrCo_{0.8}Fe_{0.2}O_3$. Lithiation of the oxides was found to increase conductivity by promoting p-type conduction. Lithium can displace metals at particular lattice sites and introduce holes (or electron vacancies) through which electrons may flow. These samples were tested at 900° C in an atmosphere of 96% H_2 and 4% H_2S. It was determined that lithiated $Y_{0.9}Ca_{0.1}FeO_3$ could be a viable cathode candidate. It was later tested in a full cell run at 650° C under a gas composition of 3.7% CO_2, 25.8% CO, 4.6% H_2O, 65.6% H_2, and about 3000 ppm H_2S. The H_2S removal rate was 1.2×10^{-6} gmol cm^{-2} min^{-1} under an applied current density of 75 mA cm^{-2}.

2.2.7 Cell Housing Passivation

Besides cathode durability, other factors may also detract from the lifetime of the cell such as cell housing deterioration and loss of electrolyte. Macor cell housings have been used in many of the past runs, but this ceramic material is not practical for industrial setting. Stainless steel is a cheap, durable material that can be used as a housing and current collector, but it has other problems. It cannot only be corroded by the sour fuel stream, but it can also react with the electrolyte and the ambient atmosphere. Analysis by Robinson showed electrolyte absorption and reaction with CO_2 and O_2 in the ambient atmosphere. These processes result in electrolyte loss, which can be up to 5 grams

evaporated per day in bench-scale trials.[28]   This also causes a shorting in the cell, so it results in loss of power and current efficiency.

Passivation of the cell housing area that is not in contact with the electrodes is critical for housing preservation while also maintaining a good seal and a specified active electrode area. Aluminum has been applied to the outside of the cell housing to form an insulative alumina barrier at high temperatures.   In contact with the electrolyte, a lithiated alumina film is formed by

$$Al_2O_{3(s)} + Li_2CO_{3(l)} \rightarrow 2LiAlO_{2(s)} + CO_{2(g)} \tag{27}$$
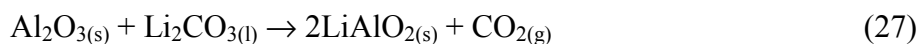
This film insulates the outer cell housing area contacting the membrane and aids in forming a seal with the electrolyte. Al_2O_3 should shield the rest of the cell housing from the ambient environment.

2.2.8 Optimal Electrode Design

The electrodes need not only be chemically stable and conductive, but they must also possess a structure idealized for gas transport to the electrolyte-electrode interface. It must therefore have a porous structure that optimizes this triple phase region. The electrode pores should be wetted with electrolyte but not flooded. From molten carbonate fuel cell studies, optimal electrode characteristics have been estimated to be pore diameter of 3-10 microns and a thickness of 0.8-1 mm.[29]

Another problem is the preservation of this porous structure if a stable sulfide material is formed in situ. For example, pure cobalt has shown a volume increase upon formation of the Co_9S_8 phase.[30] Care must be taken to preserve the optimal porous structure and wetting of the electrode. One way to accomplish this would be to start with

an overly porous and thin electrode, which then sulfurizes to the optimal size and

porosity upon reaction with H_2S and sulfide.

CHAPTER 3. TECHNICAL APPROACH AND EXPERIMENTAL METHODS

3.1 Technical Approach

There are two aims of this research to build upon past work. The first is to examine the maximum H_2S removal rate and gather experimental evidence to support or refute the sulfide membrane diffusion-limited theory. The second is to study cathode materials in full cell operating conditions.

3.1.1 Fundamental Sulfur Transport Limitations

In the primary aspect of this work, the temperature and membrane thickness were varied to analyze fundamental limitations that govern the H_2S removal rate. Past work suggests that transport of sulfur species is the rate-limiting step. It has been proposed that temperature dictates whether bulk, gas phase H_2S diffusion or sulfide membrane diffusion is limiting— where membrane diffusion should be the rate-determining step below a certain temperature. This temperature depends on cell design, as sulfide membrane diffusion rate is sensitive to membrane properties (i.e. thickness, porosity, and tortuosity).

While there is plenty of data that can be fitted to either one limitation or the other, there has not been any direct experimental evidence to support sulfide membrane diffusion limitations. This work is aimed towards determining whether or not sulfide membrane diffusion is a rate-determining step in H_2S removal. If membrane diffusion is the limiting step in sulfur removal, then theory indicates that using a membrane twice as thick should approximately halve the rate of H_2S removal.   Theory also suggests that the removal rate should increase by raising the temperature unless the gas phase transport becomes the rate-determining step. By examining how the maximum H_2S removal rate varies according to temperature, inlet sour gas concentration, and membrane design, insight may be gained

towards understanding sulfur transport limitations and H_2S reaction mechanism(s). Clarifying the rate-limiting step may expedite scale-up of the cell once a suitable cathode material is found. This information may also help determine the best industrial setting for this technology. This general theory may also be applied to other EMS processes.

3.1.2 Analysis of Cathode Materials

In another aspect of this work, cathode candidates will be tested to find suitable candidates for EMS scale-up. Recent studies have shown success with a cobalt sulfide cathode [22,26] as well as lithiated $Y_{0.9}Ca_{0.1}FeO_3$.[23] However, these materials have not been finalized as cathode choices because questions still remain concerning their versatility in operating environments and long-term stability. The aim of this research is to evaluate the stability of possible cathode candidates, considering cobalt sulfide and $Y_{0.9}Ca_{0.1}FeO_3$ as well as other novel oxide materials. Scanning electron microscopy (SEM) and X-ray diffraction (XRD) will be used to examine structural and compositional stability.

3.2.3 Novel Metal Oxide Cathode Materials

To research new materials, the stability and electrical conductivity of oxides with transition metals Mo, V, and Ti will be investigated. Double perovskite oxides Sr_2FeMoO_6, and Sr_2CrMoO_6 have three-dimensional structures and $Mo^{+5}(d^1)$ ions, so they both have high electronic conductivity. For example, Sr_2FeMoO_6 is metallic and its conductivity is 120 S cm^{-1} at 27° C.[31] In reductive atmosphere at high temperatures, these oxides tend to lose some oxygen and reduce the valence of Mo to introduce more electrons into the conduction band, increasing electronic conductivity. All these oxides can be synthesized only in highly reductive atmosphere, such as Argon with 4%~20% H_2 above 1000°C.[32]

Oxides of the form $Gd_2Ti_{2-x}Mo_xO_7$ (x = 0.0-2.0) with pyrochlore type structure have been proposed as anode materials for fuel cells. They have high mixed ionic electronic conductivity and good stability in a wide oxygen partial pressure range. Higher conductivity is present in the lower partial oxygen pressure atmosphere, which is good for application under fuel gas. In addition, $Gd_2Ti_{2-x}Mo_xO_7$ oxides are synthesized in a mixed CO/CO_2 gas, thus showing CO_2 tolerance.[33]

Perovskite oxides with $V^{3+/4+}$ (d^2/d^1) ions are electrically conductive and stable in extremely reductive atmosphere.[34, 35, 36] For example, $SrVO_3$ is synthesized in pure H_2 at 1000^oC, and its conductivity at 800^oC is about 1000 S cm^{-1}.[34] All these oxides are good alternatives as the cathode materials for H_2S removal. Considering the possibility that the electrodes may react with carbonate electrolyte under the operation conditions, the stability and conductivity of these oxides were examined with or without electrolyte while exposed to sour syngas.

3.2.4 Evaluation of Cathode Performance

For promising cathode materials with good electrical conductivity and chemical stability, a bench-scale set-up will be used to evaluate electrode performance in full cell runs. Cathode performance is registered in terms of continued removal flux of sulfur across the membrane and resistance to microstructure degradation. SEM analysis will be used to analyze the morphology and microstructure of the cathode while XRD will be employed to check for change in phase composition and crystal structure. H_2S levels at the cathode and anode will be monitored throughout the run to check for removal performance and gas crossover, respectively. CO_2 concentrations at the anode will also be measured to observe the competing reaction of CO_2 transport.

3.2 Experimental Methods

An experimental set-up was constructed that is capable of performing bench-scale EMS trials. A custom furnace was constructed to fit into a fume hood and house the operating environment for an electrochemical cell. The electrochemical cell itself was then constructed for use in full cell runs. By ramping the current in each run, the maximum H_2S removal rate could be found for that cell at its particular operating conditions. Using one versus two membranes in the full cell runs, it could be determined whether or not H_2S removal was limited by sulfide diffusion across the membrane.

3.2.1 Cell Components

The electrolytic cell has five basic components as shown in Figure 5: cell housing, an inert ceramic membrane, a molten electrolyte, an anode, and a cathode. The cell housing provides flow channels for the fuel and purge streams and may also act as a current collector to which lead wires can be attached.
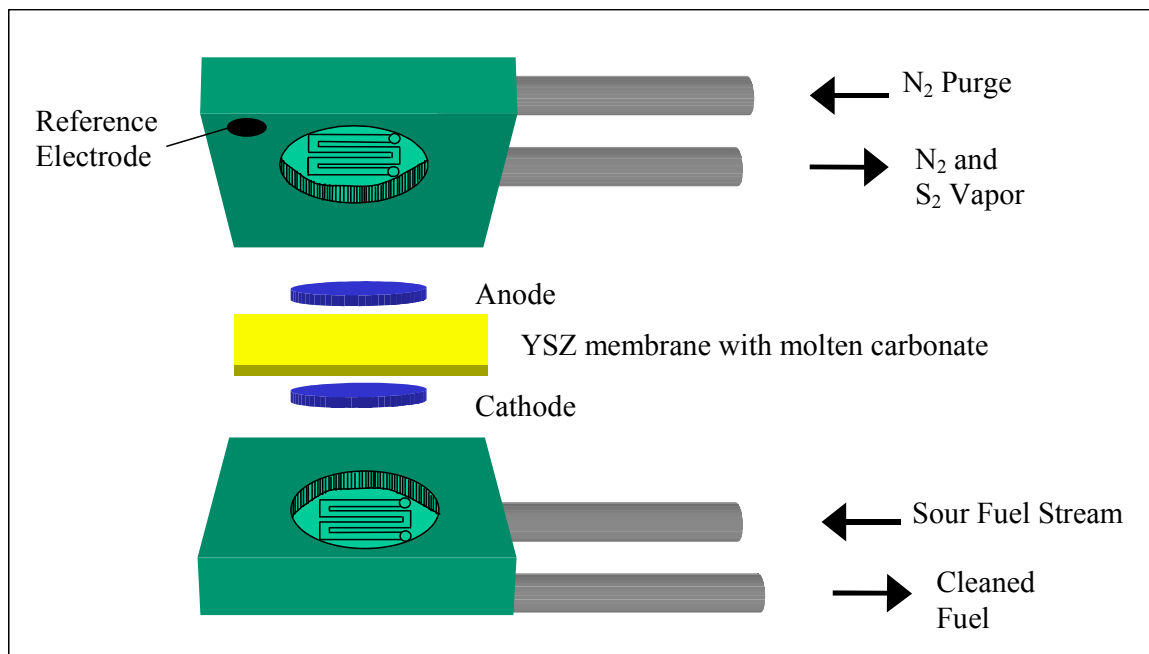
Figure 5. Bench-scale design of electrolytic cell

The inert, porous ceramic membrane separates the purge and fuel streams while holding molten electrolyte, which aids in forming a wet seal with the cell housing. Yittria-stabilized zirconia (YSZ) was the chosen membrane material because of its resistance to high bubble pressure as well as inertness and stability in molten carbonate and molten sulfide. Zircar, Inc. supplied the pre-rigidized, woven membrane.

The electrolyte must melt well below the operating temperature, allow sulfide species to form, and be stable and ionically conductive in the operating environment. The molten carbonate fuel cell (MCFC) electrolyte, $(Li_{0.62}K_{0.38})CO_3$, was chosen for this work as it satisfies these criteria.

The anode material, lithiated NiO, was used for its stability under the anode side operating conditions, as shown by Ingram and Janz.[37] It has done quite well in most runs

by maintaining its porous structure and composition in the oxidizing environment. However, if it is exposed to over 60 ppm H_2S, it converts to Ni_3S_2.

The cathode material must mirror the performance of the anode in a reducing, sour environment. Research has focused on finding a material that can withstand the corrosive reducing environment under sour hot-gas. After testing many pure metals and metal sulfide compounds, metal oxide compounds with high conductivity at temperatures above 600° C are now being studied.

3.2.2 Equipment

A custom furnace, shown in Figure 6, was built to provide the operating environment for the cell. The furnace utilized an Omega temperature controller with a solid state relay. Rotameters were used to control the gas flow rates, and mass flow meters were used to verify and monitor flow rates. A 200 mL bubbler, filled with 1.0 N sulfuric acid solution and coiled by heating tape, was used to hydrate the fuel stream before entering the furnace.
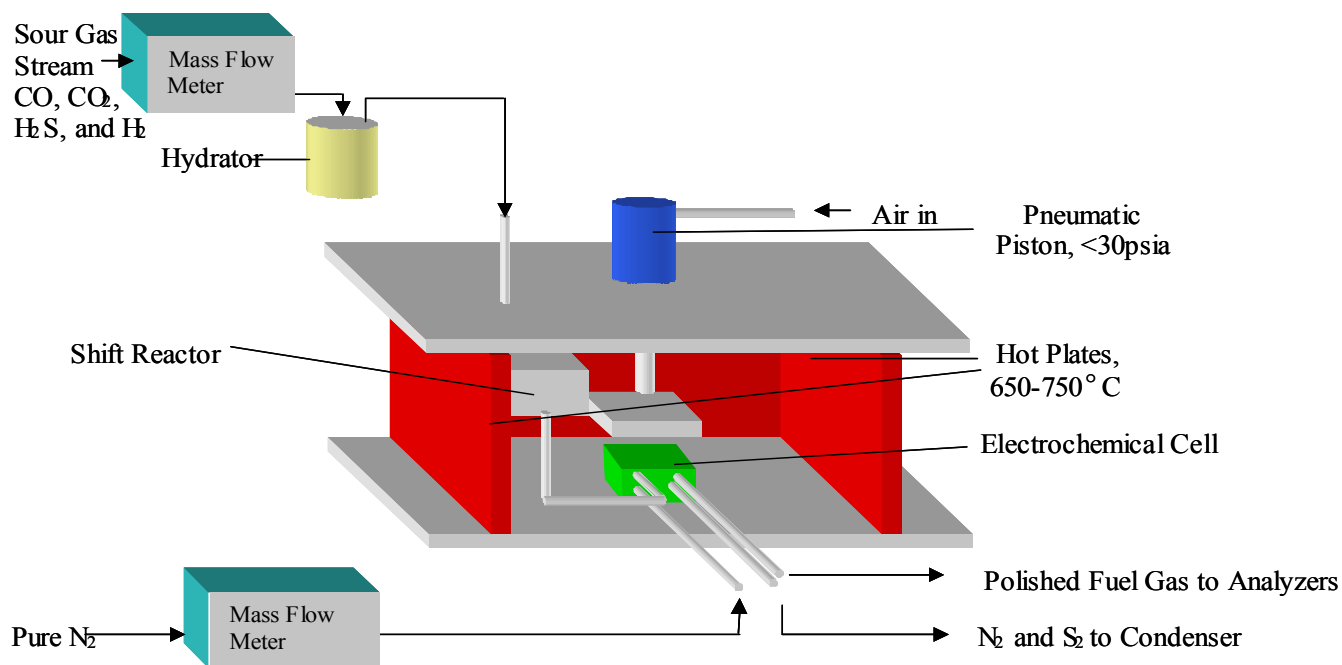
Figure 6. Schematic of Furnace Set-up

An EG & G 273A potentiostat/galvanostat was used to apply a steady current to the cell. Multimeters were connected in parallel to monitor the cathode-reference and anode-reference potentials. Multimeters were also connected in parallel to the cell to monitor voltages between each electrode and the reference. A flame-photometric gas chromatograph (GC) was used to measure H_2S concentration. The GC was a Perkin-Elmer Auto System XL. To measure the anode side CO_2 levels, an infrared detector was used; it was a Model PC04 purchased from CEA Instruments. Cathode microstructure and cracking in the ceramic membrane were examined with a Hitachi S-800 scanning electron microscope. X-ray diffraction was used to determine the bulk crystal structure and phase composition of electrode materials before and after a run using a Philips PW 1800 XRD with CuK_α radiation.

44

For the stability runs, the same custom furnace and bubbler system was used to provide the operating environment. Each powder sample was put in an alumina boat, and
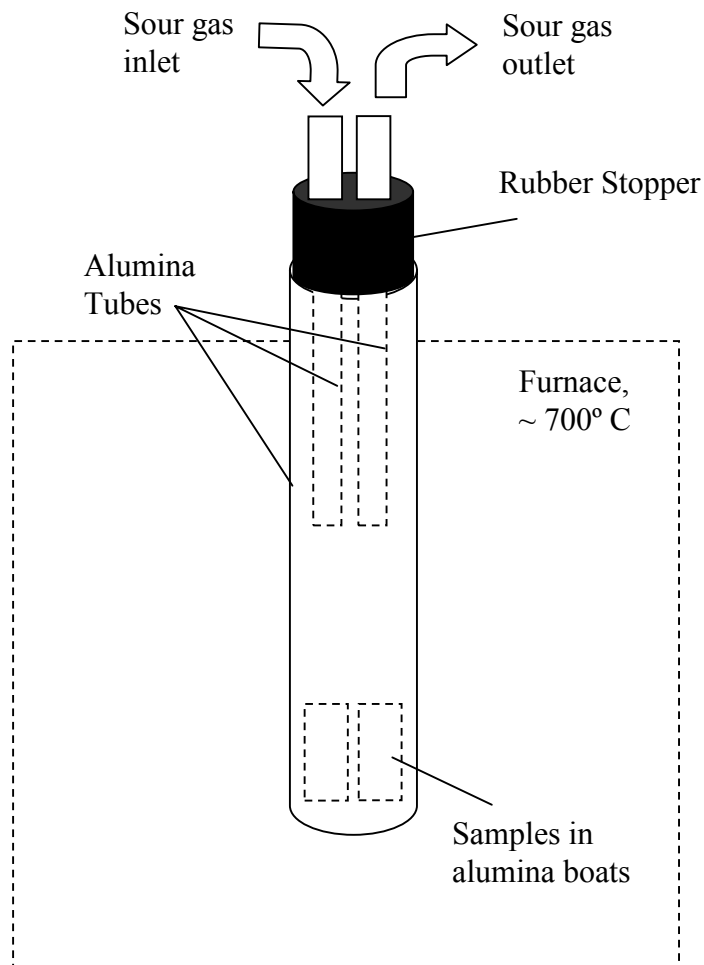
Figure 7. Diagram of stability run configuration

up to four of these boats were tested at a time. The samples were placed in a 1" diameter alumina tube, which was sealed at the top with a rubber stopper—see Figure 7. Inlet and outlet gas tubes were poked through the rubber stopper, and vacuum grease was applied over all seals to prevent leakage. A good seal was verified by monitoring the outlet gas flow with a bubble meter.

3.2.3 Electrode Fabrication

Nickel mesh sheets with 80% porosity were provided by Fuel Cell Energy, Inc. After being cut into 7.9 cm^2 disks, they were heated in a furnace at 600-800° C for at least 4 hours to convert the nickel into nickel oxide. The disk was soaked in 4 M LiOH at room temperature, air dried, and then sanded so that it would fit snugly into the cell housing without protruding into the membrane. This was the anode material for each run.

For the lithiated nickel cathode, the same nickel disks used for the anode were sanded to prevent protrusion into the membrane upon sulfidation. The 7.9 cm^2 disk was soaked in a solution of 4 M LiOH to lithiate the electrode, and, during heat-up, it was purged with nitrogen before fuel gas exposure to help prevent conversion to nickel-oxide.

Metal sulfide electrodes were fabricated using dry-pressing techniques. For example, 1.5 grams of CoS_2 was added to 0.2 g of binder. A 7.9 cm^2 disk was then pressed by a 3-cm pneumatic die at 4000 psi and sintered in air at 450˚ C for 3 hours and then at 615˚ C for 3 more hours. Cooling to room temperature took place at a rate of 2°C min^{-1}. The CoS_2 electrode was converted to Co_9S_8 and Co_4S_3 in situ under sour fuel gas.

For the $Y_{(0.9)}Ca_{(0.1)}FeO_3$ cathode, a combustion synthesis was used. Metal nitrates $(Y(NO_3)6H_2O$, $Ca(NO_3)_2$, and $Fe(NO_3)_39H_2O)$ and glycine were used to prepare the precursor solution for the combustion synthesis of $Y_{0.9}Ca_{0.1}FeO_3$. Glycine was added in solid form. The glycine-to-nitrate ratio in the precursor solution was set to be 0.60. A stoichiometric mixture of oxidant and fuel might be defined by

$$(9/x)\ M(NO_3)_x + 5NH_2CH_2COOH \rightarrow 10CO_2 + 7N_2 + 25/2H_2O + 9/xMO_{x/2} \qquad (28)$$

where x = 2.45 for the combination of metal nitrates necessary to prepare a product consisting of a mixture of iron oxide, yttrium oxide and calcium oxide or other phases

having the same average metal oxidation state as in the precursor. A stoichiometric

oxidant/fuel mixture would thus contain 0.56 glycine molecules per nitrate ion.

Combustion of the metal nitrate/glycine solutions was performed in glass beakers on an

infrared hotplate, with typically 10 ml of the precursor solution (0.2 mol with respect to

iron) burned at a time. The precursors were concentrated by heating until excess free

water was evaporated, at which point spontaneous ignition occurred and resulted in black

ash. The ash was then calcined at $800^{\circ}C$ for 2h to get $Y_{0.9}Ca_{0.1}FeO_{3-\delta}$. X-ray diffraction

analysis showed that the powder had orthorhombic structure. Isothermal

adsorption/desorption investigation showed that the specific surface area of the powder

was 143 m^2 g^{-1}, about seven times higher than that for the powder prepared by solid-state

reaction (19 m^2 g^{-1}). A 3-cm circular die was used for one gram at 7000 psi. PVA was

added as binder and starch as pore former. The cathode was sintered at $1000^{\circ}C$ for 2

hours before using. The porosity of the cathode was 43% as measured by the standard

Archimedes method.

The electrode materials Sr_2FeMoO_6, Sr_2CrMoO_6, $La_{1-x}Sr_xVO_3$ (x=0.3 and 1.0), and

$Gd_2Ti_{2-x}Mo_xO_7$ (x=1.0 and 1.4) were synthesized with a solid state reaction method. The

precursors are $SrCO_3$ (Aldrich, 98%), Gd_2O_3(Alfa, 99.9%), Fe_2O_3(Aldrich, 99%),

Cr_2O_3(Aldrich, 98%), MoO_3(Aldrich, 99.5%), TiO_2(Aldrich, 99.9%) and V_2O_5(Aldrich,

99.6%). Stoichiometric amounts of precursors were mixed thoroughly, pressed into pellets,

and then heated in 4% H_2/Ar gas at $1150^{\circ}C$ for 16 hours. The pellets were ground, pressed

into pellets, and heated for another 16 hours. $La_{1-x}Sr_xVO_3$ (x=0.3,and 1.0) was synthesized in

pure H_2 gas at $1000^{\circ}C$ for 6 hours. XRD was used to check if the expected oxides were

formed. For the stability tests, the oxide powders were mixed with the electrolyte ($Li_{0.62}$,

$K_{0.38})_2CO_3$ in the volume ratio of 1:1 and then exposed to the syngas with 0.3% H_2S (40% H_2, 30% CO_2, 30% CO) or 2.2% H_2S (60% H_2, 15%CO_2, 15% CO and 8% of H_2O) at 700° C, 750° C, or 800° C for at least 40 hours. Upon exposure to H_2S, the carbonate electrolyte becomes partially sulfide. The phase composition of each the sample was checked by XRD.

3.2.4 Conductivity Samples

Rectangular bars cut from pressed pellets were used to measure the conductivity with a SI 1255 impedance analyzer in the frequency range of 100 Hz – 5 MHz. Pt wires were connected to the end of the sample bars by Pt paste as the electrodes. The conductivity measurement was run in syngas with 0.3% H_2S or in Ar with 4% H_2. SEM (Hitachi S-800) was used to check the morphologies of the sample powders.

3.3.3 Cell Housing Fabrication and Passivation

Cell housings were fabricated from stainless steel 304 blocks (2"x 2"x 0.75"). A 1 mm deep circular indention was cut for the electrode cavity. A rectangular flow channel was cut into this indention for gas to flow across the electrode. Cell dimensions are depicted in Figure 8. Metal tubing extended from the cell housing to outside of the furnace to make gas flow and circuit connections. Finally, a quarter-inch diameter hole was drilled in an upper corner of the cell housing to be placed on top in order to provide access for a reference electrode to the membrane. The reference gas composition was 15% CO_2, 3% O_2, and balance N_2, and either a gold or platinum wire touching a corner of the membrane was used as a current collector.

In an attempt to avoid corrosion of the steel cell housing, a thin layer of alumina was layered on its surface, which contacts the membrane but not the electrode. A solution of aluminum hydroxide was applied to the clean surface of the cell housing and then heated (to about 100º C for 2-3 hours) to leave behind a thin alumina layer. The rest of the cell housing sides that are exposed to air were also painted with the aluminum hydroxide solution to prevent reaction with the ambient air. For some runs, an alumina layer was sputtered onto the surface of the cell. No difference in passivation performance was discernable between each method.

1mm deep layer taken off in 3.2 cm diameter circle centered on block

Hole, ¼ " Diameter, about ¼ " in from each side

Gas flow through channel ~ 0.355 cm deep and 0.355 cm wide

0.7 "

0.38"

0.85"

0.85"

0.38"

0.38"

0.7 "

Blow-up of gas flow channel
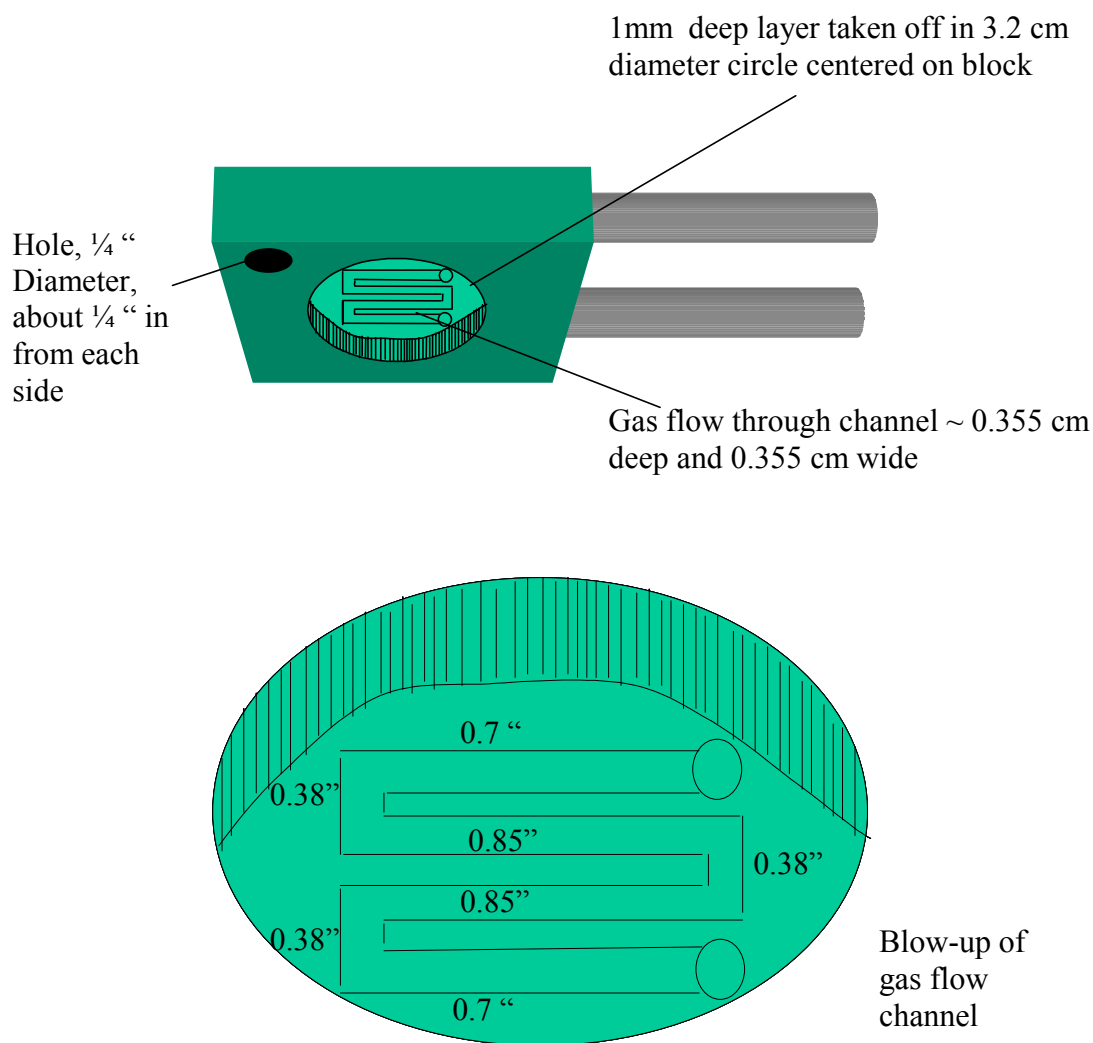
Figure 8. Schematics of cell housing dimensions

3.2.5 Assembly of Cell Housing, Electrodes, Membrane, and Electrolyte

Before heat-up, the cell was assembled as shown in Figure 5. The cell was heated at a rate of 100ºC hr^{-1}, and N$_2$ was supplied to the cathode side to prevent oxidation if needed. A piston, applying 5-15 psi, was used to compress the materials together after the electrolyte melted at 490˚ C. At this point, clean fuel gas was supplied to the cathode side of the cell, and the N$_2$ purge was switched to the anodic side. Flow rates in and out

of the cell were checked to verify that there was a good seal between the membrane and cell housings.

After verifying CO_2 transport, a synthetic, sour gas mixture of 36.56% CO, 24.65% CO_2, 38.74% H_2, and 489-2541 ppm H_2S was fed into the system. After passing through a hydrator at 60˚ C and a shift reactor with Girdler, CCl and Houdry catalysts, the gas then entered the electrolytic cell. The hydrator was used to mimic wet gas streams and to prevent carbon deposition in the reactor via the Boudouard reaction. The water vapor content leaving the hydrator was calculated by using Raoult's law to estimate the water vapor present in the fuel stream before being heated to operating temperature.

The presence of steam hampers the formation of CO, thus minimizing carbon deposition. Entering the cell, the gas inlet had a composition of 34.14% CO, 22.16% CO_2, 35.13% H_2, 8.51% H_2O and 450-2500 ppm H_2S at 600˚ C due to the gas-water shift reaction:

$$CO_2 + H_2 \leftrightarrow H_2O + CO \qquad K_{eq(600\ C)} =\ 0.373 \qquad (29)$$

About two to four days were allotted for the system to reach steady state—at which point the outlet H_2S concentration reached the inlet concentration. During this period, the cathode material changed from an oxide to a sulfide compound (if favored), and the electrolyte sulfide/carbonate ratio attained equilibrium. Either no current or very little current (1-5 mA) was applied over this equilibration period. Applying a small current helped ensure that the cathode material was not being oxidized by the low oxygen partial pressure ($\sim 10^{-20}$ atm).

3.2.6 Analytical Techniques

Cells were run at open circuit until the outlet H_2S level reached a magnitude equivalent to the inlet. At this point, the cell was operated galvanostatically to initiate electrochemical transfer. Ohmic resistance was estimated using the current-interrupt method with a storage oscilloscope. Voltages and H_2S concentrations were recorded over the course of each run.

H_2S levels were measured using a flame-photometric GC. Gas samples of 60 μl were injected into the column (chemsorb 102). The temperature of the column was 120° C, and the injection temperature was 250° C. Samples of known concentration were used to calibrate the column, which is accurate to within 10% at concentrations above 40 ppm. Cleaning the syringe with ethanol between samples produced the most consistent measurements.

Infrared spectroscopy was used to monitor the CO_2 levels leaving the anode side. The data were used to verify continued electrochemical activity because CO_2 transport is a side reaction that can be monitored according to Faraday's law. Monitoring CO_2 percentage at the cathode offers little insight because the shift reaction leaves the CO_2 concentration virtually unchanged. This detector could also detect H_2/H_2S crossover that may be present at the anode—though not quantitatively.

3.2.7 Cathode Material Stability Test

To expedite the search for possible cathode materials, stability tests were used to characterize chemical stability and conductivity under process conditions. Samples of potential cathode materials were exposed to sour fuel gas at 700-750° C for 2-3 days. In some cases, electrolyte was also added to the sample, and the electrolyte was washed

away in a water bath after the run was over. XRD analysis was used to determine whether or not each sample had changed phase and/or composition. The electrical conductivities of the materials were estimated under operating conditions (i.e. sour gas at ~700° C) using a pressed pellet of the material.

CHAPTER 4. RESULTS

The results section is divided into two parts. The first part describes the full cell operation and performance, and the second part discusses the stability studies carried out to find promising cathode candidates.

4.1 Full Cell Runs

4.1.1 CO_2 Transport

Clean fuel gas was tested first to verify proper functioning of the cell before exposure to H_2S. In a process reverse to that of a standard MCFC, current is applied to transport CO_2 across the membrane via the reactions:

$$\text{Cathode: } CO_2 + H_2O + 2e^- \rightarrow H_2 + CO_3^{2-} \tag{12}$$

$$\text{Anode: } CO_3^{2-} \rightarrow \tfrac{1}{2} O_2 + CO_2 + 2e^- \tag{15}$$
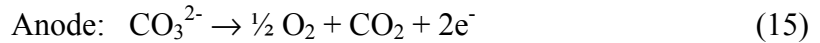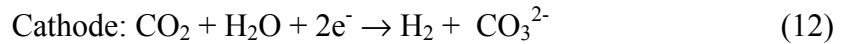
The results in Figure 9 have good stoichiometric agreement with Faraday's law. As the current is stepped upward, more CO_2 is proportionally transported across the membrane. Because a majority of the current went towards this reaction even when gas was sour, the CO_2 level at the anode was monitored to verify continued electrolytic activity. If the removal was not near stoichiometric, then it was known that the cell was not functioning properly.
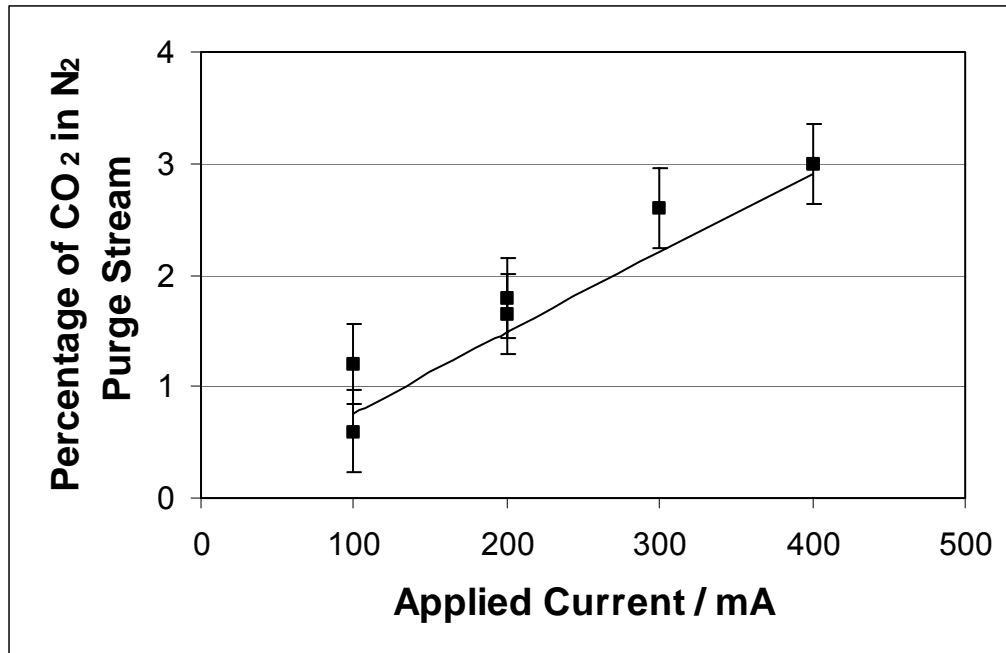
Figure 9. CO$_2$ transport data versus the theoretical percentage of CO$_2$ at the anode calculated by Faraday's law.

4.1.2 H$_2$S Removal

Following the CO$_2$ transport verification, H$_2$S transport was investigated at a given operating temperature and various inlet H$_2$S levels. In Figure 10, H$_2$S removal rate depends linearly upon log-mean average H$_2$S concentration in the sour gas stream. All of the data are taken from steady-state points at which the current had been ramped to approach the maximum achievable H$_2$S removal rate. The applied currents used to acquire this data are not shown here for each data point, but each applied current is higher than the theoretical current needed to remove only sulfur because of the interference of side reactions due to CO$_2$ transport and possible H$_2$ crossover.
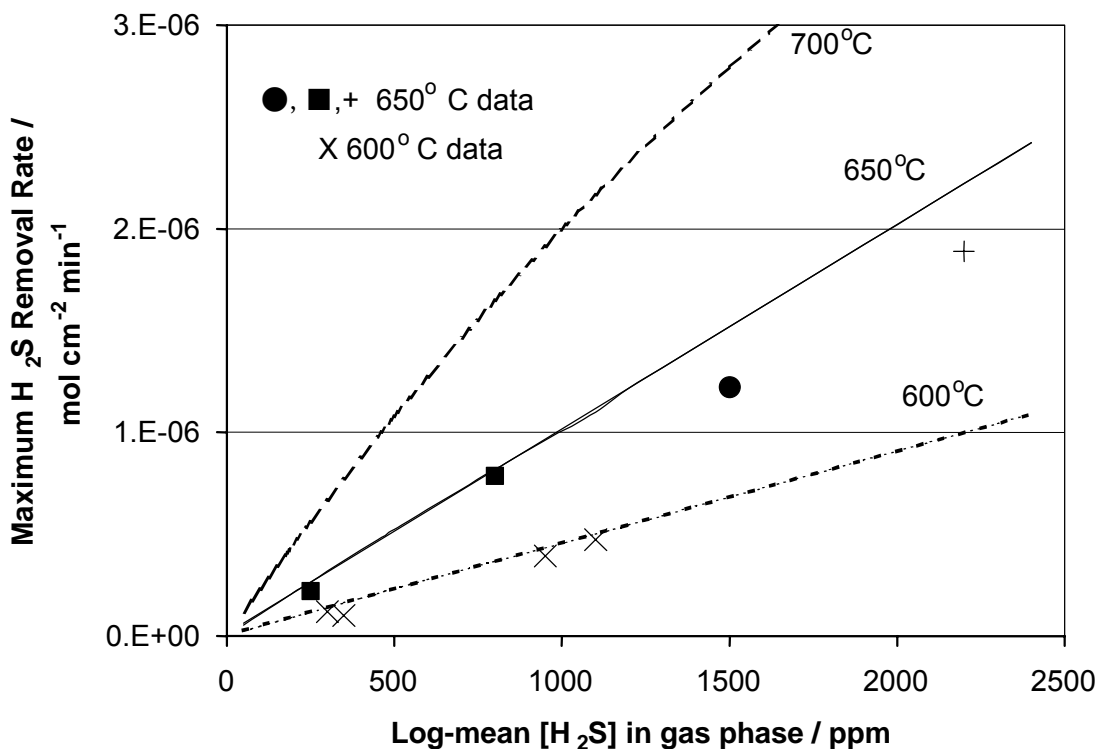
Figure 10. **Effect of Temperature on H₂S Removal Rate as a Function of Log-mean [H₂S].**

Theoretical plots based upon: $x \sim 0.9$ mm, $A = 7.9$ cm^2, and $\tau = 3.8$.

■ : $LiY_{(0.9)}Ca_{(0.1)}FeO_3$ cathode & pre-rigidized YSZ membrane (0.9 mm), at 650°C; 500-1000 ppm H₂S inlet at 80 mL min^{-1}

● : $LiY_{(0.9)}Ca_{(0.1)}FeO_3$ cathode & pre-rigidized YSZ membrane (0.9 mm) at 650°; 3000 ppm H₂S inlet at 100 mL min^{-1}, [23]

＋ : $LiCoO_2$ cathode & pre-rigidized YSZ membrane (0.6 mm) at 650°C; 3400 ppm H₂S inlet at 100 mL min^{-1}, [26]

X : $LiY_{(0.9)}Ca_{(0.1)}FeO_3$ cathode & pre-rigidized YSZ membrane (0.9 mm) at 600°C; 1300 ppm H₂S inlet at 75 mL min^{-1}

Comparisons of various data from this and previous studies are shown in Figure 10.

In accordance with theory, data taken from 650° C show higher removal capabilities than

those from 600° C. Indeed, higher temperature has only been detrimental to performance

when it has led to thermal breakdown of one or more of the cell components.

4.1.3 H$_2$S Removal—Effect of Membrane Thickness

By comparing data that vary only by membrane thickness, removal data can be compared to determine whether or not diffusion across the membrane is rate-limiting. The data in Figure 11 indicate that a membrane half as thick enables about double the removal performance under the given operating conditions.
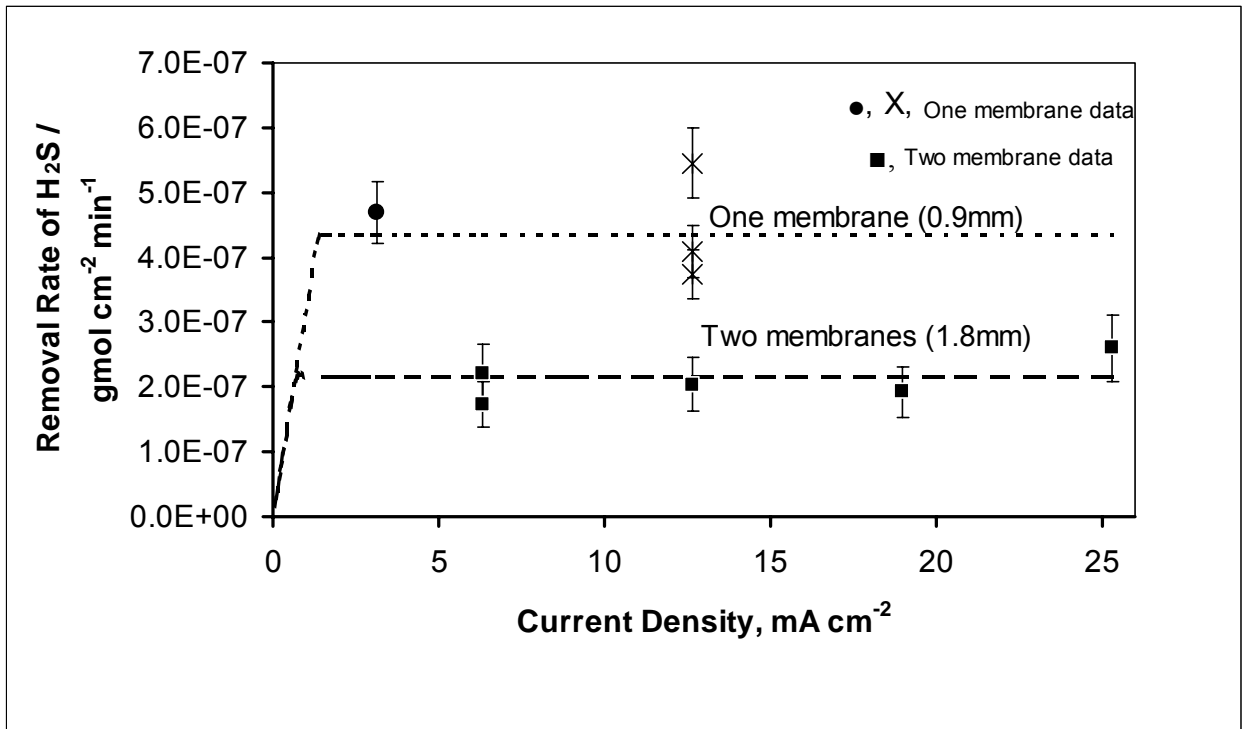
Figure 11: Effect of Membrane Thickness at 600° C.

Data of two-membrane system vs. one-membrane system.

Inlet [H$_2$S] = 1200 ppm +/- 50.

Fuel gas flow rate was maintained at 200 mL min^{-1}.

Diffusion-limited plots were calculated using a tortuosity value of 3.8.

■ : nickel cathode. ● : CoS$_2$ cathode. X: LiY$_{0.9}$Ca$_{0.1}$FeO$_3$ cathode.

Data taken at 650°C add further support that membrane sulfide diffusion is the rate-limiting step for H$_2$S removal (see Figure 12). This agrees with the data taken at 600°C.

The next step was to test the system at 700° C with one versus two membranes to see whether sulfide diffusion is still limiting and to obtain higher removal fluxes (as seen in Figure 10). The $La_{0.7}Sr_{0.3}VO_3$ and Gd_2MoTiO_7 cathodes were employed to gather this data as they performed most successfully in the high temperature stability runs. Unfortunately, each of these runs suffered from gas crossover before removal performance could be acquired. Therefore, these runs were only used for cathode stability analysis.
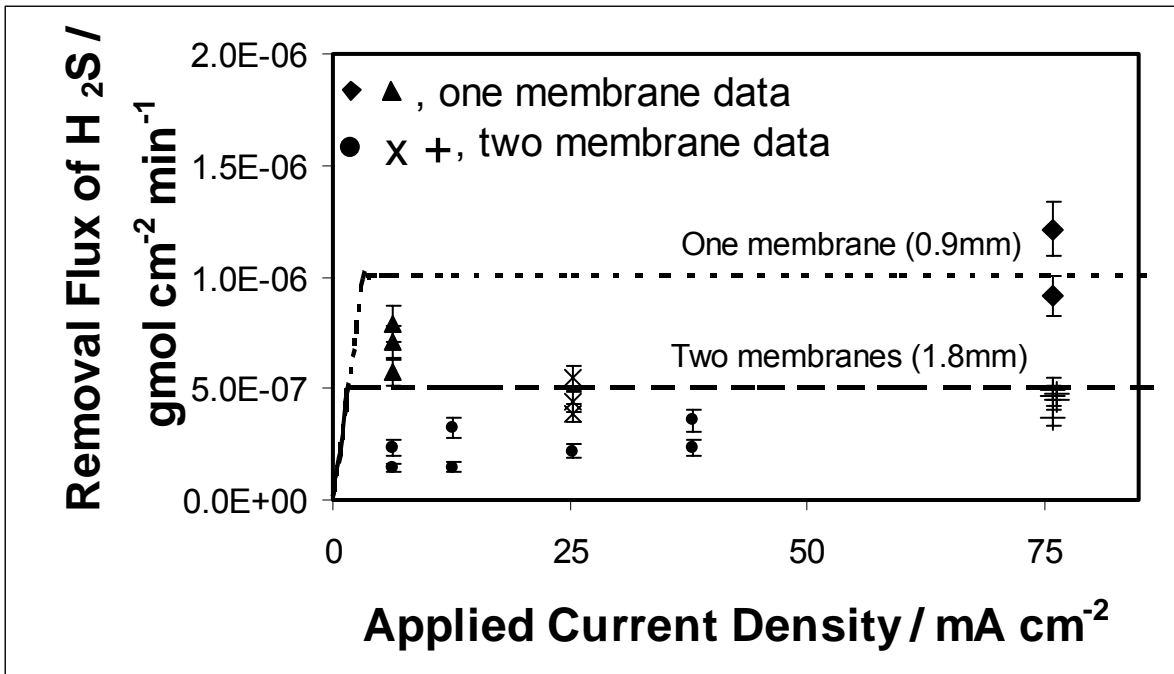
Figure 12. Effect of Membrane Thickness at 650˚ C
     Data of two-membrane system vs. one-membrane system.
     Inlet $[H_2S] = 1200$ ppm +/- 50.
     Fuel gas flow rate was maintained at 200 mL min^{-1}.
     Diffusion-limited plots were calculated using a tortuosity value of 3.8.

   ▲, X, ◆[11], & ● : $LiY_{0.9}Ca_{0.1}FeO_3$ cathode. ＋ : Gd_2TiMoO_7 cathode.

4.1.4 CO$_2$ Purge Stream

For inhibiting CO$_2$ transport, it makes sense to flow CO$_2$ past the anode. This has the effect of raising the potential required to oxidize carbonate at the anode. In run 6, a purge stream of 60% CO$_2$/bal. N$_2$ was used. It was observed that the resulting potential was higher than in runs that used a pure N$_2$ purge stream, but the maximum removal rate appeared to be reached at a slightly lower current density. This makes sense because the competing reaction will be inhibited unless it is forced by lack of sulfide at the anode surface. Because this system was operated galvanostatically, a certain amount of current must flow through the cell. When the current is above the membrane diffusion limitations of sulfide removal, the excess current must go towards CO$_2$ transport, even though it may require more power to do this. This results in forced carbonate oxidation at the anode when sulfide is not present in sufficient quantities.

For potentiostatic operation, excess CO$_2$ at the anode may aid in conserving power and increasing current efficiency. However, the flux of sulfide removal will not be increased because it is inherently limited by diffusion limitations through the membrane and in the bulk gas stream. Also, there must be careful selection of an operating voltage/current to maximize sulfide transport and minimize CO$_2$ transport.

4.1.5 Dynamics of Cell Operation

Any of the following can happen during operation, causing an increase in H$_2$S removal flux: increase in fuel flow rate, increase in temperature, or an increase in H$_2$S concentration. Slight shifts in these variables during the long cell trials make steady state difficult to obtain. This must be a carefully controlled process to be optimally run. In some runs, however, these increases did occur and a higher removal rate was seen. For

data to be considered at steady state, all variables were closely monitored for 3 hours to ensure no drastic changes that could influence the H_2S removal rate.

4.1.6 Pre-mixing Sulfide Electrolyte

Several attempts were made to pre-mix the carbonate/sulfide ratio that would be in equilibrium with a cell operating at 700ºC. Unfortunately, none of these trials were successful. The K_2S in the lab consists of many impurities, so Li_2S was used to add all sulfide to the mixture. Li_2CO_3 and K_2CO_3 were then added to form a ternary mixture that should melt according to thermodynamic plots.[38] This procedure resulted in a poorly mixed electrolyte that did not melt at operating temperatures. Heating over 1100º C to ensure melting and adequate mixing resulted in a solid electrolyte that was very difficult to pulverize into a powder form. Therefore, to ensure electrolyte melting (at least initially before it turned to sulfide), the $(Li_{0.62}K_{0.38})_2CO_3$ eutectic was used instead.

4.2 Cathode Stability Analysis

4.2.1 Stability Results in Full Cell Runs for Previously Used Cathode Materials

The results with the cobalt sulfide electrode were discouraging because the electrode melted during operation. Post-mortem XRD analysis showed that the CoS_2 electrode, which had been sintered at 600˚ C for 4 hours to obtain a mixed Co_3S_4/Co_4S_3 phase, had transformed into a mixture of Co_9S_8, which melts at 835º C, and Co_4S_3, which melts around 1100º C (see Figure 13 for XRD analysis). This data conflicts with several of Weaver's runs, in which cobalt sulfide was successful. He began with pure cobalt and formed the cobalt sulfide cathode in situ, but, in the most successful runs, a low CO_2 level was present in the fuel stream. The CO_2 concentration in this study was much

higher than that used by Weaver and Smith; hence, Co_9S_8 may not be stable under this gas phase.
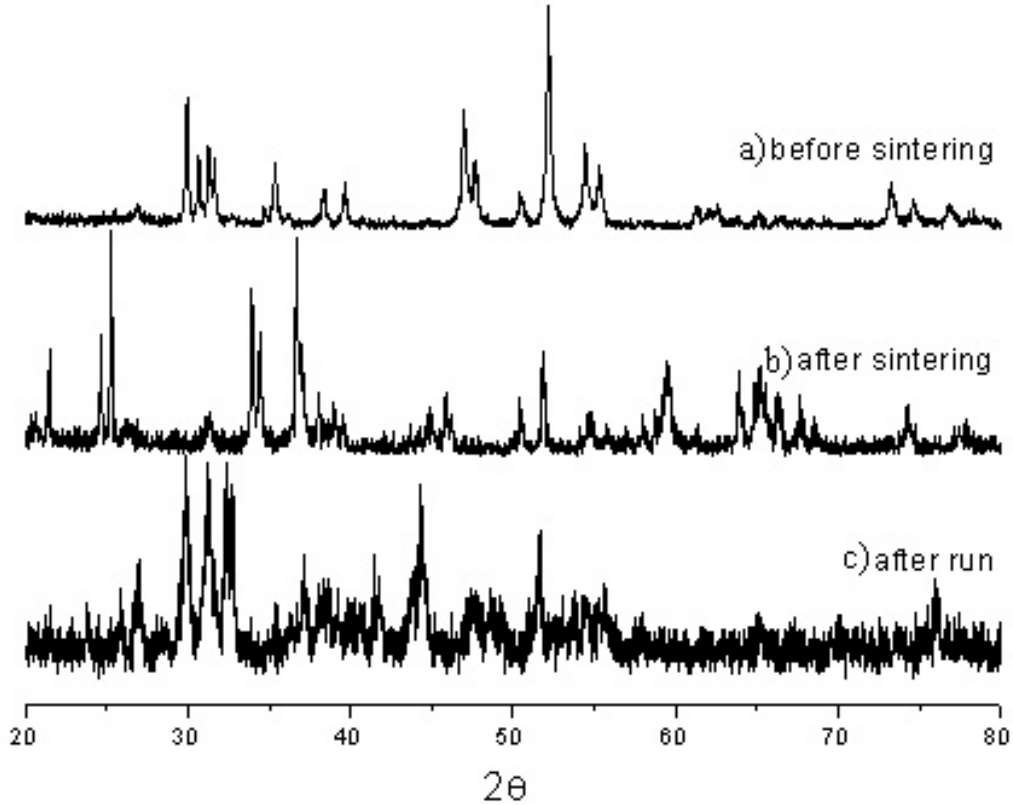
Figure 13. X-ray diffraction of cobalt sulfide electrode
The XRD patterns correspond to the following structures: (a) CoS_2,
(b) Co_4S_3/Co_3S_4 mixed phase, and (c) Co_9S_8/Co_4S_3 mixed phase.

A possibility is that $CoCO_3$ was formed in the runs with high CO_2 and H_2O levels.

$CoCO_3$ is unstable at high temperatures and will decompose. But even temporary

formation of this compound may induce degradation of the cobalt sulfide structure. This

may account for the poor stability of cobalt sulfide in recent runs, even though post-

mortem XRD spectra reveal cobalt sulfide phases that should be stable above 700° C.

The $Y_{(0.9)}Ca_{(0.1)}FeO_3$ cathode also failed after about 150 hours, but it was able to run

at 650º C, thus showing better performance. Post-mortem analysis agreed with earlier

results, as $Y_{(0.9)}Ca_{(0.1)}FeO_3$ was seen to convert from a metal-oxide semiconductor to a

metallic conductor via sulfurization into a Y_2O_2S, FeS mixed phase (see Figure 14). The

conductivity remains around 15 S cm^{-1} throughout proposed operating temperatures (600-

800º C).[23] Higher sintering temperatures (of at least 1000˚C) prior to insertion into the

cell aids in stabilizing the microstructure of the cathode, allowing it to endure longer

periods of operation.
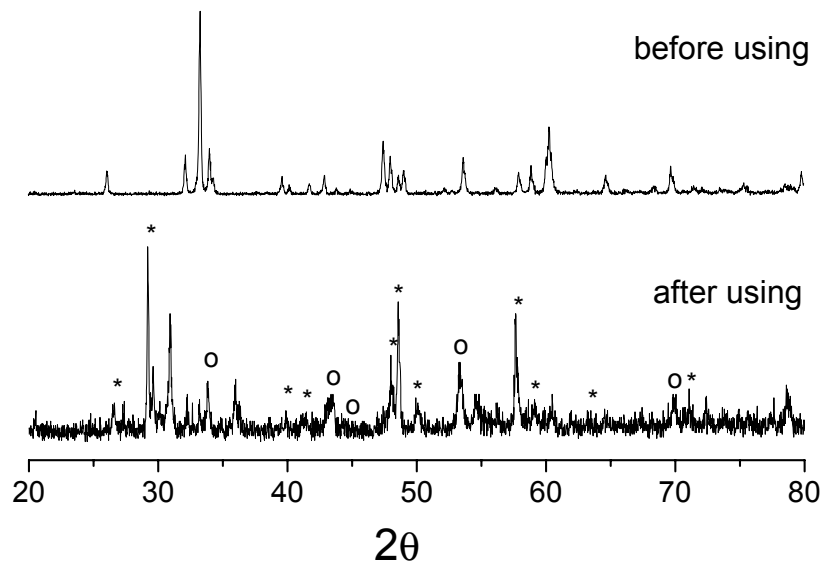
Figure 14. X-ray diffraction of $Y_{0.9}Ca_{0.1}FeO_3$ Shown above is a comparison between before and after using the cathode for electrochemical removal of H_2S. Before using, the composite has a structure of $YFeO_3$. After using, the material consisted of Y_2O_2S (*), FeS (o), electrolyte and possibly $YFeO_3$.

$Y_{0.9}Ca_{0.1}FeO_3$ has been used in multiple full cell runs and has been very useful in

acquiring data at 600-650° C. However, potential FeS absorption into the electrolyte and

evidence of microstructural changes give reason to search for other materials. In a full

cell run at 700º C, a hole through the cathode material was slowly formed where the sour

gas first makes contact with the cathode. This is strong evidence that this material cannot

be used at this temperature.

The nickel cathode material was initially good at 600° C, but failed after about 150

hours of operation under H_2S. The industrial grade nickel cathode material had fewer

defects than the cathode materials made by hand, so nickel samples were analyzed to

ascertain the degradation mechanism at the cathode. XRD results showed that the nickel

cathode was turned, as expected, to a predominantly Ni_3S_2 phase known as

heazlewoodite—see Figure 15.   An extra peak at $2\theta = 63$ offered evidence that the

cathode also contained a NiO phase.
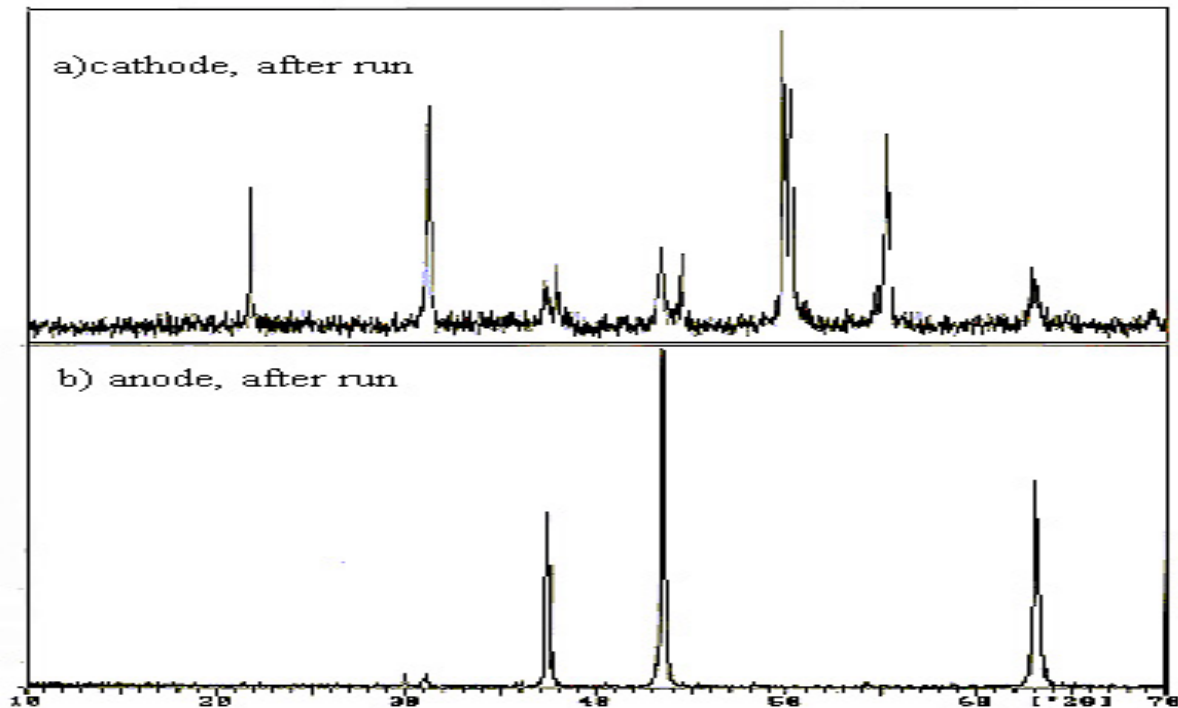
Figure 15. XRD of nickel cathode and anode after full cell trial.
a) cathode shows hazelwoodite structure, Ni_3S_2
b) anode shows no phase change, stable NiO

SEM analysis offered evidence to the breakdown of the porous structure in the nickel cathode in Figure 16. A loss of cathode wetting and/or pore size can both result in diminished H_2S gas exposure to the cathode-electrolyte interface. The NiO anode shows no significant sign of damage in Figure 17 and also no sign of sulfur absorption. This is evidence that the sulfide is oxidizing immediately at the anode and not reacting with the NiO anode; hence, modeling of the anode sulfide concentration approaching zero is a good approximation.

4.2.2 Internal Heat Production—Ohmic Losses

It should also be noted that the nickel cathode, even though converted to Ni_3S_2, which melts at 636º C, did not melt. This offers proof that the internal heat produced by ohmic losses does not significantly contribute to an increase in cell temperature. This heat may not be negligible in a larger scale cell, but as long as these temperature rises do not cause degradation of cell components, this should actually help increase kinetics, diffusivities, and overall cell performance (especially since higher sulfide concentrations in the electrolyte are favored at higher temperatures). The relative consistency of IR drops across the cell staying in the range of 1-2 ohms at current densities up to 75 mA cm^{-2} shows that the maximum heat produced is only 6-11 mJ cm^{-2}. In these small bench-scale trials, this heat will dissipate rapidly through the metal cell housings to the surrounding air.
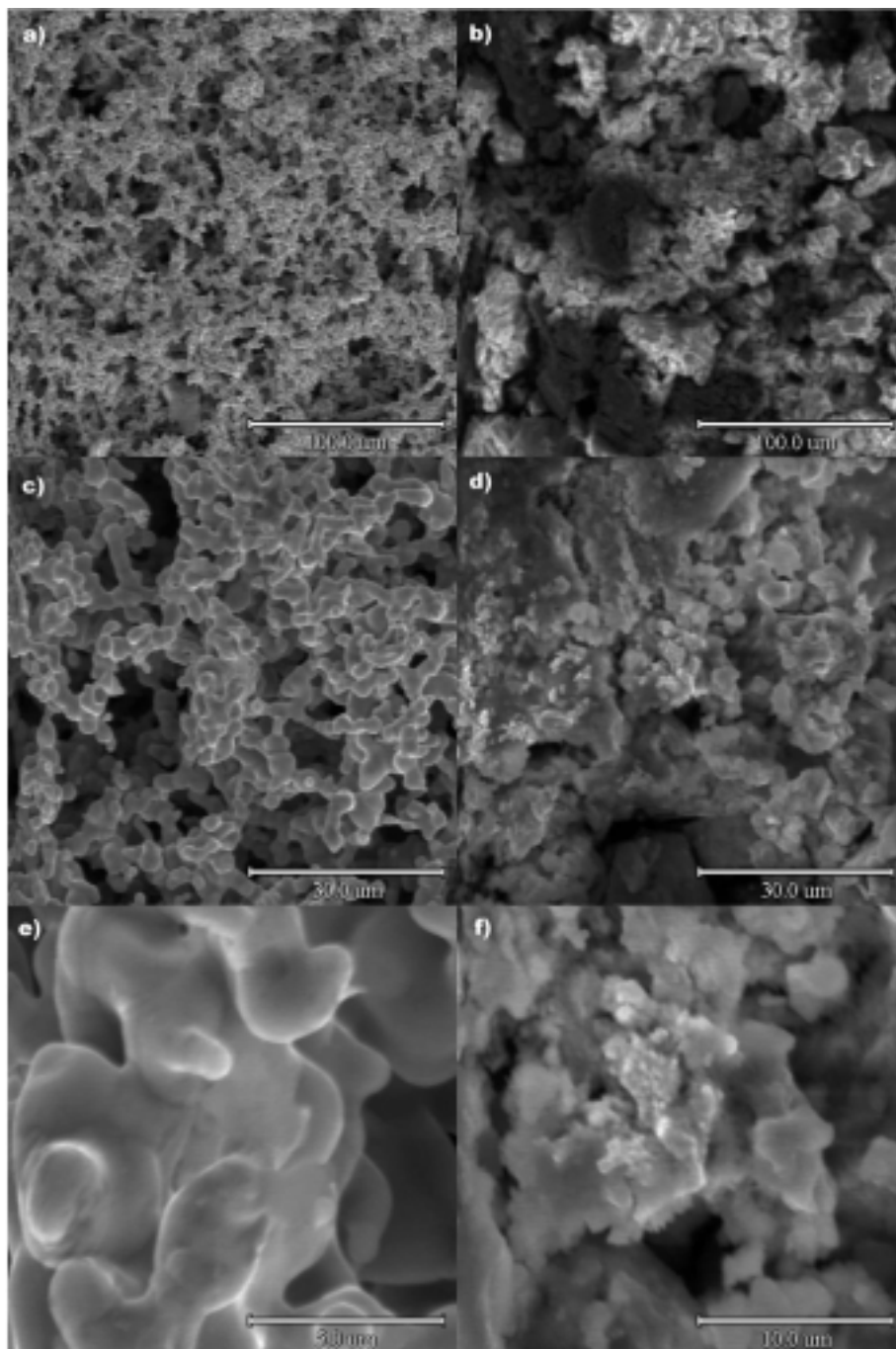
INCLUDEPICTURE "../My%20Documents/SEM%20pics/11-
14%20nickel/10b.JPG" * MERGEFORMATINET \d \z

Figure 16. Scanning electron micrograph of nickel cathode
Shown above is: before (a) and after (b) run, 300x, before (c) and
after (d) run, 1000x, and before (e), 6000x and after
run (f), 3000x. Notice the clogging of pores after the run.
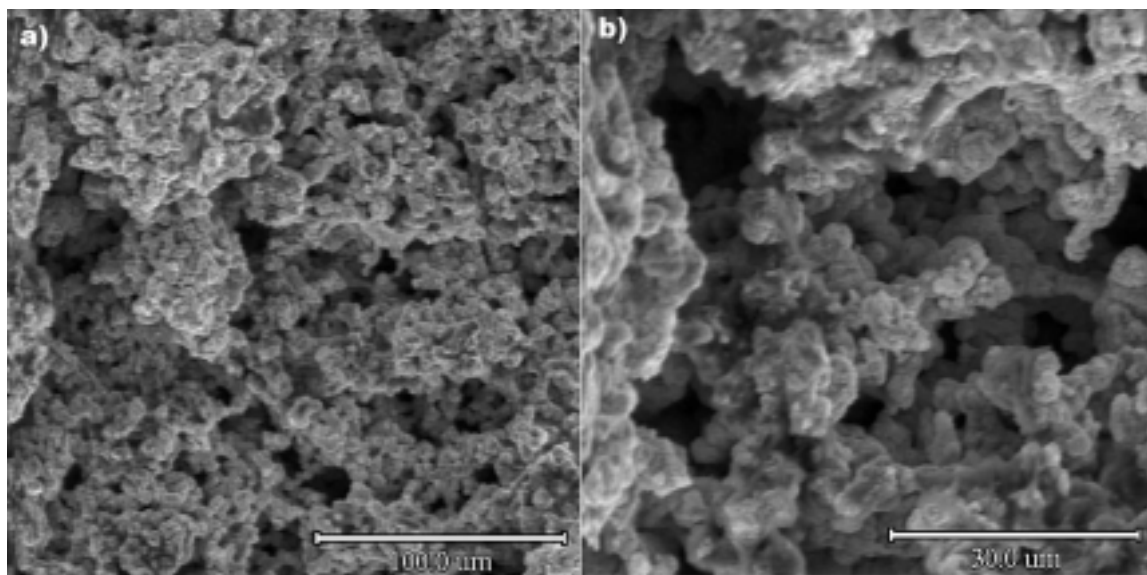
Figure 17. SEM of nickel oxide anode after full cell run.

Pores appear to be in good condition. (a) 300x (b) 1000x

4.2.3 Stability Run Results

The following materials were all been tested for chemical stability in the cathodic

operating environment.

Perovskites	Pyrochlore	Others
(single)	Gd_2TiMoO_7	$BaLa_2MnS_5$
$SrVO_3$		$CoS_2/LiCoO_2$
$La_{0.7}Sr_{0.3}VO_3$		$Zn_{0.98}Al_{0.02}O$
$La_{1-x}Sr_xCrO_3$		$CuIr_2S_4$
Sr_2VO_4		TiN
$Y_{0.9}Ca_{0.1}FeO_3$		
$La_{0.9}Sr_{0.1}Ga_{0.8}Cr_{0.2}O_3$		
$LaCr_{0.9}Ti_{0.1}O_3$		
$SrCo_{0.8}Fe_{0.2}O_3$		
(double)		
$SrFeMoO_6$		
Sr_2CrMoO_6		
$BaLaMnMoO_6$		

Table 2. Materials analyzed as possible cathode candidates

These oxides have high electrical conductivity when they are partially reduced, but they needed to be tested for chemical stability under prolonged H_2S and electrolyte exposure. Results of each successful candidate are described below.

$Gd_2Ti_{2-x}Mo_xO_7$ (x=1.4) mixed with electrolyte decomposed completely after being heated for 40 h in syngas with 0.3% H_2S. The only phase that can be indexed from the XRD of the sample is Gd_2O_2S (Figure 18). Because the stability of $Gd_2Ti_{2-x}Mo_xO_7$ increases with increasing Ti content, we measured the performance of Gd_2TiMoO_7 and found that there is no obvious change in the XRD spectra after it was heated for 40 hours at 800° C (see Figure 19). Its electrical conductivity in 4% H_2/Ar is presented in Figure 20. It is about 6 S cm^{-1} at 650° C. We had the cell performance test with Gd_2TiMoO_7 as the cathode material. The feeding gas for the test is syngas with 2.2% H_2S. It was found that Gd_2TiMoO_7 decomposed to Gd_2OS_2, $TiO_{1.04}$ and other phases after 4 days at 650° C. Because $TiO_{1.04}$ has high electrical conductivity (5000 S cm^{-1} at 25^oC),[39] the composite derived from Gd_2TiMoO_7 should have adequate electrical conductivity. A previous report has confirmed that $TiO_{1.04}$ has good H_2S tolerance;[40] hence a Gd_2TiMoO_7 derived composite is a good cathode candidate for H_2S removal.
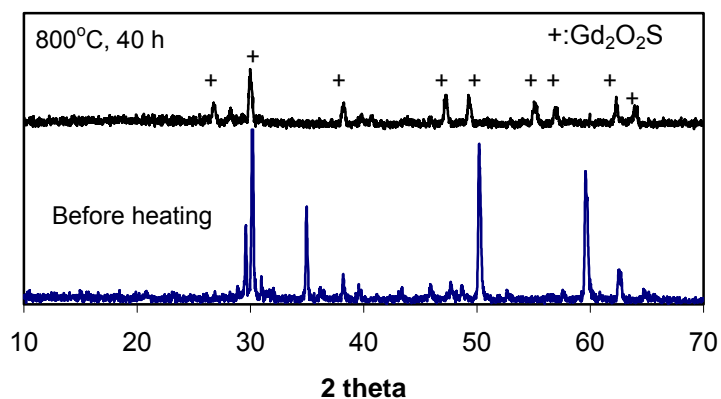
Figure 18. XRD of $Gd_2Ti_{0.6}Mo_{1.4}O_7$ immersed in electrolyte at 800° C for 40 h in syngas with 0.3% H_2S
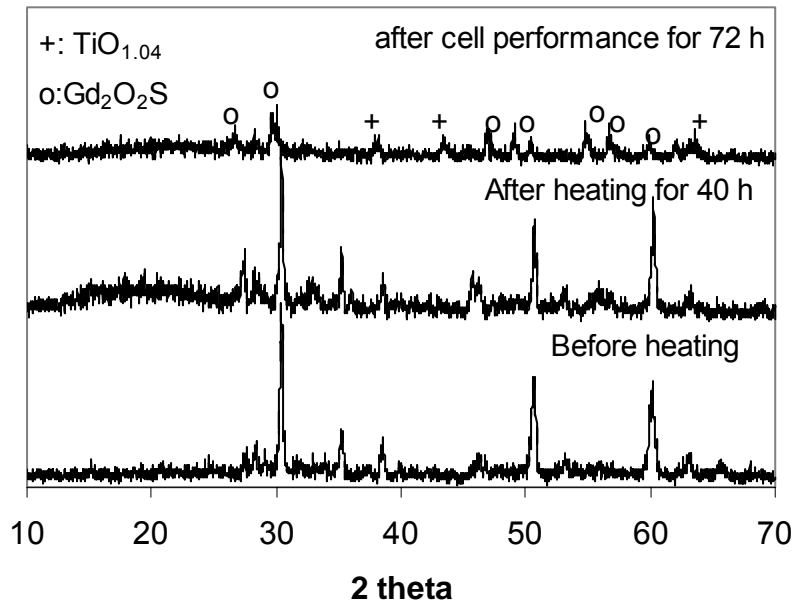
Figure 19. XRD of Gd$_2$TiMoO$_7$ immersed in electrolyte at 800°C for 40 h in syngas with 0.3% H$_2$S and the sample after cell performance for 3 days.
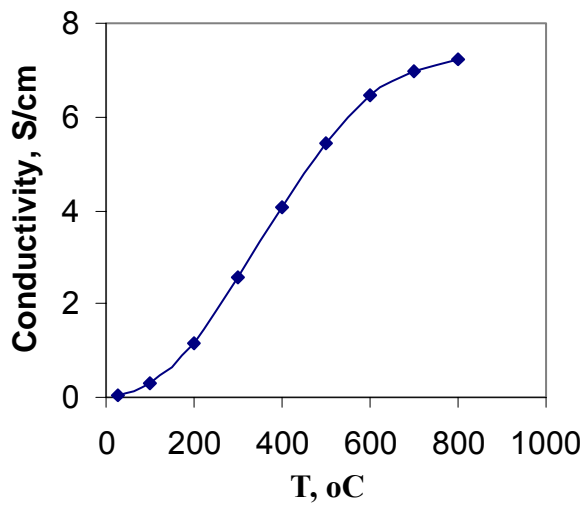
Figure 20. Electrical conductivity of Gd$_2$TiMoO$_7$ in 4% H$_2$/Ar

In another test, a small amount of SrS was indexed from the XRD spectra of

La$_{0.7}$Sr$_{0.3}$VO$_3$ sample after it was heated without electrolyte at 750°C in syngas with 2.2%

H_2S for 72 h. When it was mixed with electrolyte in a 1/1 weight ratio and heated in syngas with 0.3% H_2S at 750°C for 72 h, no $LiVO_2$ was indexed from its XRD, and only a small amount of SrS was found. No change was observed after the sample was heated for another 72 h in the same conditions (see Figure 21). These facts indicate that, when electrolyte is present, $La_{0.7}Sr_{0.3}VO_3$ has much better stability than $SrVO_3$ does. SEM showed that $La_{0.7}Sr_{0.3}VO_3$ did not melt at 750°C in the mixture with electrolyte for 6 days (see Figure 22). Figure 23 presents the electrical conductivity of $La_{0.7}Sr_{0.3}VO_3$ in 4% H_2/Ar atmosphere. It is about 30 S cm^{-1} at 650°C.
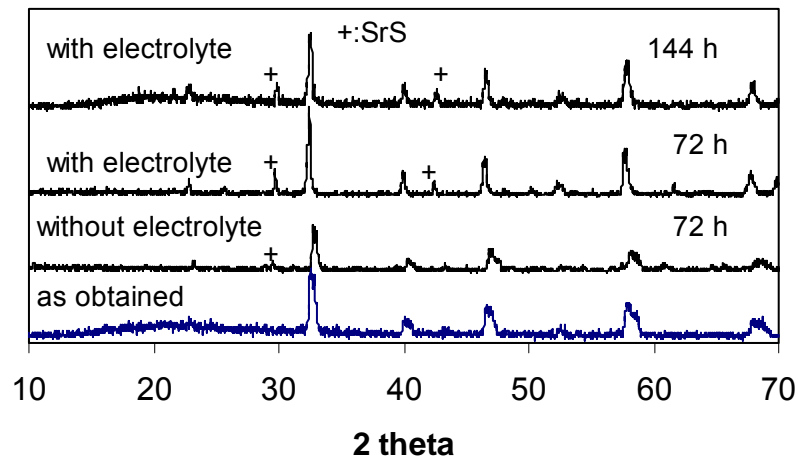
Figure 21. XRD of $La_{0.7}Sr_{0.3}VO_3$ immersed in electrolyte at 750°C for 72 hours and 144 hours.
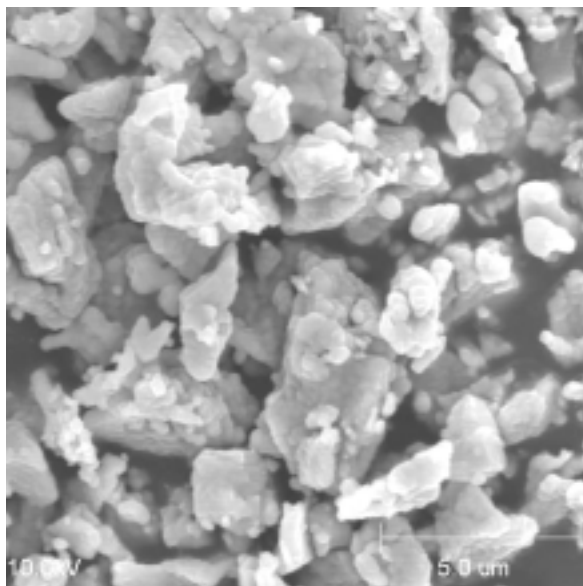
Figure 22a. An SEM micrograph of La$_{0.7}$Sr$_{0.3}$VO$_3$ as obtained.
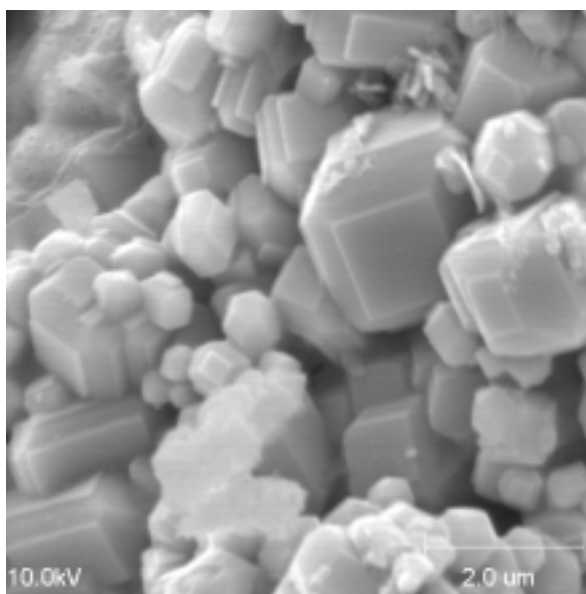
Figure 22b. An SEM micrograph of La$_{0.7}$Sr$_{0.3}$VO$_3$ after heating for 144 hours at 750°C in H$_2$S gas and immersed into electrolyte. The electrolyte was washed out before the image was taken.
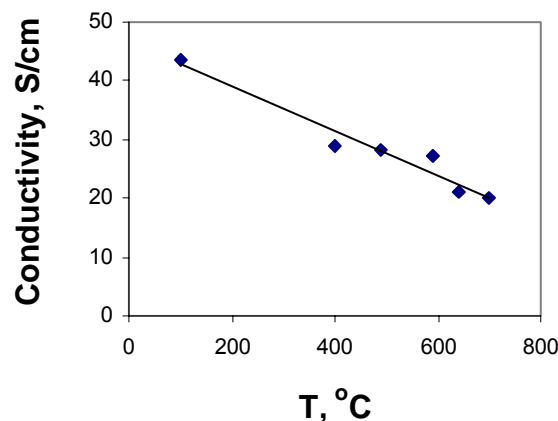
Figure 23. The electrical conductivity of La$_{0.7}$Sr$_{0.3}$VO$_3$ in 4% H$_2$/Ar.

La$_{0.7}$Sr$_{0.3}$VO$_3$ is the most stable perovskite oxide with high electrical conductivity in H$_2$S

containing atmosphere analyzed to date. Its stability increases with increasing La content,

though its conductivity decreases. The low Sr containing members, La$_{1-x}$Sr$_x$VO$_3$ (x<0.3), are

potential cathode materials for H$_2$S removal. La$_{0.7}$Sr$_{0.3}$VO$_3$ did not melt in the stability runs

and has an electrical conductivity of about 20 S cm^{-1} at 650° C under reducing gas.

4.2.4 Stability Results in Full Cell Runs for Novel Cathode Materials

For the materials that looked most promising in the stability trials, porous disks were

prepared for use in full cell runs. Cell performance was continually monitored, but even if

there was gas crossover, the run was continued to observe the physical change of each

cathode material in the working cell environment.

Gd$_2$TiMoO$_7$ has shown resilience to pore deformation under the sour, reducing

conditions. Figure 24 shows the SEM of the cathode before and after a run at 650° C

with 600 mA of current applied over its 7.9 cm^2 surface. XRD revealed that the

Gd$_2$TiMoO$_7$ derived composite converted to electrically conductive TiO$_{1.04}$ and Gd$_2$O$_2$S

with high melting point. It has good stability and high electrical conductivity. Even

though the composition changed, the pore structure appeared to be okay, signifying that

the material may be made in situ without accounting for change in volume and/or

porosity. This material also achieved the highest removal rate achievable under the

operating conditions (5.0×10^{-7} gmol cm^{-2} s^{-1} at 650° C with two membranes). A

separate run at 700° C also gave further support that this material has promising

stability—see Figure 25. The electrolyte side showed a stable porous structure, but the

side exposed to the gas had deformation—probably due to formation of Gd_2O_2S.
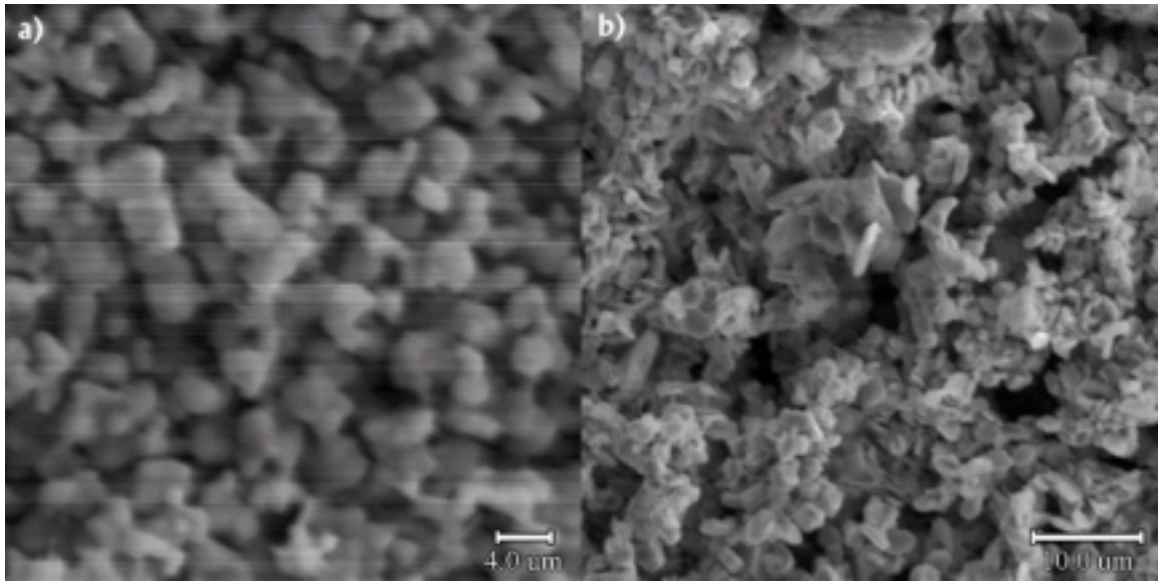
**Figure 24. SEM of Gd$_2$TiMoO$_7$ before (a) and after (b) full cell operation at 650° C.
Note that the pore structure is still intact.**
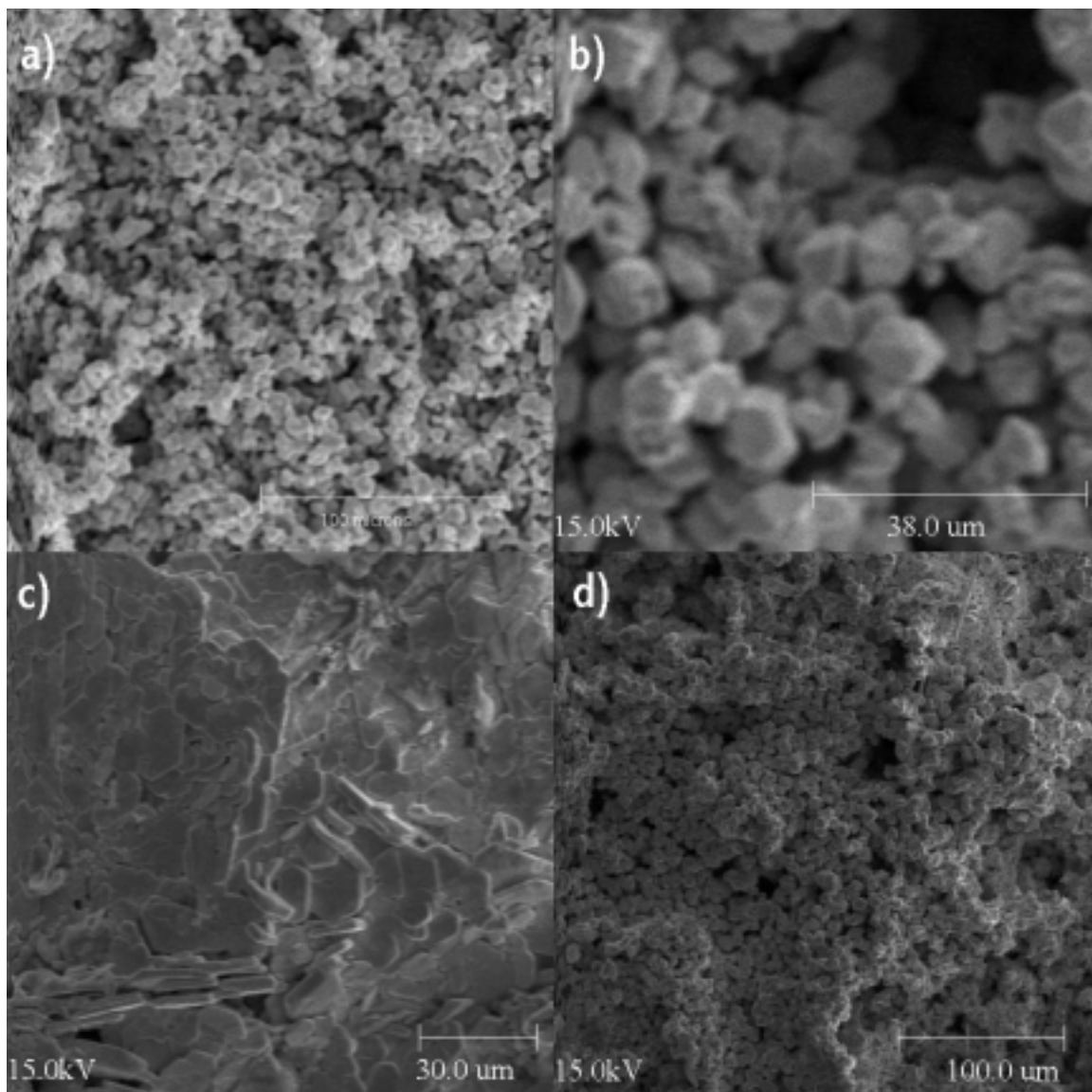
Figure 25. SEM of Gd₂TiMoO₇ coated with LiCoO₂ at 700° C
a) standard, 1000x, before run
b) washed, 800x, electrolyte side, after run
c) washed, 700x, gas side, after run
d) washed, 150x, electrolyte side, after run

$La_{0.7}Sr_{0.3}VO_3$ did not show good removal performance, but the XRD data show that this material keeps its perovskite structure in this operating environment—see Figure 26. In this XRD plot, however, there is much noise—possibly a result of sulfide.

The SEM pictures in Figure 27 show that the electrolyte side of the cathode kept its

porosity. The problem appears to be the side directly exposed to the electrolyte, opposite

the case with Gd_2TiMoO_7. Perhaps a pure $LaCrO_3$ or $La_{1-x}Sr_xVO_3$ layer could help shield

Gd_2TiMoO_7 from the sour gas. In a best-case scenario, Gd_2TiMoO_7 would be wetted

with electrolyte, and $La_{0.7}Sr_{0.3}VO_3$ would handle the direct exposure to the sour fuel gas.

This way the materials would complement each other, and each would be more isolated

in an environment in which it is stable.
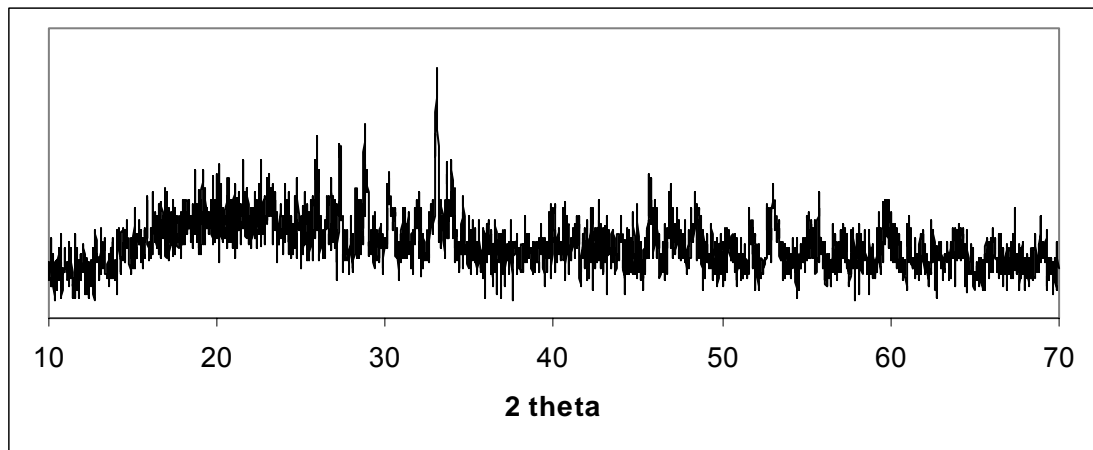
**Figure 26. XRD of $La_{0.7}Sr_{0.3}VO_3$ after run, shows deformation from
original structure (compare to Figure 21)**
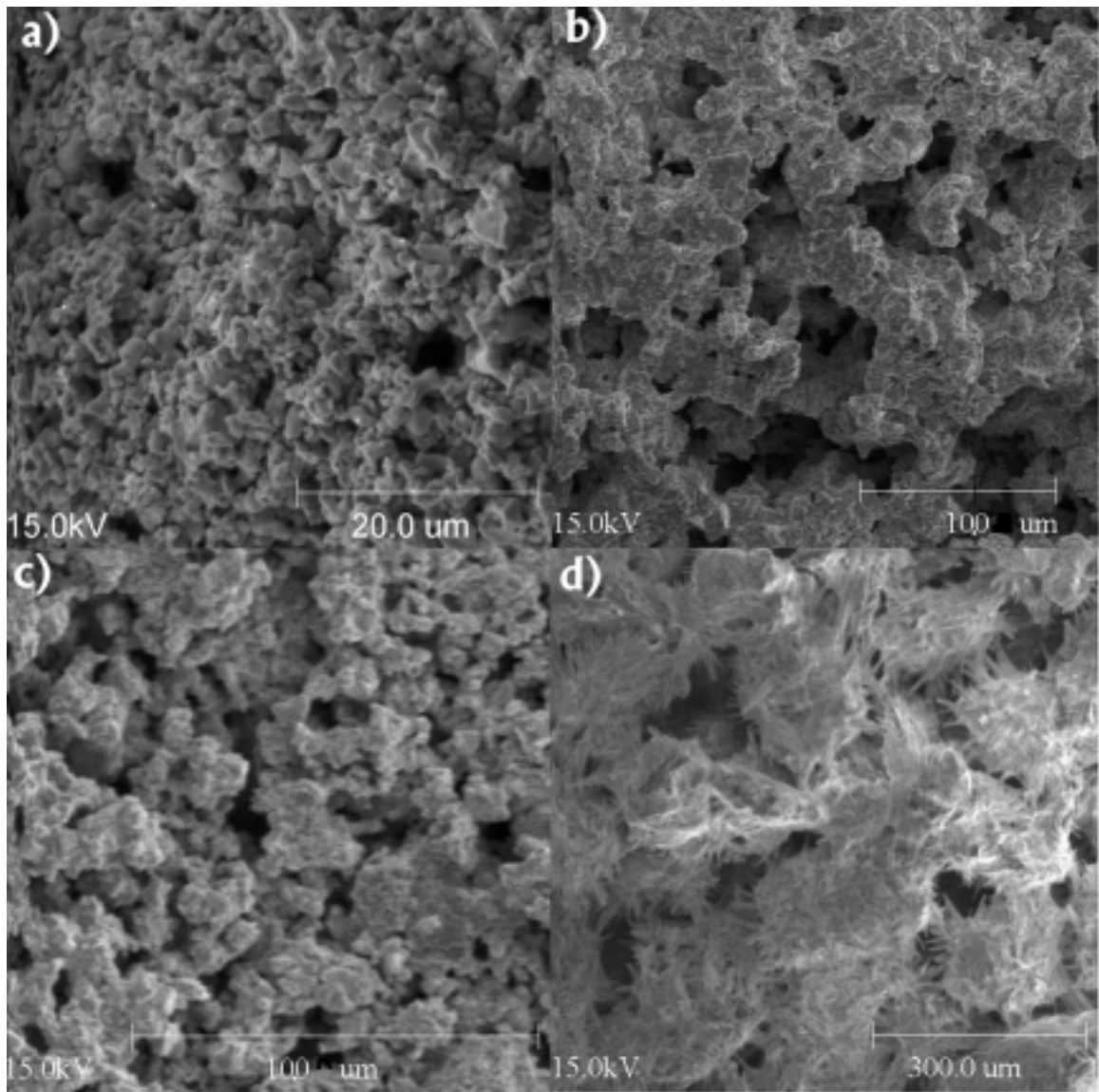
Figure 27. SEM of La$_{0.7}$Sr$_{0.3}$VO3 after use in full cell run.
 a) standard, 1500x, before run
 b) washed, 200x, electrolyte side
 c) washed, 300x, gas side
 d) La$_{0.7}$Sr$_{0.3}$VO$_3$ turned white upon exposure to oxygen, 100x,
   electrolyte side

CHAPTER 5. DISCUSSION

5.1 H₂S Removal

5.1.1 Temperature Effects

The thermodynamic data in Figure 28 imply that higher H_2S removal rates are possible at higher temperatures because more sulfide is favored in the electrolyte via Reaction (6). This enables higher current efficiency for sulfur removal because the concentration gradient across the membrane in Equation (5) will increase (assuming the anode side concentration remains the same--approximately zero). Additionally, higher temperatures generally increase electrode kinetics and diffusivities of species in the electrolyte. The maximum flux attained at 650° C was 1.1×10^{-6} gmol H_2S min^{-1} cm^{-2}.[23]
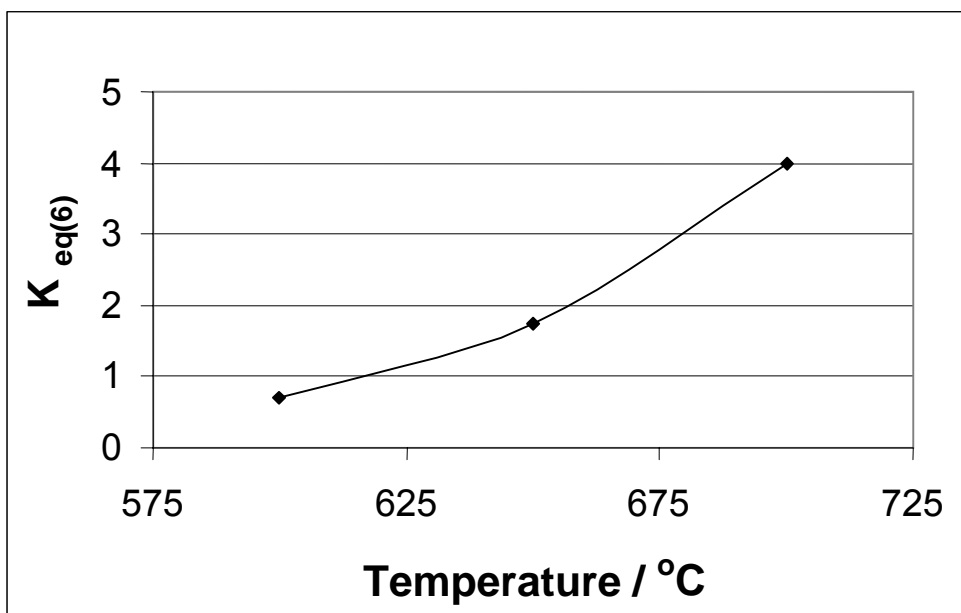
Figure 28. **Equilibrium constants for Reaction (6)**
Calculated from Gibbs free energy of reaction via $\Delta G_{rxn} = -RT \ln(K_{eq})$.[41]

5.1.2 Effect of Membrane Thickness

The most convincing evidence supporting membrane diffusion as the limiting process is the comparison of one versus two membranes used in the cell. Equation (5)

shows that a membrane twice as thick will decrease the removal rate by half if all other parameters are held constant.

Each membrane is approximately 0.9 mm thick, so when two membranes are used, the membrane thickness is 1.8 mm. Weaver also used a membrane thickness of 1.8 mm, and it should be noted that his data—run at 650º C with a higher H_2S inlet concentration—fit with the diffusion-limited theory.[22] He raised the applied current to reach an H_2S removal rate of 3.3 mA cm^{-2}, which would be about 26 mA going towards H_2S removal on a 7.9 cm^2 surface, and the log-mean H_2S concentration across the cathode was 2400 ppm. This resulting H_2S removal flux, 1.03 x 10^{-6} gmole cm^{-2} min^{-1}, approaches nearly half the value predicted by the 650° C plot in Figure 10, as it should, because the membrane thickness used is twice that of the plot. Further increase of the current may have led to the maximum removal flux, which would be about 1.2 x 10^{-6} gmole cm^{-2} min^{-1} for his operating conditions as calculated by Equation (5). This argument is also assuming that the membrane in Weaver's system had roughly the same ratio of $\varepsilon/\tau \sim 0.1$ that was used in this study.

In every plot, the effective tortuosity used to fit the data to Equation (5) is 3.8--a reasonable value for a woven membrane comprised of sub-micron sized particles. Errors arising from Equation (5) can be attributed to either a non-linear activity profile through the membrane and/or sulfide ion levels lower than that of equilibrium in the electrolytic melt caused by formation of polysulfides or other side reactions. Despite supporting evidence, anode sulfide concentration may also be non-zero. Any of these inaccuracies would reduce the concentration gradient, which would reduce the maximum removal rate

of H_2S. The tortuosity value could be compensating for any of these possibly erroneous assumptions.

Considering an average data point for a one-membrane system from Figure 11, the current going towards H_2S removal is 1.31 mA cm^{-2} with the applied current being 12.66 mA cm^{-2}. The applied current is 332.2% of i_{theo} and results in a molar removal flux of 4.08×10^{-7} gmol H_2S min^{-1} cm^{-2}. The current efficiency here is 10.4%, which is lower than Robinson's model predicts but is consistent from trial to trial. The discrepancy occurs because the model accounts for neither H_2 crossover nor membrane diffusion limitations. The CO_2 and H_2O levels used in Robinson's model are also considerably lower than those used in this study.

5.2 Membrane Optimization

Recent analysis of the yittria-stabilized zirconia (YSZ) membrane using quantitative microscopy has revealed that the pore structure is not as optimized as it should have been. The porosity is only 36% on average, much lower than the porosity of most molten carbonate fuel cells (about 60%).[42] A more porous membrane would allow for higher sulfide fluxes, thus attaining higher H_2S removal rates. With an optimized membrane, sulfide diffusion across the membrane may no longer be the rate-limiting step as the cell can attain gas phase diffusion limitations at lower temperature.

5.3 Electrolyte Loss and Gas Crossover

Some runs at 600 and 650°C failed due to gas crossover across the membrane. This was caused by cracks in the membrane or excessive loss of electrolyte. Once high sulfide levels are obtained in the electrolyte, solidification may occur, resulting in membrane cracking and gas crossover. Higher temperatures may be able to keep the electrolyte

from solidifying; however, the electrode materials must be able to withstand these higher temperatures. Besides solidification, electrolyte evaporation is another concern already discussed. A gas tight cell or electrolyte reservoir could help avoid electrolyte depletion.

5.4 Catalytic Reaction Scheme

Because the data seem to fit to a model based upon the equilibrium of Reaction (6), it is very possible that the catalytic reaction mechanism proposed by Banks provides the electrolyte with sulfide.[3] In the presence of high CO_2 and H_2O concentrations, the dissociation of H_2S is catalyzed by excess carbonate in the electrolyte. Cyclic voltammetry studies with a high CO_2 fuel stream would be able to confirm or refute this reaction mechanism. Diluting the fuel stream with nitrogen, as would be done in an air-blown process, may increase performance by lowering CO_2 and H_2O levels, thus inhibiting the competing reaction at the cathode. However, this action will also be diluting the fuel stream, thus lowering its calorific value.

5.5 Nernstian Effects

The Nernstian cell potential, E_{eq}, may deviate from the standard potential, E^o, because of concentration (activity) differences at each electrode as shown in Equations (14) and (15). Additionally, taking E_{eq} to be equivalent for both sets of reactions, one can estimate the relative extent of each reaction.

For instance, at 600º C and 1 atm, the standard potentials for Reactions (12) and (13) are $E_{12}^0 = -0.245$ V and $E_{13}^0 = -1.04$ V (thus H_2S dissociation is favored). Given the typical gas stream tested, the cathode side molar composition is 35.1% H_2, 22.2% CO_2, 8.5% H_2O, and a log-mean average of 1000 ppm H_2S. With the sum of liquid phase activities at the cathode being unity, thermodynamic data for Reaction (6) were used to

estimate mole fractions of 0.964 and 0.036 for carbonate and sulfide, respectively (assuming activity coefficients are equal to one). On the anode side, during current application, the activity of sulfide ions approaches zero while that of the carbonate ion approaches one.

Next, an operating Nernstian potential, E_{eq}, must be chosen to calculate the CO_2 present at the anode from Equation (15). This potential is free of ohmic and other non-Nernstian overpotentials. With E_{eq} = -0.75 V, a value common when trying to achieve maximum H_2S removal and compensating for IR drop and overpotential, an average CO_2 mole percentage of 0.1% exists at the anode (oxygen would then have half of this value).

Finally, setting an anode side sulfur level allows one to determine the sulfide activity at the anode from Equation (14). Under these operating conditions, experimental removal data suggest that a log-mean average sulfur level at the anode would be approximately 100 ppm. For this value and the same E_{eq} value of –0.75 V, the carbonate/sulfide activity ratio in the anolyte is on the order of 10^6. Therefore, a significant sulfide concentration gradient exists through the membrane, and the current efficiency is about 16% (the percentage of current contributing to H_2S removal).

Experimentally, however, there is much more CO_2 transport—most likely due to H_2 crossover. Because of this, a lower current efficiency is observed (normally 5-10%). However, with the small H_2S concentrations present and the small currents applied, this low efficiency can still generate excellent removal performance without suffering unacceptable power losses.

5.6 Using CO_2 as the Purge Stream

Instead of using N_2 as the sweep gas at the anode, CO_2 can be used to aid in inhibiting the competing reaction of CO_2 transport. As can be seen from the Nernstian relation in Equation 15, a higher anode side CO_2 pressure should further lower the operating potential of the cell. However, this will not increase the rate of H_2S removal that is limited by mass transport of sulfide species. Additionally, for a system run gavanostatically, the power requirement may actually be increased because a higher potential would be required to oxidize carbonate at the anode—as calculated from Equation 15. With all sulfide that reaches the anode oxidizing immediately, that only leaves carbonate to fulfill the remaining current demands. In a system operated potentiostatically with CO_2 at the anode, the current efficiency should be higher and the power requirements minimized if an optimal cell voltage is used.

5.7 Model of Sulfide Membrane Diffusion-Limited System

A computer simulation of the membrane-diffusion limited system has been developed to aid in predicting the applied current needed for a given removal rate/percentage under various operating conditions and scales. It may also help gain insight into the activities of carbonate and sulfide species at each electrode under various operating potentials (especially once more data are gathered for direct comparison with the model). If gaseous mass transfer is determined to be limiting at higher temperatures (as theorized), then the model can be adjusted to accommodate for this limitation. Please see Appendix F for an algorithm of this model.

5.8 Preliminary Economic Study

Past studies have shown the capital investment of EMS to be less than half of that a Sulfinol/Claus plant investment (84.26 MM\$ versus174 MM\$).[5] The same study also calculated the operating costs to be less than half: \$2.292/1000 SCM coal gas versus \$5.644/1000 SCM coal gas. With these numbers, the lifetime of the EMS could be roughly half that of the Sulfinol/Claus process, and EMS would still be economical. It should also be noted that the cost of cooling the gasified stream and reheating it are not taken into account here. The absence of these steps in EMS offers considerable more savings, estimated at 20% savings of the entire plant electricity used. It would also decrease process steps, equipment, and space.

The medium heating value (48 MJ kg^{-1}) of the coal analyzed in Alexander's work closely resembles the heating value of diesel fuel reformate—40-45 MJ kg^{-1}. This heating value is exceptionally high; most coal heating values, after accounting for the latent heat of evaporation of water, amount to 25-30 MJ kg^{-1}. Consequently, much more fuel would have to be treated to maintain the same power generation. This results in either larger cell area required or higher H_2S removal fluxes. But considering the smaller application as Perna and Scoles have, EMS should retain its capital cost advantages.

Another consideration is the operating cost in for this process. For a 2.5 MW application that obtains 60% the calorific value of the fuel consisting of 60% H_2, 16% CO_2, 17% CO, 6% H_2O, and 1% H_2S, the required flow rate at 650º C and 4 atm assuming ideal behavior is roughly 26200 L min^{-1}. From the removal fluxes seen in bench-scale trials, it can be assumed that the average current density going to H_2S removal would be at least 3 mA cm^{-2}. This translates into a required cell area of 1485 m^2.

Considering 1.0 m x 1.0 m square cells that are 2 cm in thickness, the 1032 cells alone

would take up nearly 30 m^3. This could be acceptable in a building power generator, but

much effort would be put into minimizing this space, as it is limited. Optimal membrane

design and the extraordinarily high flow rates may help increase average current density.

From industrial electricity costs, estimated at $0.04/kW hr, the cost of powering the

cell can be calculated. Taking from bench scale trials the efficiency of about 15%, the

total average applied current would be 20 mA cm^{-2} at a voltage of about -0.75 V. This

comes to a power requirement of 223 kW at a cost of $0.32/kg$_{H2S}$ removed. This is about

twice the cost of Alexander's estimates, but a comparison in Table 4 shows that these

operating costs are still competitive with other sulfur removal technologies. The lower

heating value fuel stream considered here causes these estimates to be higher than

Alexander's economic analysis. To put it simply, the coal stream in Alexander's report

has much less CO_2 and more H_2. The sulfide current densities that he proposes during

each step of sulfur removal are much higher than 3 mA cm^{-2}. But under less CO_2 and a

higher log-mean H_2S concentration in addition to optimum membrane design, a sulfide

current density in excess of 100 mA cm^{-2} is feasible.

	Liquid Scavengers	Solid Scavengers	Liquid-redox system	Claus & Tailgas cleanup	EMS
Operating Costs, $/kg H$_2$S removed	20	6.65	0.30-0.35	Very low	0.32
Capital Costs	Low	Moderate	Moderate	High	Moderate
Limits	< 50kg/d	50-200 kg/d	< 20 tons/d	>15 tons/d, > 15% H$_2$S	Scalable < 5% H$_2$S?

Table 3. A list of current technologies versus EMS[10]
Please see Appendix G for a full explanation of EMS operating costs.

EMS also shows that this can be effective for small or large-scale removal. Since a

majority of the operating costs are based solely on electricity, scale will not affect the

overall price. In adsorption processes, when the adsorbent needs to be regularly replaced and regenerated, the handling costs become very great for large-scale (coal) processes. For smaller applications, building a sulfinol and Claus plant is impractical. EMS offers scalability at a price competitive with other methods in use.

In general, these factors promote more economic operation by increasing the maximum H_2S flux possible across the membrane:

1) Higher H_2S concentration (as long as cell materials can handle it)
2) Lower CO_2 concentration
3) Higher Temperature (until gas phase diffusion limitation reached)
4) Thinner membrane
5) Higher pressure (in theory)

A possible way to save space and avoid low current efficiency at polishing levels would be to couple this process with a post-adsorption step. The adsorbent lifetime would be dramatically increased by only having to operate at these low (sub 100 ppm) contamination levels, and this would ensure that the H_2S concentration is reduced to an acceptable level—adding a failsafe for preventing possible corrosion of generators and/or fuel cells downstream.

The high CO_2 levels used in this study mirror some of the harsher environments that EMS may encounter. The high CO_2 levels compete with H_2S for reduction sites and evidently are involved with a catalytic process with the electrolyte via Reaction (6). Air-blown coal gasifiers produce streams diluted by N_2; hence, the H_2S and CO_2 concentrations are already reduced, thus requiring less competitive side-reactions. However, the fuel itself is also diluted, and it loses calorific value. Fuel will have to be processed at higher rates to obtain the same energy output. However, if this is still economical, it should help EMS performance by reducing CO_2 concentration. Previous

studies have shown that the cobalt sulfide cathode performs adequately while exposed to CO_2 levels below 10%.[22, 26]

5.9 Development of Cathode Materials

5.9.1 Cathode Stability

Recent studies in sulfide compounds and transition metal oxides may help explain why certain materials performed better than others. Sulfur binding energy in transition metal sulfides has recently been related to catalytic activity in hydrotreating processes. Toulhoat et al. have shown that those materials with intermediate sulfur binding energies (45-60 kcal mol^{-1}) have the highest catalytic activity.[43] In addition, mixtures of low and high sulfur binding energy compounds can produce a synergistic effect, resulting in the high catalytic activity seen in intermediate sulfur binding energy compounds. Cobalt, iron, and nickel all have low sulfur binding energy and exhibit metallic behavior. Mixing cobalt with molybdenum or nickel with tungsten can produce the synergistic effect, although the compound may inherit the semiconductive nature of the high sulfur binding energy metals. Low sulfur binding energy could be good for the EMS system, however, because that could allow sulfur ions to be released from the cathode surface more easily. The metallic nature is also preferable, as this would help decrease cell resistance.

5.9.2 Novel Oxide Cathode Materials

For perovskite structured oxides, explanations for stability are based on resistance to sulfide formation. For a generic ABO_3 perovskite compound, a tri-valent A-site ion helps stabilize the 3+ valence state of the B-site ion at low oxidant pressures. This is how lanthanum helps stabilize the perovskite $LaVO_3$. Substituting strontium for lanthanum results in 4+ vanadium ions in the lattice that induce the semiconductive, n-type behavior

of $La_{0.7}Sr_{0.3}VO_3$. A balance between conductivity and stability is achieved by the proper selection of atoms to fill the A and B lattice sites.

Pyrochlore structures and their conductive mechanisms are based on oxygen vacancies in the lattice. In Gd_2TiMoO_7, it is the presence of molybdenum that promotes conductivity by its changing valence. However, after its structure changes upon exposure to H_2S, it appears that titanium oxide is responsible for the conductivity. SEM has shown that Gd_2TiMoO_7 keeps its porosity despite this phase change (at least on the electrolyte side of the cathode). This means that a suitable cathode material may be made in situ by starting with a pyrochlore structure. More pyrochlore structures need to be analyzed to gain further insight into the resulting phases under sour operating conditions.

CHAPTER 6. CONCLUSIONS AND RECOMMENDATIONS

6.1 Conclusions

It is apparent from this study that the diffusion of sulfide across the membrane is the rate-limiting step in H_2S removal. The maximum H_2S removal flux attainable will be limited by this step. Temperature and membrane effects offer the evidence needed to arrive at this conclusion. If this system were gas phase-diffusion limited, then the changes in membrane thickness and temperature would not have resulted in such dramatic change in H_2S removal rate. However, if a system were designed with a membrane that has optimized structure, then the gas phase diffusion of H_2S to the electrode/electrolyte may be limiting. Higher temperature will also promote gas phase limitation, because the sulfide ion diffusion flux increases with temperature whereas the gas phase diffusion flux remains relatively constant.

In the search for a suitable cathode material, more insight was gained towards the stability of promising materials in the full cell operating environment. $Li-Y_{0.9}CaFeO_3$ and cobalt sulfide cathodes were found to have limitations to temperature and CO_2-H_2O levels, respectively. Of the many novel metal oxides tested for stability in the sour operating environment, Gd_2TiMoO_7 and $La_{0.7}Sr_{0.3}VO_3$ were chosen as the best candidates. Each showed slight deformation in the full cell operating environment, but these materials may be able to complement each other. Gd_2TiMoO_7 appears to be stable under sour gas when the carbonate electrolyte is also present. $La_{0.7}Sr_{0.3}VO_3$ is stable under pure sour gas, but forms SrS when exposed to the electrolyte. A layered electrode could offer a solution to this dilemma. An inner Gd_2TiMoO_7 layer could be wetted by the electrolyte and shielded from the sour gas by an outer layer of $La_{0.7}Sr_{0.3}VO_3$.

Progress has been made towards fundamental understanding and materials selection for an environmentally benign H_2S removal process that can continuously clean coal gasification streams in hot-gas clean-up. While promising cathode candidates have been found in Gd_2TiMoO_7 and $La_{0.7}Sr_{0.3}VO_3$, uncertainty still remains concerning long-term stability and catalytic activity.

6.2 Recommendations

6.2.1 Chemical Combustion Vapor Deposition (CCVD)

A CCVD unit recently acquired from Microcoating Technologies (MCT) is now available and operational. Porous, catalytic layers can be coated onto a given substrate on the order of 10 nm to 0.5 micron. This could be useful in coating electrodes or other materials--possibly even the membrane at some point. $LiCoO_2$ has already been successfully deposited onto a quartz substrate. This will aid in forming composite materials to be used in full cell runs.

6.2.2 Sol-Gel Processing of Membrane

Another important avenue for continued research is the optimization of the porous membrane structure that separates the anode and cathode and immobilizes the molten electrolyte. To circumvent sulfide membrane diffusion limitations, a novel membrane should be developed. The desired membrane must be physically, thermally, and chemically stable, electrically insulating, and resistant to cracking. It must act as a barrier to convection and gas diffusion while allowing selective S^{2-} diffusion.

Zirconia membranes with porosities up to 60% could be synthesized by sol-gel processing with zirconium chloride octahydrate as a precursor. This procedure is detailed in work by Shi, Tin and Wong.[44] The sols are then dried to form gels, which are fired to

form zirconia membranes. Adding yittria stabilizes the membrane at high temperatures. Methyl celluloses and polyvinyl alcohol (PVA) are added to the sols to increase membrane porosities and to prevent the formation of cracks during drying. The porosities are controlled by the amount of organics added to the sols and by the firing temperatures.

6.2.3 Future Cathode Possibilities

Besides the pursuit of metal oxide cathodes that possess a balance of stable and conductive structures, cobalt-based alloys should also be examined. In one case, a Co-15 wt. % Y alloy showed reduced sulfidation rates in comparison to pure cobalt.[45] In another case, rhenium addition to cobalt has shown a decrease in sulfidation rate.[46] This decrease is attributed to slower outward diffusion of cobalt cations in the Re-Co alloy as opposed to pure cobalt. Although a cobalt sulfide cathode is still formed, its lifetime is increased. But these studies were done with only H_2/H_2S atmospheres. Stability analysis that includes CO, CO_2, and H_2O needs to be done to see whether these cobalt alloys have increased tolerance to high CO_2 level fuel gas streams as well.

Composite materials are also a matter to be considered. This study has shown that a two layered cathode, with Gd_2TiMoO_7 wetted by the electrolyte and $La_{0.7}Sr_{0.3}VO_3$ exposed to the sour gas directly, might preserve the stability of each phase in the full cell operating environment. In this two-layer electrode, each material is shielding the other from the environment in which it is not stable. This possible synergistic effect should be studied, and other materials that have complementing traits (such as stability from one component and conductivity from another) should be explored.

6.2.4 Full Cell Runs at Higher Temperature

In theory, operation at higher temperature offers many advantages, but scant data have been gathered above 650º C to support this claim. Future trials should strive for higher temperatures and operation times. Complete isolation of the cell from ambient air may also help preserve electrolyte at temperatures above 650º C. Gas crossover was the main problem in runs operated at 700º C. This crossover is attributed to either electrolyte evaporation or solidification at these higher temperatures.

6.2.5 Full Cell Runs at Higher Pressure

Operation at higher pressure will also favor higher H_2S removal rates as long as sulfur does not condense at the anode. This is another avenue for exploration as long as safety issues are properly addressed. High-pressure operation should allow for greater adsorption rates and conservation of plant space and energy. Additionally, if the purge stream is composed of CO_2 instead of an inert, it should help inhibit the competing reaction of CO_2 transport. However, change in pressure can affect the magnetic properties and electrolyte wetting of the electrode materials. Therefore, the electrode materials will have to be tested at these pressures as well.

REFERENCES

[1] J. Winnick. US Patent 79-17064 (1981).

[2] H. S. Lim and J. Winnick. *J. of the Electrochem. Soc.* **131** (3), 562-568 (1984).

[3] E. Banks and J. Winnick. *J. of the Electrochem. Soc.* **16**, 583-590 (1986).

[4] K. White, III and J. Winnick. *Electrochimica Acta*, **30**(4), 511-519 (1985).

[5] S.R. Alexander and J. Winnick. *J. of App. Electrochem.*, **24**, 1092-1101 (1994).

[6] S.R. Alexander and J. Winnick. *AIChE Journal.*, **40**(4), 613-620 (1994).

[7] J. Robinson, D. S. Smith, and J. Winnick. *AIChE Journal.*, **44**, 2168-2174 (1998).

[8] J. Robinson and J. Winnick. *J. of App. Electrochem.*, **28**, 1343-1349 (1998).

[9] Mark A. Perna and S. W. Scoles. "Navel Distillate Reforming for Navy Ship Service Applications", 2000 Fuel Cell Seminar. 10/30-11/2, 2000, Portland, OR. MTI 00-28.

[10] Gary J. Nagl. *Chemical Engineering*, **108(7)**, 97-100 (2001).

[11] F. A. Uribe and T. A. Zawodzinski, Jr. "The Effects of Fuel Impurities on PEM Fuel Cell Performance" 2001 Joint Meeting of The Electrochemical Society and the International Society of Electrochemistry. San Franscisco, CA. Abstract No. 339.

[12] R. J. Gorte, H. Kim, and J. M. Vohs. *Journal of Power Sources*. **106**, 10-15 (2002).

[13] C. Bauer. Plenory Discussion. 5th International Symposium on Gas Cleaning at High Temperature (2002). Morgantown, WV.

[14] P. Nowacki. <u>Coal Gasification Processes</u>, p. 326-334, Noyes Data Corp., NJ (1981).

[15] A. Atimtay and D. Harrison. <u>Desulfurization of Hot Coal Gas</u>, p. 91, Springer, Germany (1998).

[16] R. Siriwardane and J. Abbasian. Overview-Sorbent Development for H_2S Removal. 5th International Symposium on Gas Cleaning at High Temperature (2002). Morgantown, WV.

[17] E. Majewski and D. Walker. *Earth Planet. Sci. Lett.*, **160**, 823-830 (1998).

[18] F. P. Incropera and D. P. DeWitt. <u>Fundamentals of Heat and Mass Transfer,</u> 2nd edn, J. Wiley & Sons, New York (1987).

[19] M. A. Volgin and A. L. L'vov. *Issled. Obl. Khim. Istochnikov Toka.* **2**, 26-31 (1971).

[20] M. A. Volgin, A. L. L'vov, and V. A. Loskutkin. *Electrochimiya,* **9**(3), 368-71, (1973).

[21] H. Cheng, D. B. Reiser, and S. Dean, Jr. *Catalysis Today*., **50**, 579-588 (1999).

[22] D. Weaver and J. Winnick. *J. Electrochem. Soc.*, **139**, 492-498 (1992).

[23] S. Wang, M. Liu, J. Winnick. *J. Solid State Electrochem.*, **5**, 188 (2001).

[24] A. Burke, J. Winnick, C. Xia, and M. Liu. *J. Electrochem. Soc.*, (2002)

[25] T. Rosenquist. *J. Iron & Steel Inst.*, p. 37-57 (January, 1954).

[26] D. S. Smith. Georgia Institute of Technology, Ph.D. Dissertation, Atlanta, Ga, 1999.

[27] Z. Grzesik. *Solid State Ionics*., **141-142**, 295-299 (2001).

[28] J. Robinson. Georgia Institute of Technology, Ph.D. Dissertation, Atlanta, Ga, 1996.

[29] D. Weaver. Georgia Institute of Technology, Ph.D. Dissertation, Atlanta, Ga, 1988.

[30] S. Mrowec, M. Danielewski, and A. Wojotowicz. *J. of Materials Sciences*., **33**, 2617-2628 (1998).

[31] B. Garcia-Landa, C. Ritter, M. R. Ibarra, J. Blasco, P. A. Algarabel, R. Mahendiran, and J. Garcia. *Solid State Comm.*, **110**, 435 (1999).

[32] T. Nakamura, and J. H. Choy. *J. Solid State Chem.*, **20**, 233 (1977).

[33] O. Porat, C. Heremans, H. L. Tuller. *Solid State Ion.*, **94**, 75 (1997).

[34] S. Hui, and A. Petric, *Solid State Ion.*, **143**, 275 (2001).

[35] A. Nozaki, H. Yoshikawa, T. Wada, H. Yamauchi, and S. Tanaka. *Phys. Rev. B*, **43**, 181 (1991).

[36] K. Maiti, N. Y. Vasanthacharya, and D. D. Sarma. *J. Phys. Condens. Matter*, **9**, 7507 (1997).

[37] M. D. Ingram and G. J. Janz. *Electrochemica Acta.*, **10**, 783-792 (1965).

[38] K. Babcock and J. Winnick. *J. Chem. Eng. Data*, **33**(2), 96 (1988).

[39] A. A. Valeeva, A. A. Rempel, and A. I. Gusev. *JETP Lett.,* **73**, 702 (2001).

[40] D. Weaver, and J. Winnick. *J. Electrochem. Soc*. **138**, 1626 (1991).

[41] I. Barin and O. Knacke, Thermochemical Properties of Inorganic Substances, Springer-Verlag, Berlin, 1973.

[42] H.C. Maru, L. Paetsch, and A. Pigeaud. "Review of Molten Carbonate Fuel Cell Matrix Technology", Proceedings of the Symposium on Molten Carbonate Fuel Cell Technology. p.20-53. The Electrochemical Society, Inc., Pennington, NJ(1984).

[43] H. Toulhoat, P. Raybaud, S. Kasztelan, G. Kresse, and J. Hafner. *Catalysis Today*, **50**, 629-636 (1999).

[44] L. Shi, K. Tin, and N. Wong. *J. Mat. Sci*., **34**, 3367-3374 (1999).

[45] Y. Niu, F. Gesmundo, C. Zeng, W. Wu, and F. Viani. *Oxidation of Metals*, **48(3/4)**, 243-262 (1997).

[46] R. Shiring and D. L. Douglass. *Oxidation of Metals*, **52 (5/6)**, 353-377 (1999).

[47] R.M. Souto, and H. Alanyali. *Corrosion Science*, **42**, 2201-2211 (2000).

[48] H. F. Pen, L. H. Tieng, E. Pellegrin, F. M. F. de Groot, G. A. Sawatzky, M. A. van Veenendaal, and C. T. Chen. *Phys. Rev. B*., **55**, 15500 (1997).

[49] H. R. Kunz. *J. Electrochem. Soc.*, **134 (1)**, 105-113 (1987).

Run 1-12/1/00 to 12/8/00

Following the work of Wang,[23] lithiated $Y_{0.9}Ca_{0.1}FeO_3$ was used as the cathode material. One membrane was used, and the cathode had been sintered beforehand at 800° C for 6 hours. The cell was run at 600° C for 140 h, but over the last 20 h, temperature control was lost, and the temperature rose to 740° C. By this time, cross-cell potential had dropped, signifying gas crossover, and the run was ceased.

Visual observation of the cathode afterwards showed serious degradation with almost a third of the material wasted away. At 600º C, the fuel stream inlet composition was 34.1% CO, 22.2% CO_2, 35.1% H_2, 8.51% H_2O, and 450 ppm H_2S. The H_2S removal performance can be seen in Figure A1.
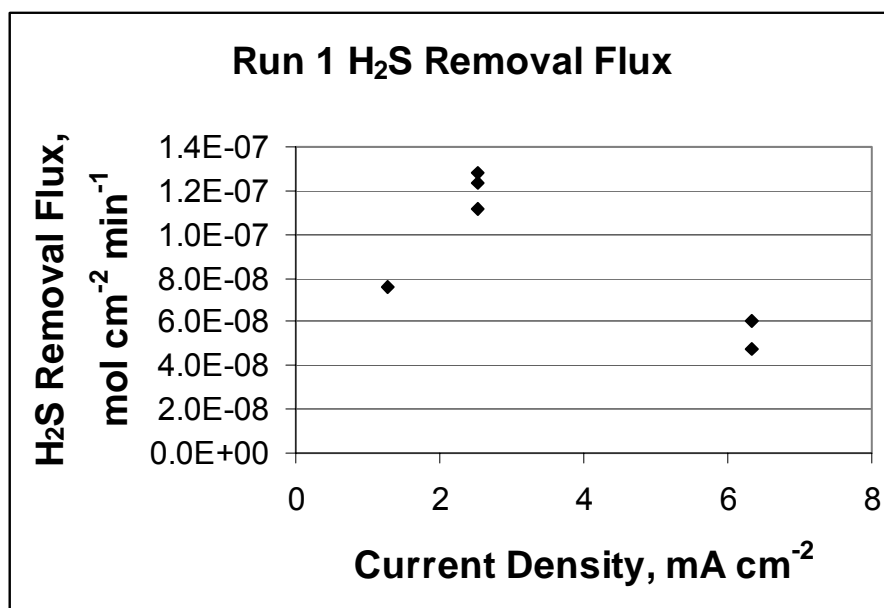
Figure A1. H_2S Removal Flux vs. Applied Current Density for Run 1.
$Y_{0.9}Ca_{0.1}FeO_3$ was tested at 600° C at a fuel flow of 80 mL min^{-1}.

Run 4 – 1/16/01 to 1/22/01

A CoS_2 cathode was made from 1.5 g starting material. After dry-pressing, it was sintered in air at 545º C for 3 h and then cooled. The final mass was 1.74 g, thus showing some oxide formation. One membrane was used, and the temperature was 600º C. The fuel flow was 195 mL min^{-1} and the inlet gas composition was (post-shift) 34.4% CO, 22.1% CO_2, 34.9% H_2, 8.39% H_2O, and 650 ppm H_2S. This run lasted 130 h under sour gas. H_2S removal performance can be seen in Figure A2.
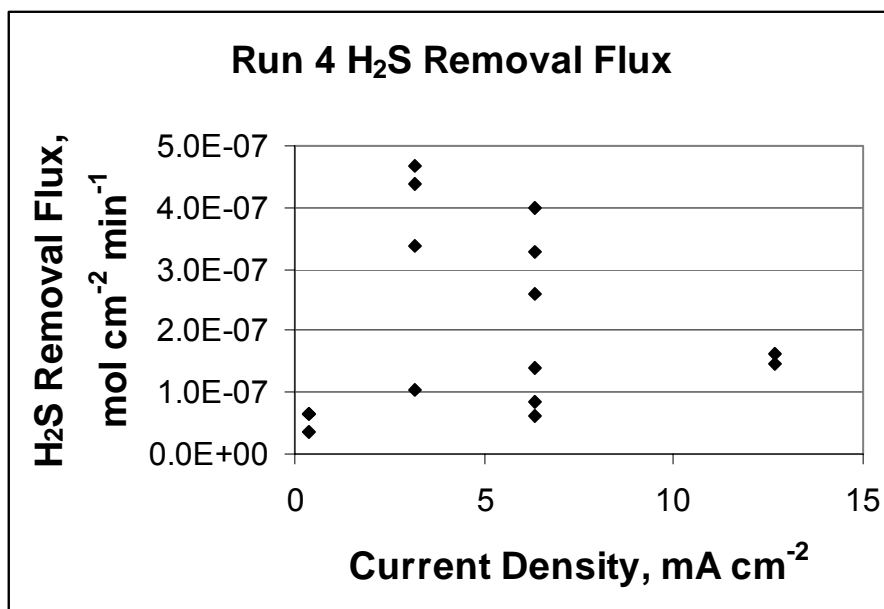
Figure A2. H_2S Removal Flux vs. Applied Current Density for Run 4.
CoS_2 was tested at 600˚ C at a fuel flow of 195 mL min^{-1}.

In this run, for a short duration, the cathode gas outlet was forced through a bubbler, causing backpressure on the cathode-side stream. This pressure forced H_2 crossover to the anode side and resulted in a positive cathode versus anode potential.

Over the last day of this run, the temperature drifted as high as 670º C, and gas crossover ensued, resulting in low cell potential and stoppage of the run. Post-mortem analysis showed that the cathode had partially melted into the gas flow channel.

Run 6 – 1/30/01 to 2/5/01

This run used a lithiated $Y_{0.9}Ca_{0.1}FeO_3$ cathode that had been sintered at 1000ºC for 6 h. One membrane was used and temperatures of 600 and 650º C were tested. A heating element went out in the middle of the run, but the cell appeared to fully recover from the temporary decrease in temperature to 340º C. The fuel flow rate was 200 mL min^{-1} and the inlet gas composition was 34.4% CO, 22.1% CO_2, 34.9% H_2, 8.39% H_2O, and 1150 ppm H_2S at 600º C and 35.6% CO, 20.9% CO_2, 33.6% H_2, 9.62% H_2O, and 1250 ppm H_2S at 650º C. Figures A3 and A4 show the IV curve and H_2S removal performance.
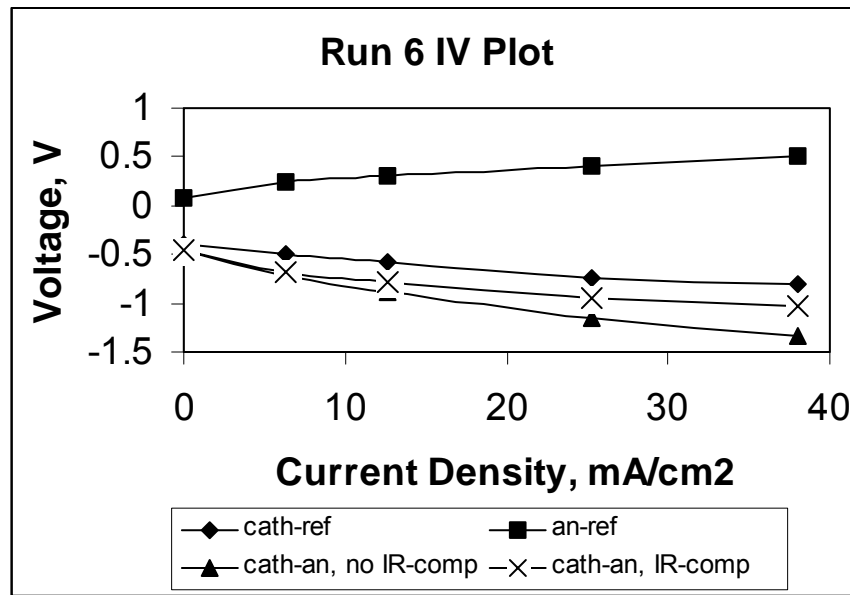
Figure A3. IV Curves for Run 6.
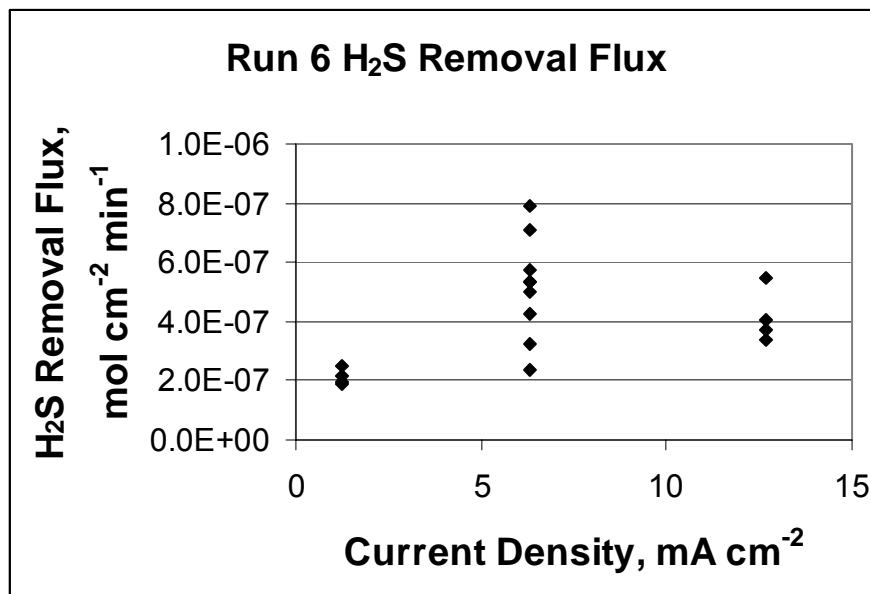
Figure A4. H_2S Removal Flux vs. Applied Current Density for Run 6. $Y_{0.9}Ca_{0.1}FeO_3$ was tested at 600˚ C and 650˚ C at a fuel flow of 200 mL min^{-1}.

Run 9 – 3/30/01 to 4/6/01

    Nickel was used as the cathode at a temperature of 600º C. Two membranes were used with six grams of electrolyte, and fuel flow was kept at about 75 mL min^{-1}. The gas composition was 35.6% CO, 20.9% CO_2, 33.6% H_2, 9.62% H_2O, and 1150 ppm H_2S. Towards the end of this run, the H_2S removal rate steadily dropped even though the potential still looked okay. IR drop was 0.5 ohms. Sixty percent CO_2 was blended into the purge stream on this run. Figures A5 and A6 show the IV curve and H_2S removal performance.

Run 9 IV Plot
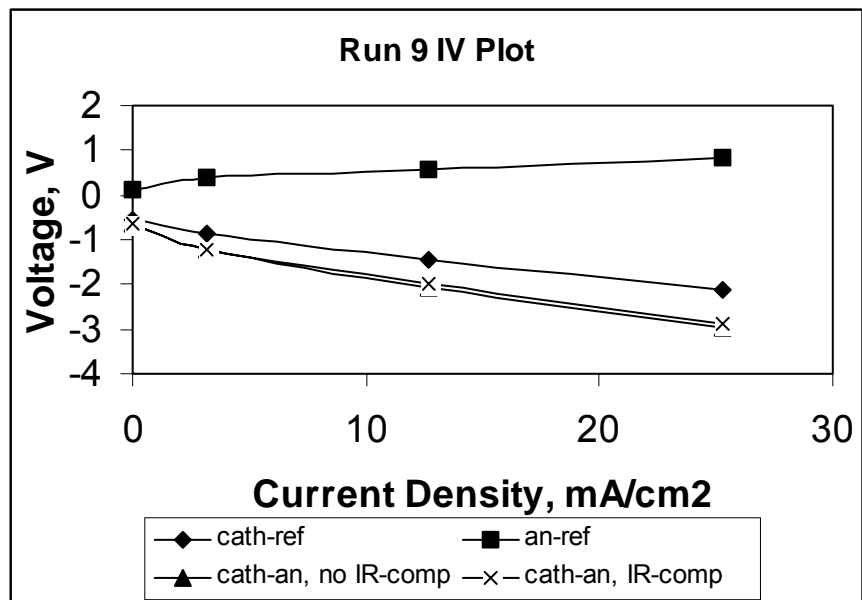
Figure A5. IV Curves for Run 9.

Run 9 H$_2$S Removal Flux
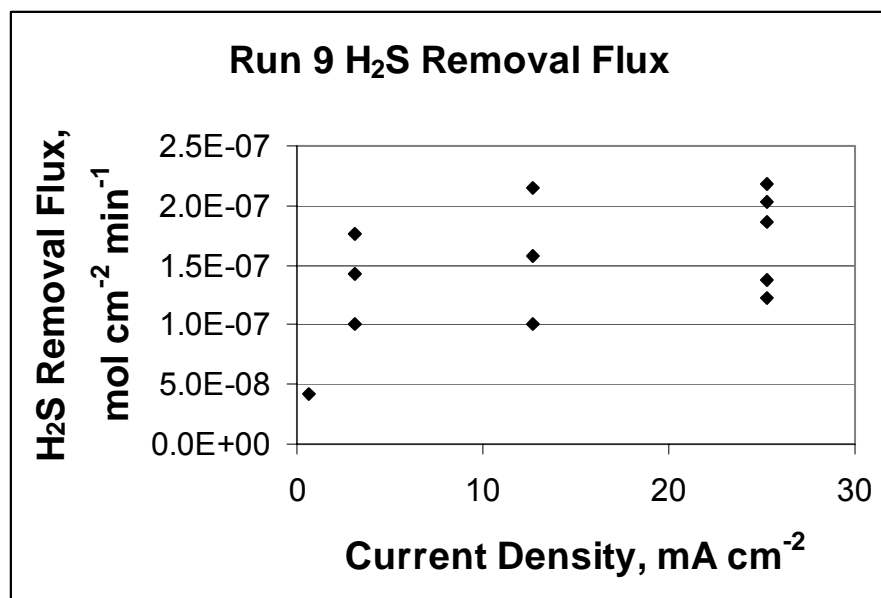
Figure A6. H$_2$S Removal Flux vs. Applied Current Density for Run 9. Nickel was tested at 600° C at a fuel flow of 75 mL min^{-1}.

Using CO_2 at the anode increased the cell potential. This is because carbonate is the

only species to be oxidized at the anode besides sulfide, and with CO_2 at a higher

pressure at the anode, the potential required to oxidize it is increased. This effect is a

result of galvanostatic operation. Potentiostatic operation should have the benefits of lower power requirements and higher current efficiency if CO_2 pressure is increased at the anode as long as an appropriate voltage is selected for operation.

Run 11 – 5/1/01 to 5/7/01

A lithiated $Y_{0.9}Ca_{0.1}FeO_3$ cathode fired at 800º C and two membranes were used in this run. Fuel flow was at 100 mL min^{-1} and the composition was 35.6% CO, 20.9% CO_2, 33.6% H_2, 9.62% H_2O, and 1150-2300 ppm H_2S.

The temperature was first at 600º C and then was raised to 650º C to better the performance. The H_2S concentration was also raised at this higher temperature. Over the course of the 136 h run, the cathode was severely degraded and partially melted into the channel. It also looked as if it were partially absorbed into the electrolyte/membrane. The measured IR-drop during operation was 1 ohm at 600º C and 0.4 ohm at 650º C. Figures A7 and A8 show the IV curve and H_2S removal performance.
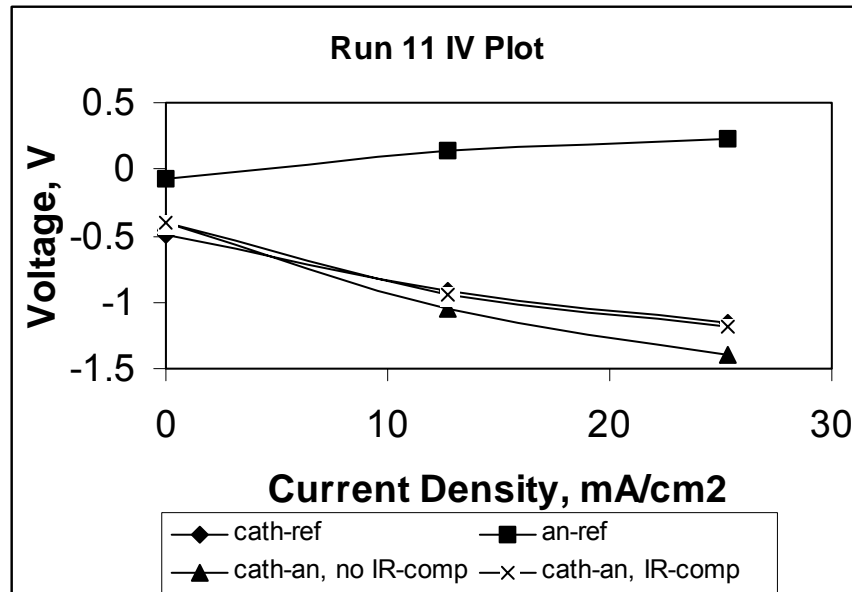
Figure A7. IV Curves for Run 11.
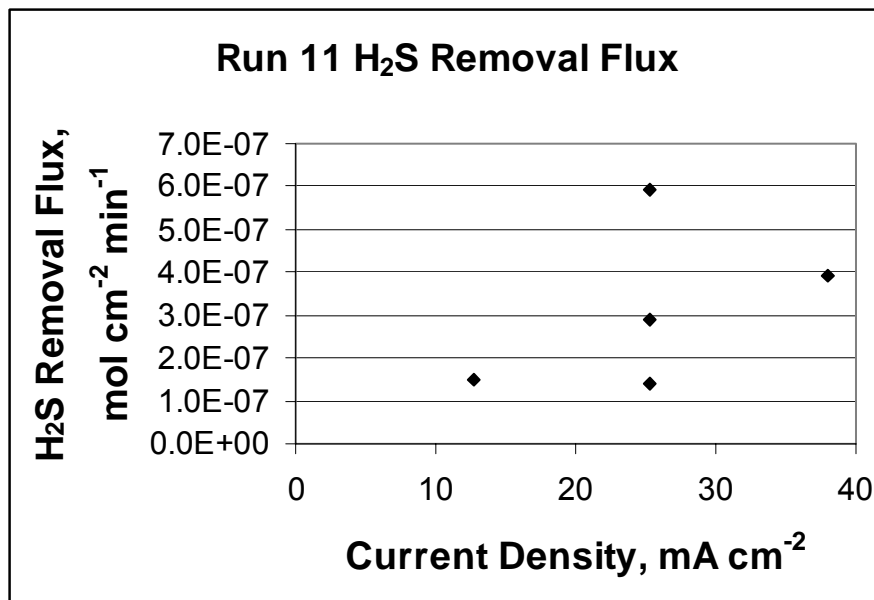
Figure A8. H$_2$S Removal Flux vs. Applied Current Density for Run 11. Y$_{0.9}$Ca$_{0.1}$FeO$_3$ was tested at 600° C and 650° C at a fuel flow of 100 mL min^{-1}.

Run 13 – 11/5/01 to 11/12/01

Using a nickel cathode, the cell was run at 600° C with a fuel flow of 200 mL min^{-1} and a composition of 34.4% CO, 22.1% CO$_2$, 34.9% H$_2$, 8.39% H$_2$O, and 1300 ppm H$_2$S. Two membranes were used, and the run lasted for 142 h. The cause of failure was gas-crossover. IR-drop was near 3 +/- 0.5 ohms for most of the run. Figures A9 and A10 show the IV curve and H$_2$S removal performance.
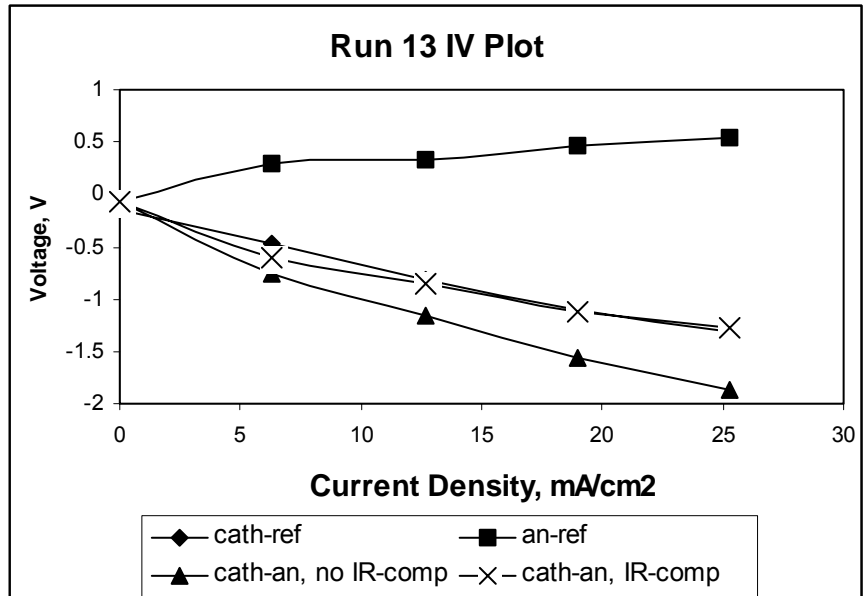
Figure A9. IV Curves for Run 13.
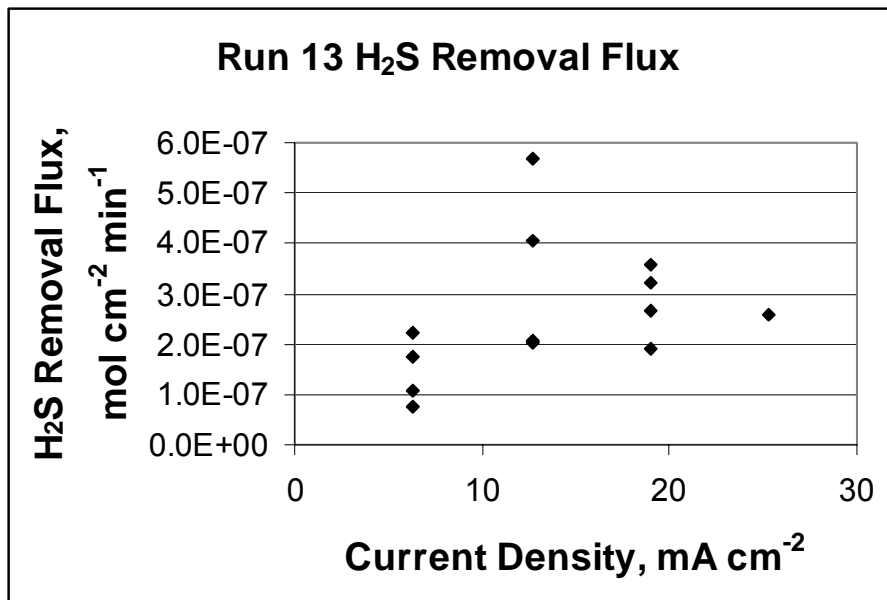
Figure A10. H₂S Removal Flux vs. Applied Current Density for Run 13. Nickel was tested at 600° C at a fuel flow of 200 mL min⁻¹.

This run used a lithiated $Y_{0.9}Ca_{0.1}FeO_3$ cathode that had been sintered at 1000º C for 6 h. Two membranes were used, and a fuel flowed at 200 mL min^{-1} with a composition of 34.4% CO, 22.1% CO_2, 34.9% H_2, 8.39% H_2O, and 1150-1700 ppm H_2S at 600º C. The run lasted for 171 h before gas-crossover was evident. The IR drop held near 1 ohm. Figures 15 and 16 show the IV curve and H_2S removal performance.
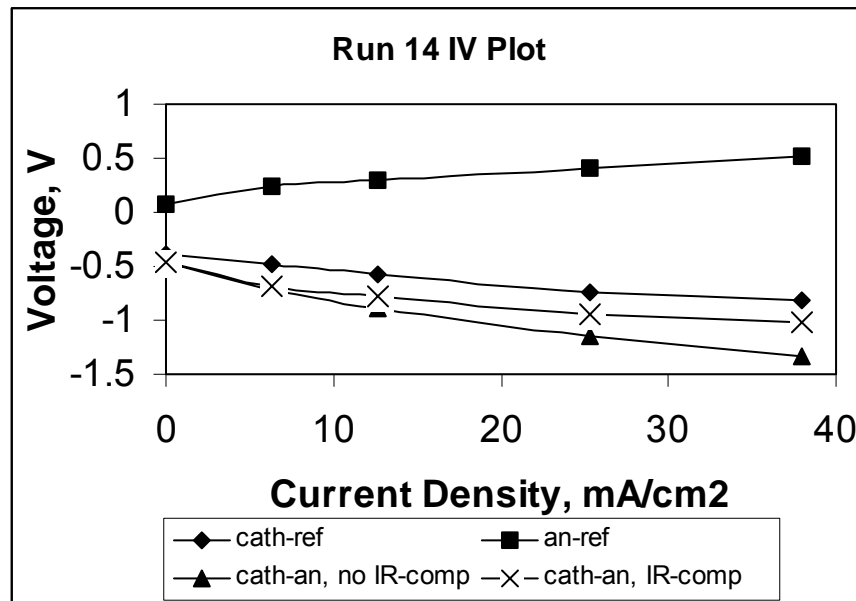
Figure A11. IV Curves for Run 14.
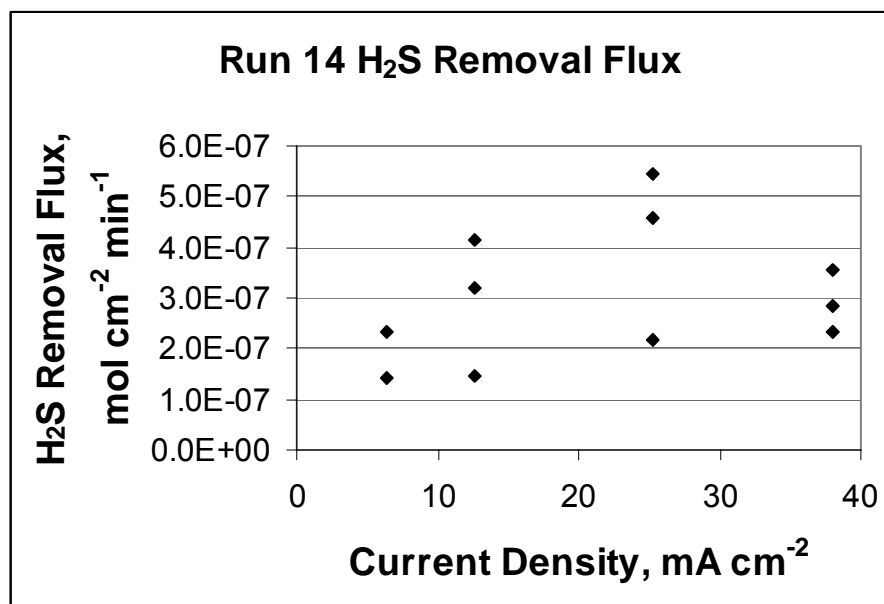
Figure A12. H$_2$S Removal Flux vs. Applied Current Density for Run 14. Y$_{0.9}$Ca$_{0.1}$FeO$_3$ was tested at 600° C at a fuel flow of 200 mL min^{-1}.

Run 15 – 3/18/02 to 3/23/02

A Gd$_2$TiMoO$_7$ cathode was prepared to run in a cell with two membranes at 650° C. The gas flowed at 100 mL min^{-1} and was composed of 33.6% CO, 21.8% CO$_2$, 33.5% H$_2$, 10.6% H$_2$O, and 2650 ppm H$_2$S. The cell ran for 70 h, but performance decreased substantially after roughly 50 h. It appeared that gas-crossover was present, but after adding electrolyte through the reference electrode hole, the cell recovered for a few hours. The removal data was acquired during this time, when the cell potential was also at its highest, and most high for any run (~ 5.6 V).

The removal rate was 5.0 x 10^{-7} mol min^{-1} cm^{-2}. The high operating potential offers serious doubts about its conductivity. However, its porous structure withstood high temperature and current very well. Perhaps too large of a current was applied (600 mA); more conservative currents should be used in future runs. This was the only current applied and the cross-cell voltage varied from 3-5 volts. It is possible that the cross-cell

voltage decreased when electrolyte was depleted, thus leading to gas crossover. In the two-membrane cell design, the cell was able to achieve the maximum removal rate as determined from Equation (5).

**Note: for runs 18 on, the reference electrode was exposed to air.

Run 19 – 1/25/03 to 1/28/03

A $La_{0.7}Sr_{0.3}VO_3$ cathode with $LiCoO_2$ coating was tested at 700º C with two membranes. Five grams of electrolyte were used. The fuel flow was 200 mL min^{-1} and composed of 34.8% CO, 20.6% CO_2, 32.3% H_2, 11.8% H_2O, and 1925 ppm H_2S. The run was ended when H_2O was found at the anode--indicating crossover. The IR drop was about 2.5 ohms for most of the run. Figures A13 and A14 show the IV curve and H_2S removal performance. The substantial drop-off of H_2S removal can be attributed to the large cell potential in this run, which drove the competing hydrolysis reaction instead of the preferred H_2S dissociation. Gradually increasing gas crossover could also be responsible as the higher currents were applied at later times in the run.
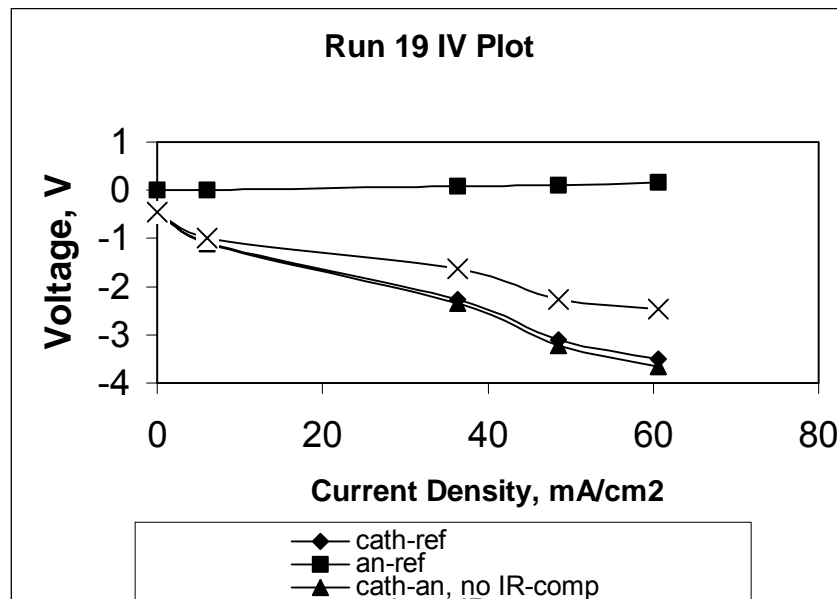
Figure A13. IV Curves of Run 19.
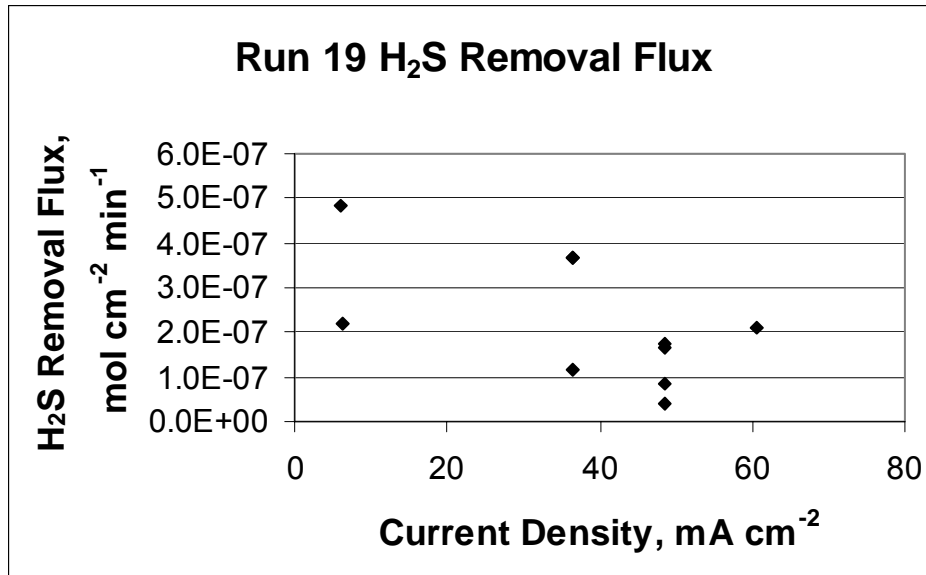
**Figure A14. H₂S Removal Flux vs. Applied Current Density for Run 19.
La$_{0.7}$Sr$_{0.3}$VO$_3$ with LiCoO$_2$ coating was tested at 700˚ C
at a fuel flow of 200 mL min^{-1}.**

APPENDIX B. Unsuccessful Run Descriptions

Run 2 – 12/13/00 to 12/16/00

A lithiated $Y_{0.9}Ca_{0.1}FeO_3$ cathode was used, but the furnace broke down, so this run had to be stopped.

Run 3 – 1/8/01 to 1/10/01

A CoS_2 cathode was prepared from 1 gram of starting material and 0.21 g cellulose ether as binder. The electrode was sintered at 520 C for 2 h and then 618º C for 1.5 h. Anode flow was 140 mL min^{-1}, and cathode flow at 42 mL min^{-1}. At 650º C, the inlet gas composition was 35.4% CO, 20.9% CO_2, 33.9% H_2, 9.75% H_2O, and 450 ppm H_2S. But by the third day, cell potential dropped and gas-crossover was observed. The run was stopped.

Run 5 – 1/26/01 to 1/28/01

A lithiated $Y_{0.9}Ca_{0.1}FeO_3$ cathode was tested again, but crossover occurred before any data could be taken.

Run 7 - 2/28/01 to 3/4/01

Nickel run. Crossover evident. No data taken.

Run 8 – 3/8/01 to 3/11/01

Nickel run, but cell housings were touching—shorted cell. Stop run.

Run 10 - 4/11/01 to 4/16/01

TiN was tested as a cathode material in this run after a recent publication discussed its excellent stability and conductivity.[47] Temperature was at first 600º C and little H_2S removal was performed. The polarization was very large and increasing the temperature to 650º C did not help performance. Electrochemical transfer was occurring to some

extent, however, so it is possible that this material is reactive with the stainless steel cell housing. The IR drop increased from 1.2 ohm to 5.6 ohms at 600º C and even got up to 10 ohms at 650º C. TiN is not a good candidate.

Run 12 – 8/1/01 to 8/4/01

A cermet cathode composed of 40% $LaCrO_3$ with 60% NiO was sintered at 1350º C for 5 hours and was used in this run with two membranes. This material never achieved stoichiometric CO_2 transport, so the run was stopped. It is believed that the cathode was not thick enough to make good contact with both the cell housing and electrolytic membrane.

Run 16 – 12/20/02 to 12/26/02

A $Y_{0.9}Ca_{0.1}FeO_3$ cathode was used with on membrane at 700º C. The inlet fuel gas flowed at 200 mL min^{-1} and was composed of 34.8% CO, 20.6% CO_2, 32.3% H_2, 11.8% H_2O, and 1925 ppm H_2S. Crossover was evident during the run, and H_2S removal performance was poor. In post-mortem analysis, it was found that the cathode had deteriorated, forming a small hole at the source of sour gas. Therefore, $Y_{0.9}Ca_{0.1}FeO_3$ should not be used at these higher temperatures.

Run 17 – 1/10/03 to 1/11/03

A $La_{0.7}Sr_{0.3}VO_3$ cathode was tested at 700º C with one membrane. Unfortunately gas-crossover was evident by the first day and no data could be taken. The cathode turned white and could have been exposed to too much oxygen upon heat-up, resulting in a non-conductive $Sr_3V_2O_8$ phase.

Run 18 – 1/13/03 to 1/17/03

A Gd_2TiMoO_7 cathode coated with $LiCoO_2$ was tested at 700º C with one membrane. The cathode had cracked during post-fabrication handling but was still used. The fuel was kept near 180 mL min^{-1} with a composition of 34.8% CO, 20.6% CO_2, 32.3% H_2, 11.8% H_2O, and 1925 ppm H_2S. Crossover was evident again, by the first day, but the run was continued for a few days to observe the chemical stability of the material in the operating environment. The cell potential was much smaller this time, reaching only –1.3V (cathode-anode) with 670 mA applied. The potential also decreased over time, signifying that crossover was getting worse. The IR drop was 0.4 ohm.

Run 20 – 2/14/03 to 2/17/03

A $LiCoO_2$ cathode was tested in a cell with one membrane at 650º C. The fuel gas flowed at 15-100 mL min^{-1} and was composed of 33.6% CO, 21.8% CO_2, 33.5% H_2, 10.6% H_2O, and 1925 ppm H_2S. After about 50 h, the cathode flow appeared to be partially blocked. Upon cooling and post-mortem analysis, it was found that the cathode material had decomposed and melted into the gas flow channel.

APPENDIX C. Stability Results of Poor Cathode Candidates

The XRD spectra of Sr_2FeMoO_6 without electrolyte heated in syngas with 2.2% H_2S at 700^oC for 72 h showed that Sr_2FeMoO_6 decomposed completely and resulted in a composite with FeS (Figure C1). Sr_2FeMoO_6 can react with the electrolyte and gaseous H_2S. It forms a composite mainly including Sr_2FeMoO_6, $SrCO_3$, FeS and other unknown phases after it was heated in syngas with 0.3% H_2S at 800^oC for 72 hours with the electrolyte (see Figure C1). For further heating in the same conditions, Sr_2FeMoO_6 will completely decompose and result in FeS containing composite. FeS can work as the electrical conducting component. Such material is similar with the $Y_{1-x}Ca_xFeO_3$ derived material. They have adequate electrical conductivity and stability for the H_2S removal cell as described by Wang.[23]

Figure C2 shows that Sr_2CrMoO_6 is much more stable than Sr_2FeMoO_6, but part of it reacted with H_2S and resulted in SrS after it was heated in syngas with 2.2% H_2S at 700^oC for 72 hours. Similar to Sr_2FeMoO_6, Sr_2CrMoO_6 reacted with the electrolyte $(Li_{0.62}K_{0.38})_2CO_3$ and H_2S, forming a composite consisting of Sr_2CrMoO_6, $SrCO_3$ and other unknown phases. It was heated in syngas with 0.3% H_2S at 800^oC for 72 hours together with the electrolyte.
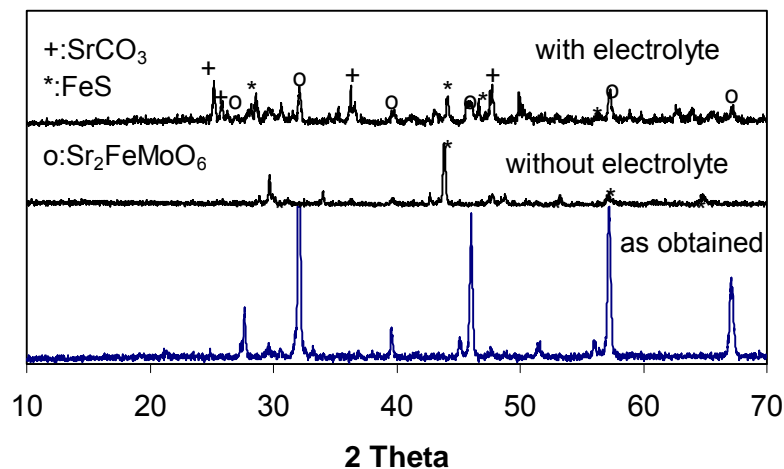
Figure C1. XRD of Sr₂FeMoO₆
(a) immersed in electrolyte at 800°C for 72 h in syngas with 0.3% H₂S.
(b) without electrolyte in syngas with 2.2% H₂S at 700°C for 72 h.
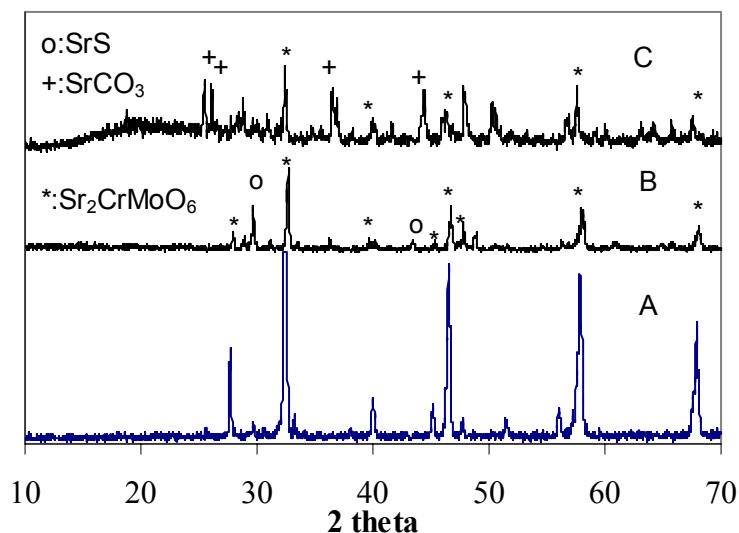
Figure C2. XRD of Sr₂CrMoO₆
(A) as obtained; (B) without electrolyte at 700°C for 72 h in syngas with 2.2% H₂S;
(C) immersed in electrolyte at 800°C for 72 h in syngas with 0.3% H₂S.

The $SrVO_3$ sample without electrolyte was very stable in the sour syngas atmosphere.

Only a very small amount of SrS was indexed from the XRD spectra of the sample heated in

syngas with 0.3% H_2S for 65 h (see Figure C3). However, the $SrVO_3$ sample, mixed with

electrolyte, changed to a composite with $SrVO_3$, $LiVO_2$ and SrS after it was heated in syngas

with 0.3% H$_2$S for 65 h. Further heating at 750°C for 72 h increased the amount of SrS. This

indicates that SrVO$_3$ kept reacting with H$_2$S and electrolyte. The final products were SrS and

LiVO$_2$. LiVO$_2$, usually used as an electrode material for Li batteries, is electronically

conductive.[48] Unfortunately, the electrical conductivity of the composite derived from

SrVO$_3$ and electrolyte was only 0.06 S cm^{-1} from 600 to 750°C. This is not high enough for

adequate cell efficiency.
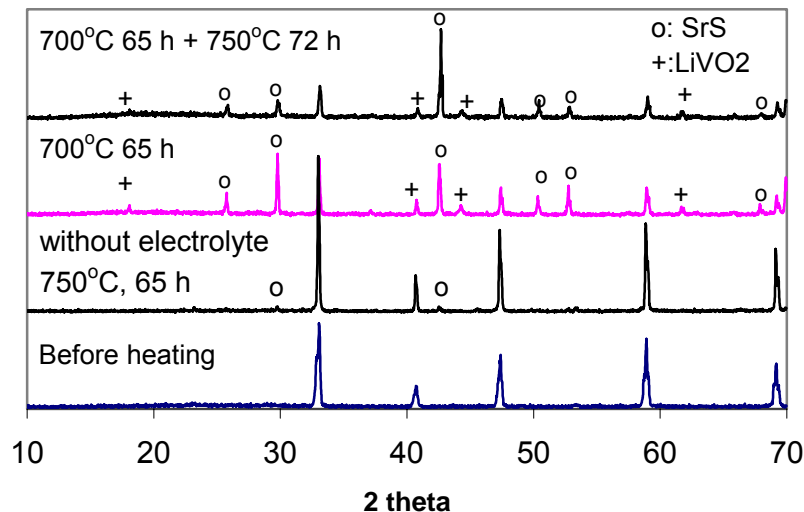
**Figure C3. XRD of SrVO$_3$ immersed in electrolyte and heated in syngas
with 3000 ppm H$_2$S.**

XRD spectra of MoSi$_2$, Co(II)MoO$_4$, and LaSrNi$_2$O are shown below. Each sample

was placed under 2% H$_2$S syngas at 700° C for 1 and 3 days. Electrolyte was mixed in

with the 3-day samples. MoSi$_2$ looked fairly promising, but we were unable to

successfully prepare a sintered disk electrode for full cell operation. The MoSi$_2$ powder

did not bind with the dry-pressing technique. Perhaps tape-casting would work better.
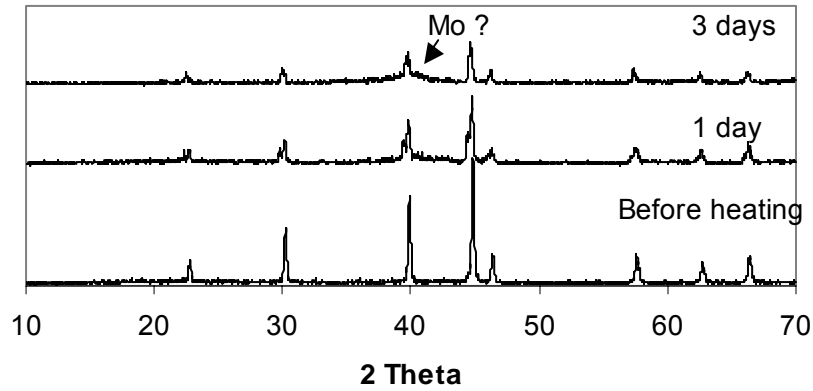
Figure C4. XRD of MoSi$_2$ heated with 2% H$_2$S syngas at 700˚ C for 1 and 3 days. Electrolyte was mixed in with the 3-day samples.
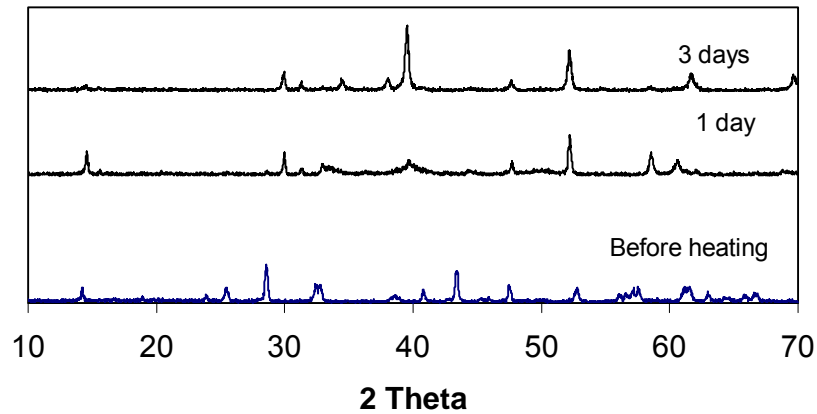
Figure C5. XRD of CoMoO$_4$ heated with 2% H$_2$S syngas at 700˚ C for 1 and 3 days. Electrolyte was mixed in with the 3-day samples.
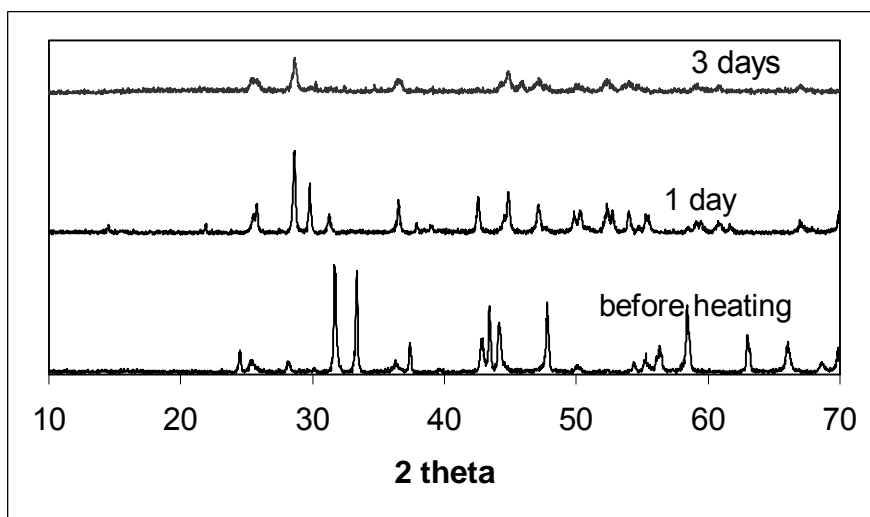
Figure C6. XRD of LaSrNi$_2$O heated with 2% H$_2$S syngas at 700˚ C for 1 and 3 days. Electrolyte was mixed in with the 3-day samples.

Many other materials were tested, as can be seen in Table 4, but not all the XRD spectra are shown. In the materials not shown, the XRD spectra were indiscernible, thus indicating that complex sulfide structures were formed. Some of these sulfide structures may indeed be stable, but the focus of these stability runs was to find materials that can resist reaction with a sour fuel stream.

APPENDIX D. Derivation of Ionic Flux Equation

The sulfide diffusion flux equation is derived directly from the Nernst-Planck equation for ions through liquid media:

$$i = -D_{AB} F z \left[\frac{dC}{dx} + \frac{zCF}{RT} \frac{dV}{dx} \right] \tag{D1}$$

where dC/dx and dV/dx are the concentration and voltage gradients across the membrane, respectively. The left-hand side term reflects the diffusion effects, and the right-hand side term corresponds to the migration effects. This equation assumes that ion movement is only in one direction along these concentration and voltage gradients. It also assumes that the ionic species move independently, not interfering with each other.

Near an electrode, both migration and diffusion are often significant, but in the bulk solution, the migration term typically dominates, rendering the diffusion term negligible. However, if supporting electrolyte is present, then the ion under consideration is "swamped" and the migration process is hindered. In this scenario, movement of the supporting electrolyte is responsible for a majority of the current in the bulk electrolyte.

To determine the fraction of current carried by sulfide in the bulk electrolyte, the transference (or transport) number must be calculated. The transference number corresponds to the fraction of current carried by a particular ion in bulk solution. First, the mobility can be calculated for each ion from

$$u_i = \frac{|z_i| e}{6 \pi \upsilon r} \tag{D2}$$

where z_i is the charge of the ion, e the quantity of charge per electron, υ the solution viscosity, and r the ion radius. Now, after estimating the concentration, C_i, of each ionic species, the transference number can be calculated by

$$t_i = \frac{|z_i| u_i C_i}{\sum_j |z_j| u_j C_j}$$ (D3)

The ions considered here are Li^+, K^+, CO_3^{2-}, and S^{2-}. In the 600° C runs with 1000 ppm H_2S, 10% H_2O and 21.2% CO_2, the cathode side electrolyte sulfide fraction would be approximately 7.2%, assuming that the activity coefficients for carbonate and sulfide are equivalent and that Reaction (6) is at equilibrium. This sulfide mole fraction corresponds to a concentration of 3.65 x 10^{-4} mol cm^{-3} at the cathode. Using half this value to represent the average sulfide concentration in the electrolyte, the calculated transference number is 0.01 for sulfide. This means that sulfide migration should account for only 1% of the total current in the bulk electrolyte. From this calculation, it appears that the presence of supporting electrolyte significantly hampers the migration of sulfide.

However, evaluation of the right-hand side term (the migration term) in Eq. (D1) implies that the migration term is several orders of magnitude larger than the diffusion term when 1V is applied across the cell. This large sulfide flux, however, is not seen in experiment. The Nernst-Planck equation does not account for interaction between the ionic species, and sulfide interaction with other species must be interfering with its migration. One example could be the formation of polysulfide, which would not only decrease the concentration but also lower the mobility of the sulfide species. Also evident from experimentation is that no sulfide deposition is found at the anode and applying higher potentials did not always result in higher sulfide removal fluxes. Because a stronger electric field does not further increase the sulfide removal flux, it must be limited by a diffusion process. Also, because no sulfide was found at the anode,

this implies that the concentration of sulfide at the anode is near zero, thus rendering the migration term insignificant near the anode.

Another problem is that the mobilities calculated by Eq. (D3) are idealized and often inaccurate in real molten solutions. For instance, experimental data shows that the mobility of K^+ is actually higher than that of Li^+, although one would not derive this from the above formula.[49] From experimental data, it appears that the sulfide mobility is lower than this theory suggests. Nevertheless, migration may dominate the sulfide transport process in some regions of the membrane, especially where sulfide concentration is high. But despite these calculations, migration does not appear to be the limiting step. All experimental evidence signifies that diffusion ultimately limits the removal of sulfide.

The presence of highly concentrated electroactive species in molten electrolyte may be the source of ion interactions and migration suppression. The swamping effect of large quantities of non-reactive electrolyte species results in double layer formation. Large capacitance values seen in sulfide melts (20-30 mF cm^{-2}) support the existence of a heavily charged double layer. This double layer produces electrode polarization by building up oppositely charged species at the electrode/electrolyte interface. Strong interactions between sulfide and other ionic species may be what hampers the migration term in Equation (D1). At higher temperatures or higher inlet H_2S concentrations, the migration term may not be negligible, but the same limitations appear to hold at 650˚ C.

Focusing back on Equation (D1), the only term left to deal with is the diffusion coefficient. When considering diffusion through a membrane, the diffusion coefficient must be modified to account for the membrane's structure—specifically the porosity and tortuosity. The porosity is simply the void volume in the membrane, while the tortuosity

refers to the ratio of the average distance a molecule travels across the membrane to the shortest possible distance across the membrane. Tortuosity reflects the actual path a molecule may follow to twist and turn its way through the membrane. With the effective diffusivity, $D_{E,AB} = (\varepsilon/\tau)D_{AB}$, the flux balance becomes

$$i = -D_{AB}zF\frac{\varepsilon}{\tau}\frac{dC}{dx} \tag{D4}$$

Now all that is left is estimation of the concentration gradient. Assuming that the concentration profile is linear across the membrane and that the concentration of sulfide goes to zero at the anode,

$$\frac{dC}{dx} \approx \frac{C_{S^{2-},cathode} - C_{S^{2-},anode}}{x} = \frac{C_{S^{2-},cathode}}{x} = \frac{\rho_{Elec}}{x}c_{S^{2-}}^{cath} \tag{D5}$$

where ρ_{Elec} is the molar density of the electrolyte, x is the membrane thickness, and c^{cath}_{S2-} is the sulfide fraction at the cathode surface. Combining (D4) and (D5) yields Equation (5).

APPENDIX E. Error analysis

All gas percentages are accurate to within 2%, as certified by the vendor, Matheson. Flow rates are also accurate to within 2%, as was calculated from repeated bubble meter measurements at constant flow rate. The potentials are verified with multimeters, but because the voltages slightly vary over time, the values recorded here are accurate to within 2%. The CO_2 levels measured with IR are accurate to within 2% as reported by the manufacturer.

The most error arises from the H_2S sampling in the GC. There is about a 10% variance in the gas samples taken during full cell operation. Each set of data is taken in 20 minute increments and saved in an individual file. Data was averaged from each data set and the operating conditions (flow rate, current, etc.) were noted for each data set. The inlet H_2S concentration was also sampled in each data set for comparison to the outlet. Error bars in the H_2S removal plots reflect the 10% variance.

The membrane itself also has variable properties. The thickness and porosity can vary slightly between all runs. The estimate of 38% porosity was calculated from a 4 in^2 sample, and this porosity was used in all calculations. A larger sample population is needed for more accuracy here, but the values for porosity and thickness used in this study can conservatively be assumed accurate to within 5%.

APPENDIX F. Algorithm of Sulfur Species Diffusion Model

```
Input:
    -stream composition
    - fuel flow rate
    -membrane porosity
    -membrane toruosity
    -membrane thickness
    -area of cell
```

↓

```
Set Temperature and
intended removal percentage of H₂S
```

↓

```
Calculate:
-water-gas shift
-log-mean H₂S concentration at the cathode
-log-mean sulfur and CO₂ conc.'s at anode
-carbonate/sulfide ratio at cathode from Rxn (6) equilibrium
-sulfide activity at cathode and anode
-Nernstian voltage from Eq.'s (14) & (15)
-Intended H₂S removal flux
-membrane diffusion limited H₂S flux
-gas phase diffusion limited H₂S flux
```

↓

```
Compare diffusion limted
fluxes.  Is the lower value of
the two greater than the
intended H₂S removal flux?
```  —— no ——→  ```
Recalculate:
-CO₂ at anode, since excess
current will go to CO₂ transport
-Nernstian voltage
-Actual removal rate of H₂S
```

yes ↓

```
Calculate:
-overpotentials
-power requirement
-cost
```

↓

```
Set new Temperature
and/or removal percentage?
```  —— no ——→  ( END )

Yes ←

APPENDIX G. Operating Costs Calculations

The first steps of cost analysis in scale-up of an EMS process is to decide on the power application needed and the type of fuel stream that is going to be treated. Considering a moderate level power application of 2.5 MW, this system could supply power to a building or several homes. Pure H_2 has a calorific value of 150 MJ kg^{-1}. Assuming that the reformed diesel stream is 60% H_2 and that the entire process obtains only 60% of hydrogen's calorific value, total gas flow at 923 K and 4 atm would be 26200 L min^{-1} as estimated from the ideal gas law.

$$MassFlowH_2 Needed = \frac{2.5MW}{(0.6)150MJ/kg_{H_2}} = 0.027kg_{H_2}/s$$

$$\dot{V} = \frac{\dot{m}RT}{M_{W,H_2} y_{H_2} P} = \frac{(27.7g_{H_2}/s)(0.0821L\_atm/mol\_K)(923K)(60s/min)}{(2g/moleH_2)(0.6molH_2/molfuelgas)(4atm)} = 26200L/min$$

Now, assuming a 1% H_2S contamination and that 3 mA cm^{-2} (30 A m^{-2}) on average goes towards H_2S removal, the required cell area would be

$$Cell\_Area = \frac{nF}{i}(\dot{n}_{H_2S}) = \frac{2(96485C/mol)}{30A/m^2}\left(\frac{(27.7gH_2/s)(0.01)}{(0.6)(2g/molH_2)}\right) = 1485m^2$$

Now assume that the average applied current density is 20 mA cm^{-2} at a cell voltage of –0.75 V. Therefore, the power requirement would be about 9% the power output, or

$$P = (i)(Area)(Voltage) = (200A/m^2)(1485m^2)(0.75V)(1kW/1000W) = 223kW$$

Obtaining the typical industrial cost for electricity at $0.04/kWhr, the total cost per kilogram H_2S removed will be equal to

$$Cost = (P/\dot{m}_{H_2S})\$0.04/kWhr = \$0.32/kg\_H_2S\_removed$$
$$where\_\dot{m}_{H_2S} = \dot{n}_{H_2S}M_{W,H_2S} = (0.231mol/s)(34g/mol) = 7.854g_{H_2S}/s$$